Chapter 2
Wood Surface Stability

2.1 Introduction

Surface stability itself is also a complex property having far-reaching connections with the general resistance to artificial and environmental influences as a function of time. Any deterioration in the physical and mechanical properties of the surface layer, changes in colour and gloss fundamentally decrease the utility and aesthetical value of a product.

The main environmental influences are the light irradiation of different wavelengths, moisture and temperature changes and fungal attacks. Artificial actions such as heat treatment with dry air, humid air or steam also influence the mechanical and aesthetical properties (colour) of the material.

In this chapter, a detailed description and analysis is given concerning the interrelationship between environmental or artificial influences and material response. The most common environmental influence is the UV irradiation causing photodegradation of the wood surface with all its consequences: destruction of physical and mechanical properties of the surface, discolouration, loss of gloss and roughening of the surface. Different artificial heat treatments are also increasingly used to modify some physical and mechanical properties, and also to change colour and colour inhomogeneity. The associated chemical reactions, however, are quite different of those involved in the changes due to light irradiation.

In wood materials, moisture is always present and plays an important role in all environmental and artificial influences. Therefore, the moisture exchange with the air and the moisture movement in wood structures are also treated.

Some mechanical properties of the surface, such as hardness and resistance to friction forces, play also an important role in utility product design. They are also discussed and practical recommendations are given.

E. Csanády et al., *Quality of Machined Wood Surfaces*,
DOI 10.1007/978-3-319-22419-0_2

2.2 General Remarks

Wood is a naturally created polymer composite. The combination of cellulose, hemicelluloses and lignin naturally arranged into tubular structures and eventually forms a cylindrically layered composite; this is the solid wood. Beside these three main components, the extractives play important role in colouring the wood. The unique formations of the woody tissues offer their excellent mechanical and physical properties. Their low density is accompanied by desirable mechanical strength. That is why wood is widely used as structural engineering material for indoor and outdoor applications. In addition, wood is easy to process.

Beside the excellent physical and mechanical properties, the wood has unique colour. Most of wooden colour is naturally inhomogeneous. The colour inhomogeneity of wood is one of the most beautiful colour harmony created by the nature, because its colour range and the colour pattern provide emotive comfort for the observer. The colour hue of wood between red and yellow gives us warm image. The hue angles (see in Sect. 3.2) for wood species are between 45° and 90°. (The 0° hue is red and the 90° belongs to yellow.) There are only a few extremely dark species with hue below 45°. This hue interval is visible by human eye as colour interval between yellow and brown.

Because of its organic nature, wood undergoes abiotic and biotic degradations. The biotic degradation consists of fungal and insect attacks. The abiotic degradations are usually surface phenomena. The abiotic degradation is influenced by the solar radiation, rainfall, heat, humidity content of the surrounding air, presence of oxygen and air pollutants (e.g. acid rain). The colour harmony of wood material is sensitive to light and heat. The most sensitive molecule is the lignin macromolecule because it is good absorber of ultraviolet (UV) light. Chemical analyses showed that the deterioration of light irradiated wood is primarily related to the decomposition of lignin (Tolvaj and Mitsui 2005; Pandey 2005a; Agresti et al. 2013; Tolvaj and Faix 1995; Popescu et al. 2011; Pandey and Vourinen 2008; Calienno et al. 2014). The extractives are also sensitive to light irradiation and heat treatment. Black locust wood changes its colour towards red visibly after only one hour exposure to sunlight. This colour alteration is generated by the degradation of its high extractive content. In contrast, Poplar (having low extractive content) suffers hardly any visible colour change during the same period of time (Persze and Tolvaj 2012).

Wood adsorbs or desorbs water rapidly, depending on the humidity of the surrounding air. The water uptake or loss is accompanied by the swelling or shrinkage of the wood. The rapid surface drying produces surface shrinkage creating cracks. The water uptake influences the colour of wood as well. The increase of moister content produces darker and more saturated colour. In heat or light induced reactions, the moisture content plays also an important role and the moisture always accelerates both photodegradation and thermal discolouration of wood materials.

The density of solid woods depends on species (genetic properties), growing conditions and on age. The density considerably influences several surface properties such as hardness, wear resistance, roughness and gloss properties.

In the following sections, a detailed description of all important questions concerning surface stability will be treated with several new data and practical recommendations.

2.3 Importance and Problems of Surface Stability

The stability as a complex notion expresses any change in the surface properties due to the combined actions of light, heat, moisture and mechanical loadings as a function of elapsed time. These actions may have environmental or artificial origins, and their components and intensities are generally time dependent and of random nature. The loss of stability is associated with serious consequences such as:

- surface material degradation and loss which lower the initial physical, mechanical and aesthetical properties considerably,
- decrease of surface resistance to friction and impact loadings and
- fading and discolouration of the surface.

Wood is a biobased material. Because of this nature, the wooden surface is sensitive to natural decompositions. One of the most important surface parameters is the colour. The colour of the natural woods is perceived by human eyes somewhere between yellow and brown. These colour hues give a feeling of warmth. The machined surface in any anatomical planes represents the colour diversity of the inside lumen surface, the cell wall, the earlywood and the latewood zones. Additionally, the machined surfaces of the different species include lots of micromirrors aligned parallel to the grain. Gloss from these micromirrors gives us more elegant, soft, natural and beautiful texture than that of plastics and metal (Masuda 2001).

The unique colour of wood is sensitive to light, heat and moisture. It is a great challenge for wood scientists to preserve this excellent colour harmony of wood. The colour of non-protected wood changes continuously in outdoor conditions. The surface starts yellowing and the rain leaches out the water soluble chromophoric components. The surface will be more and more grey. In indoor conditions, the colour of surfaces also fades and the dark colours become less saturated. The degradation effect of light can be reduced by transparent UV protective finishes. There is no effective process existing to protect the wood against thermal degradation. It is a slow alteration, but the colour change is visible after a few years.

The surface hardness and wear resistance are also an important parameter. The surface of furniture, claddings and wooden constructions suffer often from different loadings such as friction or impact. The hardness of low-density species is not high enough to protect the surface from damage. There are some transparent surface finishes to increase the resistance to wear or impact loading. The use of these

protective finishes is especially important on utility surfaces such as parquet flooring. It is also a common practice that surfaces subjected to high abrasive loadings are made of a thin layer of high-durability wood surfaces.

Wooden products are generally designed for many years in service, during which the main surface properties should be maintained as long as possible. The selection of proper materials, design parameters, the manufacturing process and the surface finish including the necessary protection are the main challenges of any designer.

2.4 Moisture Relations and Wettability

2.4.1 Moisture Exchange of Wood Surface with the Air

Capillaries make wood a porous, hygroscopic material having the ability to adsorb and desorb water. The water content of the wood plays a very important role influencing the physical properties and also the durability of the wood subjected to various treatments and environmental effect.

The most important relations of moisture exchange are the following:

- the moisture content of wood and its variation in time influences, its surface stability, the decay of wood and stability and durability of coatings.
- in internal spaces (living rooms), the wood surface has the ability to equalise the relative humidity of air through moisture exchange with the air.

The wood tends to be in equilibrium with the surrounding environment which generally changes continuously in its temperature and relative humidity. Taking a free water surface, some molecules of water having a given amount of energy can escape from the surface as a vapour into the surrounding air. At the same time, some vapour molecules may re-enter into the water surface (condensation). At equilibrium, the partial vapour pressure above the surface will be equal to the saturated vapour pressure which depends on the temperature.

The saturated vapour pressure can be calculated from the following exponential equation:

$$P_s = 1.3 \times 10^{11} \exp \frac{E}{RT} \quad \mathrm{N/m^2} \tag{2.1}$$

where

R is the gas constant (8.31 J/mol K),

T is temperature in K and

E E = 44,100 J/mol is the heat of evaporation

(This value is valid for 20°C and for other temperatures it must be modified.)

The moisture content of wood can be defined and expressed in different ways. The mass of water can be related to the total mass or the dry mass of the wood:

$$U = \frac{m_{\mathrm{w}}}{m_{\mathrm{w}} + m_{\mathrm{d}}} \quad \text{(wet basis)} \tag{2.2}$$

$$X = \frac{m_{\mathrm{W}}}{m_{\mathrm{d}}} \quad \text{(dry basis)} \tag{2.3}$$

where m_{W} is the mass of water and m_{d} is the oven-dried mass of the wood. Since wood is a porous material, in certain cases it may be advantageous to use the moisture content by volume:

$$W = \frac{V_{\mathrm{w}}}{V_{\mathrm{ws}}} \quad \text{(volume basis)} \tag{2.4}$$

where V_{w} is the volume of water and V_{ws} is the volume of wood sample. It is clear that the moisture content on volume basis also depends on the porosity n of the material. The different moisture contents are interrelated by the following equations:

$$U = \frac{X}{X+1} \quad \text{and} \quad X = \frac{U}{1-U}$$

and further

$$W = \frac{\rho_{\mathrm{ws}}}{\rho_{\mathrm{w}}}(1-n)X$$

where ρ_{w} is the water density and ρ_{ws} is the volume density of the wood sample.

Due to the cellular structure of wood, the moisture status in wood is a complicated phenomenon. The bound or hygroscopic water is found in the micropores ($r < 50$–100 nm) of wood, first in one layer of molecules and later in several layers. The range of micropores can be approximated using theoretical calculations.

It is well known that at a liquid–gas interface, the surface tension phenomenon exists which is due to intermolecular forces. Over a capillary meniscus with a radius r, due to the water rise in the capillary, the decreased static pressure corresponds to a decreased vapour pressure, which means a smaller relative humidity over the meniscus. According to the Thompson equation, the relative humidity φ over the meniscus is given by:

$$\varphi = \exp\left(\frac{2\gamma\rho_{\mathrm{v}}}{P_v\rho_{\mathrm{w}}}\right) \tag{2.5}$$

where

γ	is the surface tension of water (0.072 N/m),
P_v and ρ_v	are the vapour pressure and density, respectively,
ρ_w	is the water density and
r	is the radius of capillary.

Calculations show that $r = 0.36$ nm corresponds to $\varphi = 0.05$ and $r = 100$ nm to $\varphi = 0.98$. In the sorption process, therefore, capillaries over 100 nm radius cannot be filled with water. The amount of water taken up by the sorption process is called the hygroscopic water, and the corresponding moisture content is the fibre saturation point. This moisture content corresponds to saturation of the cell wall without containing any water in the bigger capillaries over radii of 100 nm.

The distribution of microcapillaries in wood is given in Fig. 2.1 showing an interesting picture (Stamm 1946). Most of the capillaries are in the 0.5–1.0 nm range corresponding to $\varphi = 0.2$ and appr. 5 % moisture content. The low relative humidity means a high driving potential (tension) which decreases rapidly with increasing capillary radii. The capillary tension is a real driving force (water potential) according to the following equation:

$$\Psi = \frac{2\gamma\cos\Theta}{r} \quad Pa \tag{2.6}$$

Note that the surface tension slightly decreases with increasing temperature.

Furthermore, the sap in the wood containing soluble nutrients has a smaller surface tension about 0.05 N/m. The surrounding air due to its relative humidity has also a driving potential given by the following equation:

$$\Psi a = \frac{RT}{m_w} ln\varphi \quad bar \tag{2.7}$$

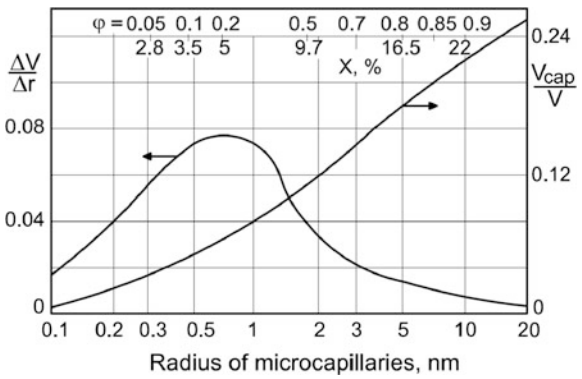

Fig. 2.1 Distribution of microcapillaries in wood

where m_w is the molecular volume of water (18 cm^3/mol) and R is the gas constant (82 bar.cm^3/mol K). An example: the air with 90 % relative humidity at 20 °C has a water potential of appr. −140 bar!

Equilibrium between the wood and the air is only possible if their water potentials are equal to each other. The main advantage of the water potential concept is in that it is valid also for different materials contacting each other and different moisture contents may be in equilibrium, e.g. heart- and sapwoods. The partial vapour pressure difference, as a driving force, can only be used for a homogeneous material having the same physical properties in its entire volume.

The equilibrium moisture content of wood as a function of air relative humidity is shown in Fig. 2.2. The equilibrium moisture content is temperature dependent, and at higher temperatures, it shifts towards lower values.

Due to the shape of the equilibrium moisture content curve, the derivative of the vapour pressure $\Delta P_v/\Delta X$ has a maximum in the φ = 0.3–0.4 range as depicted in Fig. 2.3, quite similarly to the maximum in Fig. 2.1. Consequently, the shape of the equilibrium moisture curve is dominantly affected by the distribution of micropores in the wood.

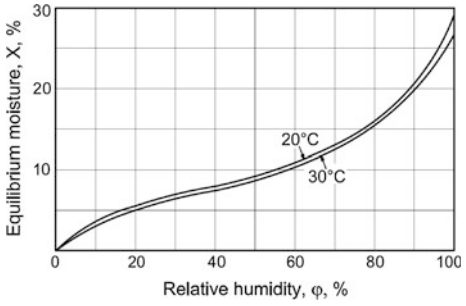

Fig. 2.2 The equilibrium moisture content of wood as a function of air relative humidity

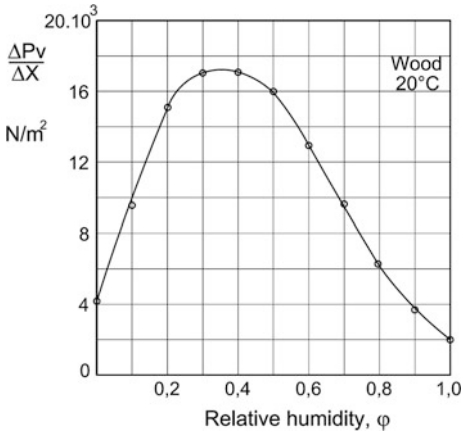

Fig. 2.3 Derivative of the equilibrium moisture content curve

Concerning a homogeneous material, the specific mass transfer on the wood surface is as follows:

$$q = \frac{\beta}{TR_V}(P_s - P_\varphi) \quad \mathrm{N/m^2 s} \tag{2.8}$$

where

β is the surface mass transfer coefficient, m/s,
P_s and P_φ are the partial pressure on the surface and in the air, respectively, $\mathrm{N/m^2}$ and
R_v is the gas constant of the vapour, m/K (47.1 m/K).

Equation (2.8) may be used in a modified form as follows:

$$q = \beta' \rho_0 (X_s - X_\varphi) \quad \mathrm{kg/m^2 s} \tag{2.8a}$$

where content corresponding to P_s and P_φ, respectively, and
X_s and X_φ is the equilibrium moisture
ρ_0 is the dry density of wood.

The mass transfer coefficients β and β' have different values, and the interrelation between them is obtained by equating the Eqs. (2.8) and (2.8a).

The moisture transferred to the surface should be conducted into the material which is described by the diffusion equation:

$$q = D\rho_0 \frac{\Delta X}{\Delta x} \quad \mathrm{kg/m^2 s} \tag{2.9}$$

where D means the diffusion coefficient depending on the moisture content and temperature, $\mathrm{m^2/s}$. The boundary condition is given by equating Eqs. (2.8a) and (2.9) in the following form:

$$\left.\frac{\Delta X}{\Delta x}\right]_{x=0} = \frac{\beta'}{D}(X_s - X_\varphi) \tag{2.10}$$

This means that the process is governed by the β'/D ratio. The accurate solution of the moisture exchange problem is rather complicated and time-consuming task. In the practice, however, a quick estimate is more desirable. Taking some simplifying assumptions, a very convenient solution may be obtained satisfying the possibility of a quick estimation.

Between certain limiting values of the moisture content, the sorption isotherm (see Fig. 2.2) can be taken as approximately a linear function and with this assumption we may write as follows:

$$\frac{dX}{dx} = -k(X - X_e)$$

where X means the instantaneous average moisture content; Xe is the equilibrium moisture content corresponding to a given relative humidity of the air; and k characterises the evaporation rate. Integration of the above equation yields the relation as follows:

$$MR = \frac{X - X_e}{X_1 - X_e} = e^{-kt} \tag{2.11}$$

where X_1 is the initial moisture content in the wood. The left-hand side of the equation is termed the moisture ratio, which characterises the moisture exchange as a decimal number until the equilibrium moisture content has been attained.

The half-time $t_{0.5}$ is termed as the time required for removal of one-half of the evaporable quantity of water, and its value is calculated as follows:

$$t_{0.5} = \frac{\ln 2}{k} = \frac{0.693}{k} \tag{2.12}$$

If the half-time $t_{0.5}$ would be known for different wood species and environmental conditions (temperature, initial equilibrium moisture content and the change in relative humidity), then the moisture uptake or moisture loss can be estimated conveniently using Eqs. (2.11) and (2.12). Furthermore, from the general theory of drying, it is well known that in parallel sided bodies (the infinite plate) the moisture profile follows a parabolic distribution.

With the parabolic assumption, the expected moisture profile for the elapsed half-time $t_{0.5}$ can easily be constructed. Figure 2.4 shows the moisture profile of a 1-inch (25-mm)-thick slab exposed on both sides, for different elapsed times. In the centre line, the decrease of moisture occurs with considerable delay. Due to the parabolic distribution, however, the moisture ratio at the centre line for the half-time $t_{0.5}$ can easily be estimated as 75 %.

The processing of a vast amount of moisture distribution profiles for quite different conditions has shown that the centre line moisture ratio is a uniquely defined function of the dimensionless time $t/t_{0.5}$ as plotted in Fig. 2.5.

The centre line moisture content tends to decrease after an elapsed time between 40 and 50 % of the half-time. Using a half-logarithmic scale, the correlation is not exactly a straight line (exponential function), but the deviation from the exponential law is not essential. Knowing the half-time for a given adsorption or desorption process, the moisture profile distribution for arbitrary time can easily be estimated. It should be noted that the above method is valid only for a uniform initial moisture distribution. With short time variations in the relative humidity, the equalizing process cannot be completed, and therefore, the initial condition for the subsequent relative humidity variations will be rather a parabolic moisture distribution. The latter

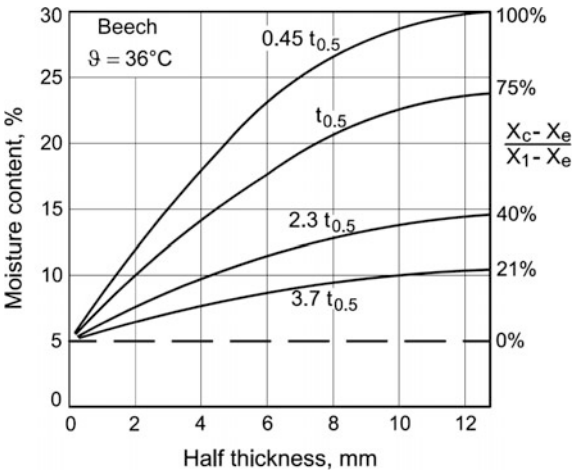

Fig. 2.4 Moisture distribution in 1-inch-thick slab

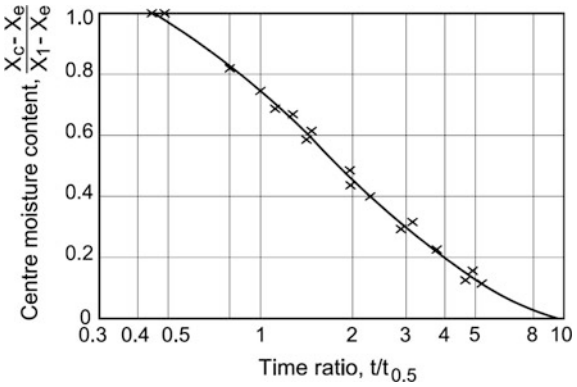

Fig. 2.5 Dimensionless plot for determining the centre line moisture content as a function of time

initial condition can be handled theoretically (Лыков and Михайлов 1959), but the solution is quite time consuming and a practice friendly elaboration would be needed.

As Eq. (2.8) suggest, the mass transfer on the surface depends on the partial pressure difference only, but not on the initial value. Equation (2.9) essentially suggests the same. At the same time, carefully conducted experimental results have shown that the adsorption and desorption process can show very anomalous behaviour at high initial moisture contents (Christensen and Kelsey 1959). The transient moisture sorption in wood at high relative humidity is governed also by non-Fickian processes which are associated with a slow sorption in the cell walls. It is also believed that this slow sorption of moisture into the cell wall is due to swelling pressure and its relaxation depends on the creation of sorption sites by molecular bond breaking and formation of micropores. Therefore, the sorption process is governed by two simultaneous different phenomena: the classical diffusion in the cavities and a moisture transfer into the cell walls.

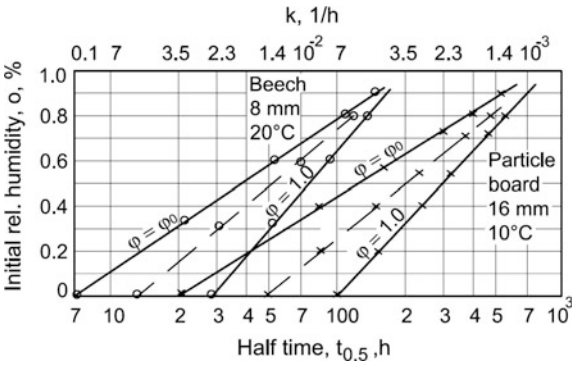

Fig. 2.6 Oblique triangle diagram representing interrelation between half-time and initial relative humidity for Beech and particle board

Instead of seeking a high theory for the above anomalous sorption process, it seems to be more reliable to generalise the existing experimental results. In this case, we will use the half-time with Eqs. (2.11) and (2.12) and Fig. 2.5. Using the detailed measurement results with particle board and several wood species (Béldi and Szabó 1979; Béldi and Bálint 1984, 1986), an "oblique triangle" diagram was found and elaborated containing all measurement results for a given wood species, sample thickness and temperature. Figure 2.6 shows the plot of experimental results on semi-logarithmic scale giving straight lines which refers to the exponential nature of the process. The left line refers to an unsteady step change in relative humidity from φ_0 to φ_1 at which φ_1 only slightly differs from the initial value φ_0. The right line ($\varphi_1 = 1.0$) means the use of saturated air at the given temperature. The broken line gives approximate middle values for $\varphi_1 = (1 + \varphi_0)/2$.

It is interesting to note that the diagrams for Beech and particle board do not differ much from each other if the difference in thicknesses is taken into account.

The effect of thickness is theoretically described by a quadratic function. In practice, however, smaller exponents were systematically found, generally in the range of 1.5 and 1.6. Therefore, half-times for different thicknesses may be corrected in the following manner:

$$\frac{(t_{0.5})_1}{(t_{0.5})_2} = \frac{L_1^{1.55}}{L_2^{1.55}}$$

There is a definite difference in half-time for adsorption and desorption. As a rule of thumb, the half-time of adsorption is 25–30 % longer than desorption for the same wood species.

The change in temperature (ϑ) influences also the rate of moisture exchange. Because the temperature variation is generally not large, a simple linear conversion may be applied:

$$\frac{(t_{0.5})_1}{(t_{0.5})_2} = \frac{\vartheta_2}{\vartheta_1}$$

The kind of wood species certainly influences the rate of moisture exchange due to their differences in their internal structures. If reliable measurement results for a given species are not available, half-times taken from Fig. 2.6 may be used as a first approximation, naturally with the necessary conversions.

Moisture exchange with humid air can be considerably reduced using different surface treatments. A more demanding treatment is the soaking of wood in an appropriate monomer (e.g. diisocyanate) using vacuum impregnation (Németh 1986) or the WAN-drying and soaking method (Burmester and Olsen 1971). The latter method allows more uptake of monomers; therefore, the wood considerably decreases its hygroscopicity. The reason for reduction of sorption is the penetration of monomers into the cell wall shifting the sorption isotherm towards lower equilibrium moisture contents as shown in Fig. 2.7 (Burmester and Olsen 1971).The half-times also increase around 40 % compared to untreated wood. The reduction in hygroscopicity by impregnation also increases the dimensional stability of wood. The reduction in shrinkage in alternating temperatures may be as high as 50 %.

A more common and cheaper treatment of wood surfaces is painting them with different finishing materials.

Because moisture plays an important role in the photodegradation of wood, it is important to protect the wood surface from excess moisture uptake, especially outdoors. The moisture exchange through coatings will mainly be influenced by the permeability of the coating material to water vapour. The colour of a coating may significantly affect the reflection properties of the surface and thus on the surface temperature. The surface temperature of outdoor wood structures is governed by solar irradiation and to a lesser extent by convective heat transfer. The reflection of painted surfaces can change between the extremes from 5 % (black) to 85 % (white), and this highly affects the instantaneous surface temperature. A higher

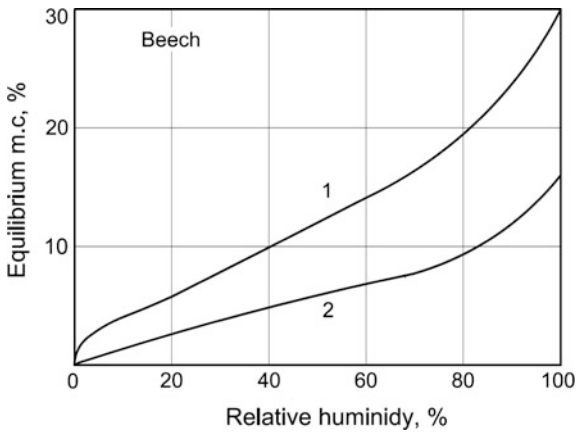

Fig. 2.7 Desorption isotherm of beech wood untreated (*1*) and soaked with diisocyanate (*2*)

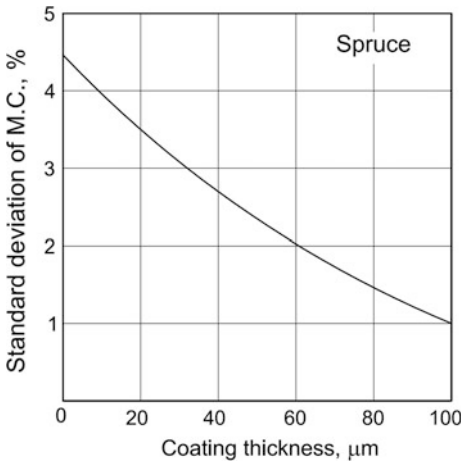

Fig. 2.8 Standard deviation of moisture content variation in a window frame as a function of coating thickness

temperature generates a higher vapour pressure inside the wood, causing a more intensive moisture exchange. This was verified experimentally as a black-painted window frame had less moisture content variations than a white-painted one (Sell 1985).

The permeability of coating generally depends on its thickness. Figure 2.8 shows the standard deviation of moisture content variation in a window frame exposed to weather as a function of paint thickness (Sell 1985).

2.4.2 Fluid Flow in Wood Materials, Infiltration

Wood is a porous material (because of its capillaries) always containing some water. Due to its hygroscopicity and permeability, wood has the ability to adsorb, conduct and lose water depending on circumstances.

The movement of moisture in wood can be described by diffusion-type equations. In many cases, the most common approach is to use the gradient of moisture content as a driving force in the form:

$$q = -D\frac{\partial W}{\partial x} \tag{2.13}$$

where D is the diffusion coefficient generally depending on the moisture content and W is the volumetric moisture content. The volumetric moisture content is related to the most commonly used moisture content by weight (X, dry basis) in the form given in the previous section.

In the soil science, the water potential is expressed in terms of energy per unit mass, J/kg, or in terms of unit volume ($J/m^3 = N/m^2$) giving pressure or pressure height.

The widely used pF number is the logarithm of the pressure height expressed in cm (1000 cm = 1 bar).

Using the water potential ψ (cm), Eq. (2.13) will be modified in the following way:

$$q = -D\frac{\partial W}{\partial \psi}\frac{\partial \psi}{\partial x} = -K(W)\frac{\partial \psi}{\partial x} \tag{2.14}$$

where

$$K(W) = D\frac{\partial W}{\partial \psi}$$

and it means the water conductivity coefficient (cm/h).

The water potential concept may equally be used for both bound and free water, and therefore, the gradient of water potential serves as the driving force within the whole range of moisture content.

The water potential as a function of moisture content is fundamentally bound to the pore size distribution in the wood material. The evaluation of the water potential curve occurs in the lower pressure range (at higher moisture contents) using the tension plate and pressure plate methods. The upper part of the water potential curve corresponds to the sorption isotherm because the relative humidity of air (φ) can be converted into tension:

$$\psi = \frac{RT}{m_w}\ln\varphi \quad \text{kJ/kg}$$

where

R is the universal gas constant (8.314 kJ/kmol K) and

m_w is the mass of the water molecule (18 kg/kmol).

Taking 50 % relative humidity, it corresponds to nearly 100 kJ/kg water potential and 1000 bar tension!

The evaluation of the water potential curve is a time-consuming procedure, and therefore, only a few studies on wood can be mentioned (Cloutier and Fortin 1991, 1993). Figure 2.9 shows the pore size distribution for a Pinewood as a function of pore radii (Sitkei 1994a). The corresponding theoretical water potential values are also given. The water potential curve of a Pinewood as a function of volumetric moisture content is given in Fig. 2.10.

It is interesting to note that the sorption isotherms for wheat corn and wood are very close to each other. Therefore, the upper part of the water potential curve is almost the same for both materials. The lower part of the curve highly dependent on porosity of the material, and therefore, different wood species, concerning the lower part of the water potential curve, may considerably differ from each other.

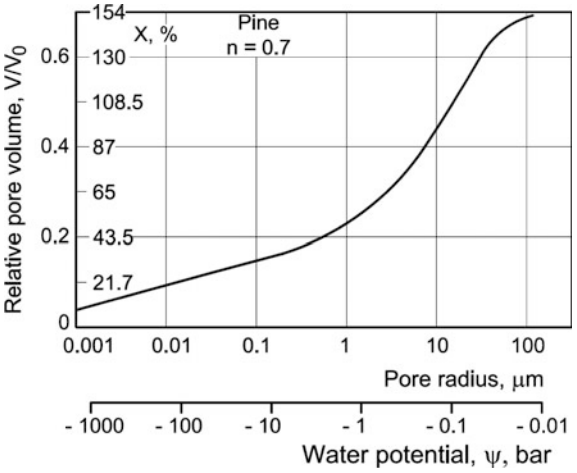

Fig. 2.9 Relative pore volume of a Pinewood as a function of pore radii. The corresponding theoretical water potential values are also given

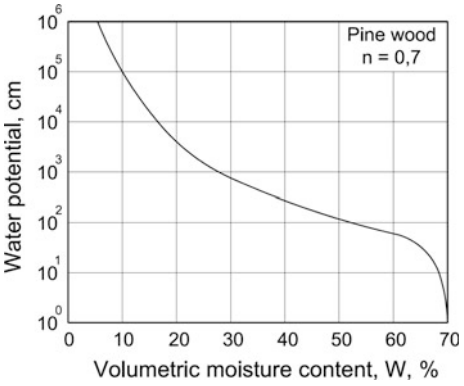

Fig. 2.10 Water potential of Pinewood as a function of volumetric moisture content

There are several mathematical expressions to describe the water potential curve. The exponential function is suitable for this purpose, except for very low tensions, in the following form:

$$\psi = -A\exp(-bW^n) \tag{2.15}$$

and

$$\frac{\partial W}{\partial \psi} = \frac{W^{1-n}}{\psi(W)nb} \tag{2.15a}$$

The exponent n has values around 0.1.

An other possible equation utilises the moisture ratio (MR) as follows (van Genuchten 1980):

$$\mathrm{MR} = \frac{W - W_\mathrm{r}}{W_\mathrm{s} - W_\mathrm{r}} = [1 + (\alpha\psi)^n]^{-m} \tag{2.16}$$

so that the exponent m and n have the following interrelation:

$$m = 1 - \frac{1}{n}$$

The residual water content W_r is taken as 0.02–0.03.

Performing the derivation of Eq. (2.16) yields the following:

$$\frac{\partial W}{\partial \psi} = \frac{(W_\mathrm{s} - W_\mathrm{r}) mn\alpha^n \psi^{n-1}}{[1 + (\alpha\psi)^n]^{m+1}}$$

If the value of W_r is small compared to W_s and so it can be neglected, a simpler expression may be used:

$$\frac{\partial W}{\partial \psi} = \frac{W_\mathrm{s} mn}{(\alpha\psi)^{mn}}$$

Concerning Fig. 2.10, the constants in Eq. (2.16) have the following values:

α = 0.03, m = 0.2126 and n = 1.27.

In order to calculate fluid flow, the conduction properties of the materials are needed. According to Eqs. (2.13) and (2.14), the conduction properties are the diffusion coefficient D and the water conductivity K(W).

The diffusion coefficient of different wood species depends on the pore size distribution of wood, the moisture content and the temperature. Measurement results for Pine and Beech are shown in Fig. 2.11 (Шубин 1965). The diffusion

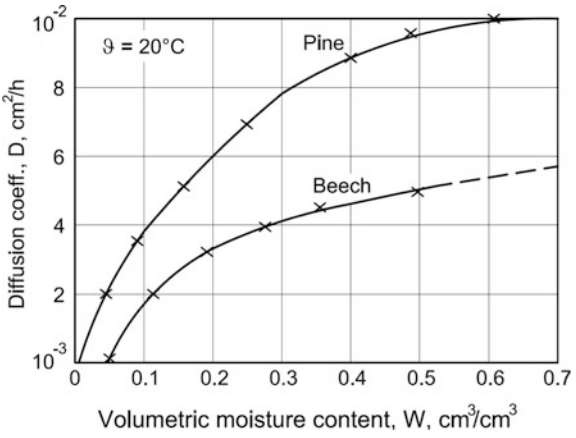

Fig. 2.11 The diffusion coefficients of Pine and Beech as function of volumetric moisture content

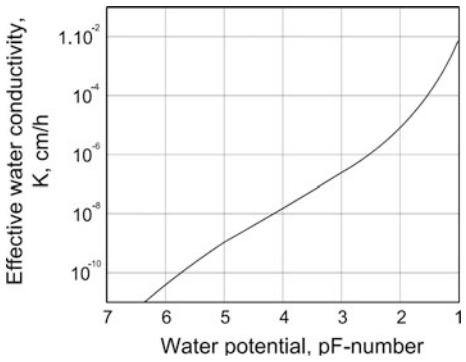

Fig. 2.12 Effective water conductivity in Pinewood as a function of water potential (tension)

coefficient increases with higher moisture contents and higher total pore volumes. An increase in temperature increases the diffusion coefficient considerably.

Knowing the diffusion coefficient and the derivative of the water potential, the water conductivity K(W) can be evaluated. Using the water potential of Pinewood in Fig. 2.10, the water conductivity as a function of the water potential is given in Fig. 2.12.

The water potential is fundamentally related to the pore size distribution of the given material. Some 50 years ago it was already demonstrated that the heat conduction coefficient for quite different soils could have been uniquely described as a function of moisture potential (Nakshabandi and Kohnke 1965). It may be supposed that the hydraulic conductivity K(W), as a first approximation, may have also general validity as a function of water potential, at least for the range $W < 50$ % (or $X < 100$ %). Depending on the overall porosity of the wood, differences may occur in the vicinity of the saturated state (K_s).

Putting water onto a wood surface, an infiltration process takes place. Water enters into the wood in response to the concentration or pressure difference, and the rate of entry is given by Eq. (2.13) or (2.14). These seemingly simple equations cannot be used because the gradients vary as a function of time and are not known. In order to examine the main characteristics of the infiltration process in time and space, the governing differential equation is needed.

For infiltration vertically downwards, the differential equation is written as follows:

$$\frac{\partial W}{\partial t} = \frac{\partial}{\partial y}\left(D\frac{\partial W}{\partial y}\right) \tag{2.17}$$

where y is the vertical coordinate, positive downwards from the surface. The problem described by Eq. (2.17) is that of diffusion of water into a wood column of infinite linear extent (semi-infinite body). Before starting the infiltration, the wood has initial moisture content W_{in}, and after starting the infiltration, the surface will become saturated (W_{s}).

In so far as the diffusion coefficient is moisture dependent (see Fig. 2.11), Eq. (2.17) can only be solved numerically. Taking a constant average diffusion coefficient for simplicity, however, Eq. (2.17) has analytical solution in the following form (Carslaw and Jäger 1959):

$$\frac{W - W_{\text{in}}}{W_{\text{s}} - W_{\text{in}}} = erfc\left(\frac{y}{\sqrt{4Dt}}\right) \tag{2.18}$$

An inspection of Eq. (2.18) reveals that the solution is a function of $y/\sqrt{t}$. Such a combination of the two independent variables, well known in the diffusion theory, has some consequences:

- the propagation distance of the diffusing material specified by a given moisture content is proportional to $\sqrt{t}$;
- a given moisture content at any distance y from the boundary surface requires a time inversely proportional to D and proportional to y^2.

To demonstrate the propagation of moisture in a solid wood, calculations were performed (Fig. 2.13) showing the instantaneous water content profiles during infiltration in a Pinewood for different elapsed times.

The initial tangent of each curve gives the moisture gradient $\partial W/\partial y$ which would have been required to use Eq. (2.13).

The moisture gradient decreases with the elapsed time, and this means that the infiltration rate also decreases with time.

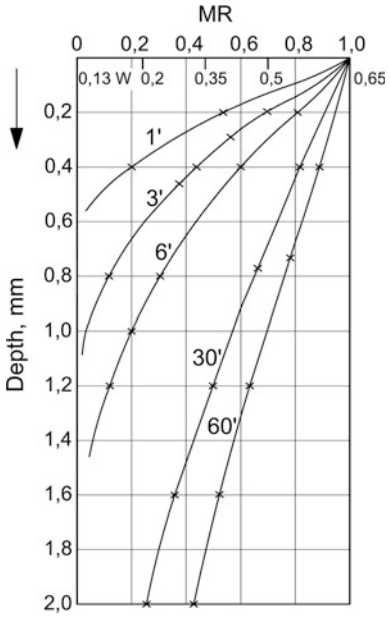

Fig. 2.13 Water content profiles during infiltration in Pinewood for different times. D = 0.03 cm^2/h, W_{in} = 0.13, $W_{\text{s}} - W_{\text{in}}$ = 0.52

The infiltration rate on the surface is given by the following equation:

$$q = (W_s - W_{in})\sqrt{\frac{D}{\pi t}} \quad \text{cm/h} \tag{2.19}$$

while the integration of this equation gives the cumulated infiltration for a given time:

$$Q = \frac{2}{\sqrt{\pi}}(W_s - W_{in})\sqrt{Dt} \tag{2.20}$$

Figure 2.14 shows the variation of surface flux and the cumulated infiltration of water in Pinewood as a function of elapsed time. The graph shows that a 1-mm layer of water requires *I* hour of infiltration time with the given diffusion coefficient.

Example: After 6-min elapsed time, the moisture gradient from Fig. 2.13 is $\Delta W/\Delta y = 0.52/0.1 = 5.2$ 1/cm and, using Eq. (2.13), $q = 0.03 \times 5.2 = 0.156$ cm/h = 1.56 mm/h. The exact value is 1.6 mm/h (see Fig. 2.14). If we would use Eq. (2.14), then we rewrite it into the following form:

$$q = K(W)\frac{\partial \psi}{\partial y} = K(W)\frac{\partial \psi}{\partial W}\frac{\partial W}{\partial y}$$

Keeping in mind that $W_{in} = 0.13$ corresponds to pF = 4.6 (see Fig. 2.10), therefore, we have

$$q = 3 \times 10^{-9}\frac{1}{10^{-7}}\frac{0.52}{0.1} = 0.156 \quad \text{cm/h}$$

which is the same result as obtained with Eq. (2.13).

From the above example, we conclude that the use of moisture gradient with Eq. (2.13) is simpler. But the use of moisture gradient as a driving force has the restriction that the material is homogeneous having the same water retention relationship in the entire space. It is well known in the practice that in a single stem, different moisture contents are in long-term equilibrium in the sap- and heartwood.

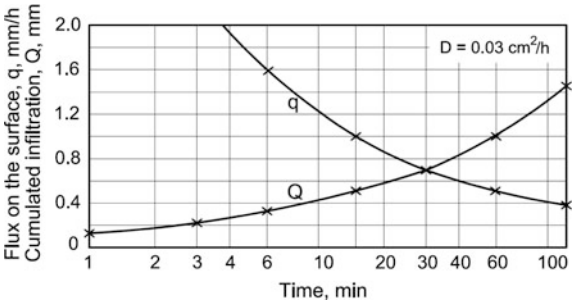

Fig. 2.14 Cumulated infiltration *Q* and water flux on the surface of Pinewood as a function of time

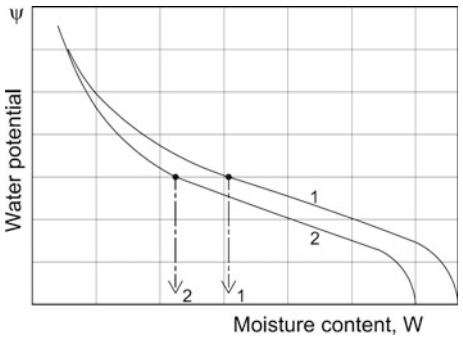

Fig. 2.15 Equilibrium of moisture in two different materials at a given moisture tension

The moisture gradient theory would say that this is simply impossible! The sap- and heartwoods have, however, different water retention properties (water potential curve), and using the water potential concept, equilibrium is possible at the same tension, but not at the same moisture content (see Fig. 2.15). It is obvious that the moisture gradient is not a true driving force in physical sense. At the same time, the space derivative of the water potential (energy) produces a force, thus corresponding to a real driving force. A further advantage is that the gradient in water potential can be used in the whole range of moisture contents.

In the possession of experimental results, and using Eq. (2.20), the average diffusion coefficient can simply and easily be estimated.

2.4.3 Surface Tension and Wetting Properties of Wood

At the boundary of a free liquid surface, the molecular forces are unbalanced and these inwardly directed forces create a new surface with *surface tension*. The molecules on the surface have greater potential energy than those in the interior, and the difference is the *free surface energy* of the liquid per unit area. The surface tension on the interface area between two liquids may equivalently be defined either through force or through energy. Surface tension is defined as force per unit length or as energy per unit area change. These two definitions are equivalent, but when referring to energy per unit of area, it is used the term "surface free energy" which is a more general term in the sense that it applies also to solid materials and not only liquids.

The surface tension is always related to two neighbouring media, i.e. liquid–air (γ_{LA}), solid–liquid (γ_{SL}) and solid–air (γ_{SA}). The surface tension has the dimensions N/m (dyn/cm) or J/m^2 (erg/cm^2), and for liquids, the surface tension may be equated with the free surface energy of the unit area. On solid surfaces, there are disturbing factors such as the work of deformation in the solid surface due to the lateral stretching effect of surface tension. Here, the surface tension and the free surface energy are not the same.

The surface tension acting on the boundary of the liquid tends to minimise the surface, and therefore, a small mass of liquid, where the gravitational force is small compared to the tension forces, will form a spherical convex body. Due to the surface tension, in the interior of the liquid a pressure is developed which is inversely proportional to the radius of the liquid surface (liquid is lying on the plane solid surface):

$$P_1 - P_2 = \gamma_{LA} \frac{1}{R}$$

The effect of gravitational forces may only be neglected if the constant A characterising the ratio of surface tension and gravitational forces:

$$A = \sqrt{\frac{2\gamma_{LA}}{\rho g}} \quad \text{m}$$

is large enough compared to the size of liquid. Using water, $A = 3.8$ mm and in this case the gravitational forces up to 1-mm water thickness may be neglected. Indeed, for $R = 1$ mm, the pressure due to surface tension is 72 N/m^2 and the hydrostatic pressure is only 10 N/m^2.

Surface tension plays important role in the wetting process of wood surfaces. Two different kinds of wetting phenomena of practical interest may occur on wood surfaces:

- the gluing process at which the emulsion of a polymer adhesive first spreads on the solid surface and the measure of its wetting power is the contact angle,, but the joint itself depends on the adhesive work of the polymer system. It is termed as *adhesion wetting*;
- the spreading of liquid on a solid surface which is termed as *spreading wetting*.

The equilibrium of the surface tension of a liquid drop is illustrated in Fig. 2.16. The equilibrium in horizontal direction requires the following relation among the surface tensions (Young equation 1805):

$$\gamma_{LA} \cos \Theta = \gamma_{SA} - \gamma_{SL}$$

or

$$\cos \Theta = \frac{\gamma_{SA} - \gamma_{SL}}{\gamma_{LA}} \tag{2.21}$$

The contact angle may be smaller or larger than 90°, and its value depends on the relative magnitude of the different surface tensions. Therefore, the wetting or non-wetting condition is determined by the solid and liquid together.

The thermodynamic energy of interaction of two surfaces was formulated by Dupré (in 1869) as the work of adhesion:

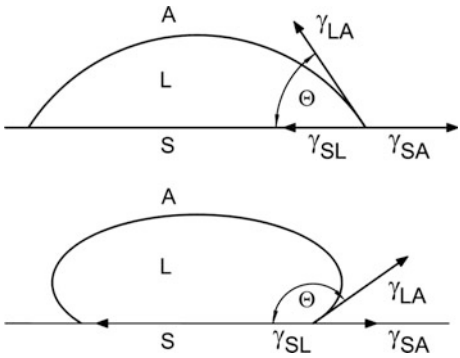

Fig. 2.16 The interfacial tensions between solid (*S*), liquid (*L*) and air (*A*) surfaces if the equilibrium contact angle (Θ) is between $0 < \Theta < 90°$ (*upper*) or between $90° < \Theta < 180°$ (*lower*)

$$-W_a = (\gamma_{SA} - \gamma_{SL}) + \gamma_{LA} \tag{2.22}$$

Similarly, the work of spreading is defined as follows:

$$W_s = (\gamma_{SL} - \gamma_{SA}) + \gamma_{LA} \tag{2.23}$$

From the above two equations, we get the following:

$$W_s - W_a = 2\gamma_{LA}$$

According to the definition, the adhesion work is always negative and the work of spreading is positive.

Combining Eqs. (2.21) and (2.22) yields the following:

$$-W_a = \gamma_{LA}(\cos\Theta + 1) \tag{2.22a}$$

$$W_s = \gamma_{LA}(1 - \cos\Theta) \tag{2.23a}$$

which are illustrated in Fig. 2.17. In theory, the contact angle $\Theta°$ may vary between zero and 180°, but in the practice, contact angles over 120° hardly ever occur. In Eqs. (2.22) and (2.23), the difference of two surface tensions, $\gamma_{SA} - \gamma_{SL}$, appears, and the measurement of the contact angle does not allow us to calculate the γ_{SA} and γ_{SL} surface tensions separately. An approximate estimation is, however, possible if we accept the validity of Antonov's rule.

Application of Antonov's rule to solid/liquid surface is based on the assumption that the interfacial tension (similar to that of between two liquids) is the difference between the surface tensions of the contacting solid and liquid. With this assumption

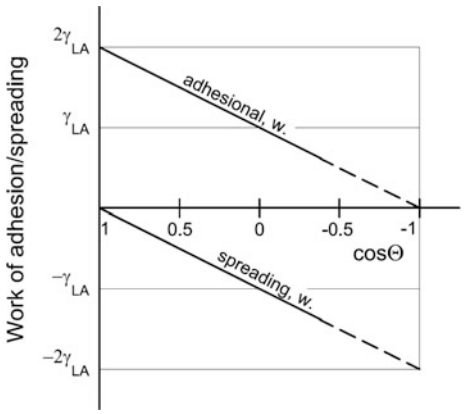

Fig. 2.17 Work of adhesion and spreading as a function of contact angle

$$\gamma_{SL} = \gamma_{LA} - \gamma_{SA}$$

and using Eq. (2.21) yields

$$\cos\Theta = \frac{2\gamma_{SA}}{\gamma_{LA}} - 1$$

and

$$\gamma_{SA} = \frac{\gamma_{LA}}{2}(\cos\Theta + 1) \tag{2.24}$$

Due to the application of Antonov's rule, the surface energy of adhesion and spreading may be expressed in the following simplified form:

$$-W_a + W_s = 2\gamma_{LA}$$

$$-W_a = 2(\gamma_{LA} - \gamma_{SL}) = 2\gamma_{SA} \tag{2.22b}$$

$$W_s = 2\gamma_{SL} \tag{2.23b}$$

Concerning wood surfaces and using water with γ_{LA} = 72 dyn/cm, the measured contact angles vary around an average of 75° (initial value), in this case γ_{SA} = 45 dyn/cm, γ_{SL} = 26 dyn/cm, and the surface energy for spreading wetting is 53 erg/cm^2 in good agreement with measured values. The surface energy for adhesion is 91 erg/cm^2. If the contact angles vary between 70° and 80°, the surface energy for spreading varies between 47.5 and 59.5 erg/cm^2.

In order to give a general overview, different measurement results were summarised and depicted in Fig. 2.18. The contact angle range of initial values for most

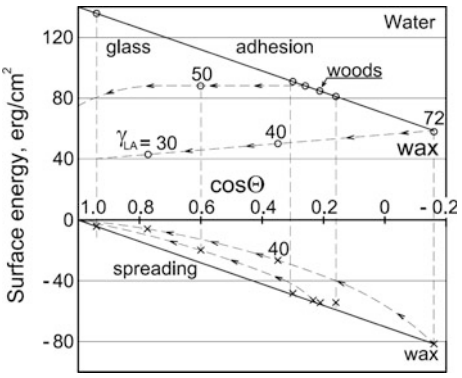

Fig. 2.18 Surface energies as a function of contact angle and surface tension

wood species is between 70° and 80°. After applying the liquid onto the surface, the contact angle rapidly decreases, due to infiltration and evaporation. Using an oil or wax surface treatment, the contact angle increases to near 90° and 102°–108°, respectively. The glass surface is given only to show the other extreme of the possible variations.

An interesting question is to substitute a liquid of lower surface tension instead of water (e.g. for petroleum γ_{LA} = 24 dyn/cm). The contact angle strongly decreases, but the work of adhesion remains more or less constant. The work of spreading decreases, however, considerably as indicated in Fig. 2.18 depending on the starting point.

Due to the complexity of the surface–liquid interaction, especially for wood surfaces, attempts were made to determine the expected various components of the total work of adhesion or spreading. It was claimed that the validity of Young's equation is limited to chemically homogeneous flat solid surface which does not adsorb liquid. The wood–liquid interaction is rather complicated because the surface of wood is rough, heterogeneous, porous, hydrophilic and anisotropic. That is why the equilibrium conditions of Young's equation are not exactly fulfilled for wood. The contact angle constantly changes over time, and this change implies problems in determining equilibrium. Liptakova and Kudela (1994) recommended: the equilibrium contact angle is defined as the contact angle measured in the moment of the change of the advancing contact angle to the receding contact angle.

The work of adhesion describes how the intermolecular forces contribute to adhesion between condensed phases. The total work of adhesion in an interfacial interaction between solids and liquids can be divided into two parts: the Lifshitz–van der Waals (LW) and the Lewis acid–base (AB) interactions (Fowkes 1983):

$$\gamma_a = \gamma^{LW} + \gamma^{AB} \tag{2.25}$$

The Lifshitz–van der Waals component can be calculated using nonpolar liquid as follows:

$$\gamma^{LW} = 0.25\gamma_{LA}(1 + \cos\Theta)^2 \tag{2.26}$$

The acid–base interactions include two different and independently variable properties expressed in the electron-acceptor (γ^+) and the electron-donor (γ^-) surface free energy parameters. This expansion leads to the "van Oss-Chaudhury-Good" model (Van Oss et al. 1987; Good 1993). The electron-acceptor (γ^+) and the electron-donor (γ^-) surface free energy parameters of wood can be calculated by applying polar liquids with known electron-acceptor and electron-donor parameters. The Young-Good-Girifalco-Fowkes equation can be applied using the measured contact angle data:

$$0.5(1 + \cos\Theta)\gamma_L = \sqrt{\gamma_S^{LW}\gamma_L^{LW}} + \sqrt{\gamma_S^+\gamma_L^-} + \sqrt{\gamma_S^-\gamma_L^+} \tag{2.27}$$

This is the geometric-mean equation, and the harmonic mean equation can also be used (Gardner 1996). The Lewis acid–base component can be calculated as follows using the acceptor–donor components:

$$\gamma^{AB} = 2\sqrt{\gamma^+\gamma^-} \tag{2.28}$$

The acid–base approach delivers the most detailed information about the surface chemistry, in giving values for acid and base components in addition to polar and disperse components of surface free energy, which is especially valuable with a chemically heterogeneous material like wood. However, it has to be stated that the results depend on the choice of test liquid. It is strongly recommended to work with minimum of three test liquids (Gindl et al. 2001).

The contact angle and surface free energy data of wood could be applied to predict the wettability of wood with different coatings and glues. The methods used to determine the surface energies of wood are generally based on static contact angle measurement of sessile drops or dynamic contact angle measurement [with Wilhelmy plate method (Gardner et al. 1991)] using the Young's equation (2.21).

Wood is a material with low free surface energy. This energy is additive. The free surface energy of wood is primarily composed of the Lifshitz–van der Waals component. Most of wood species show significant base component but only a very low acidic component. Table 2.1 presents the surface free energy parameters of some hardwood species (Gardner 1996). It is clearly visible that most of the total wood surface energy is the Lifshitz–van der Waals component. The acid–base component of the surface energy of wood is low. The base component is high enough, but the acidic component is small, almost zero. That is why the total acid–base component is small (see Eq. 2.28).

Table 2.1 Surface free energy parameters of some wood species (Gardner 1996)

Species	γ^{LW} (mJ/m^2)	γ^+ (mJ/m^2)	γ^- (mJ/m^2)	γ^{AB} (mJ/m^2)	W_s (mJ/m^2)
Ash (*Fraxinis Americana* L.)	42.63	0.001	67.35	0.52	43.15
Cherry (*Prunus serotina* Ehrh.)	47.46	0.42	28	6.84	54.3
Maple (*Acer saccharum* Marsh.)	45.48	0.46	33.19	7.85	53.3
Red oak (*Quercus rubra* L.)	39.67	0.46	37.74	8.33	48
White oak (*Quercus* spp.)	34.02	0.39	22.8	5.98	40
Walnut (*Juglans nigra* L.)	37.92	0.09	58.93	4.63	42.55

The surface energy of wood can be changed by surface modifications. Steaming is a proper treatment to modify the value of the surface energy. For this purpose, Black locust (*Robinia pseudoacacia* L.), Oak (*Quercus robur* L.), Merbau (*Intsia bijuga*) and Sapupira (*Hymenolobium petraeum*) samples were steamed at 92–122 °C (Varga and van der See 2008). During long-term, high-temperature steaming, Black locust and Merbau surfaces became strongly hydrophobic. However, contact angle between Oak and water was reduced by all of the applied steaming parameters (Fig. 2.19), which ensures a better wettability of the wood surface. Figure 2.19 shows that the value of the contact angle is decreasing rapidly right after the liquid contacts to the wood. After 2–3 s, the rapid decrease stopped and the contact angle decreased slowly.

The surface free energy of Black locust and Merbau slightly decreased during hydrothermal treatment, but there was no obvious relationship between the process parameters and the final energy value. The calculated energy values of treated Oak surfaces were higher than those of untreated samples. The surface free energy of Sapupira decreased slightly at low steaming temperatures. After long treatment at 122 °C, the surface energy of Sapupira increased significantly (Fig. 2.20). It can be concluded that the amount of surface free energy modified by steaming highly depends on the wood species.

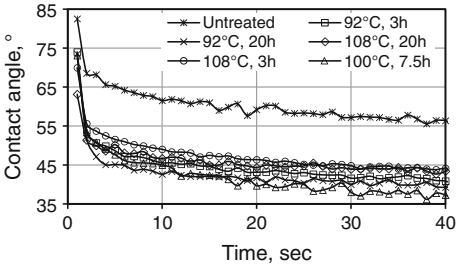

Fig. 2.19 Contact angle variation of steam-treated and untreated Oak as a function of elapsed time. *Test liquid* water (Varga and van der See 2008)

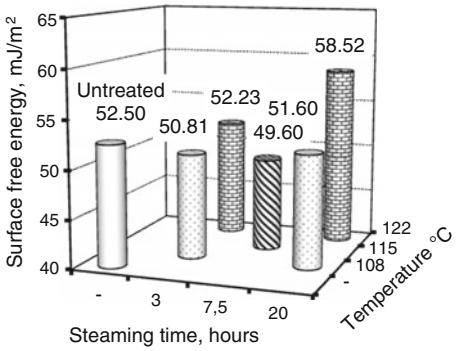

Fig. 2.20 Surface free energy of untreated and steam-treated Sapupira samples (Varga and van der See 2008)

Summarising the existing experimental results, we concluded that the interfacial interaction of wood surfaces with liquids has not been fully clarified in detail yet. We do not have a reliable relationship connecting the many variables derived from the pertinent properties of wood and liquids. Therefore, we need to seek simpler methods to characterise the spreading of a liquid on a solid surface, especially for practical purposes.

The spreading of liquids on a solid surface is the result of combined contribution of forces acting on the liquid. The surface tension of the liquid exerts a force perpendicular to the surface, and the components of this force in vertical and horizontal directions are highly dependent on the contact angle as it is shown in Fig. 2.21. For small contact angles, the horizontal components are also small enabling the horizontal spreading of the liquid. As a consequence, the thickness of the liquid layer on the solid surface will also be small. On the contrary, large horizontal forces resist spreading a liquid.

Measurements were conducted on various surfaces to determine the fluid thickness as a simple measure of spreading. Glass and variously treated wood surfaces were used, and water was applied onto the surface in different amounts. Measuring the mass and the diameter of the spreading liquid, the average thickness can easily be calculated. The results are depicted in Fig. 2.22. On the glass surface, thicknesses around 0.3 mm were measured, and on planed wood surfaces 0.7–0.8 mm were obtained, while on wax-treated surfaces the thickness was amounted to 1.9–2.0 mm. The results are in full agreement with contact angle measurements on paraffin, wax and glass giving extreme high and low contact angles, respectively (Garrett 1964).

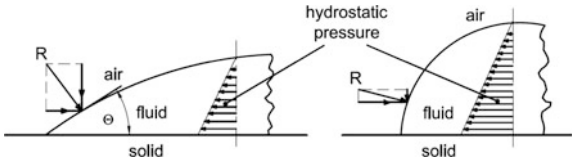

Fig. 2.21 Forces on a spreading fluid with different contact angles

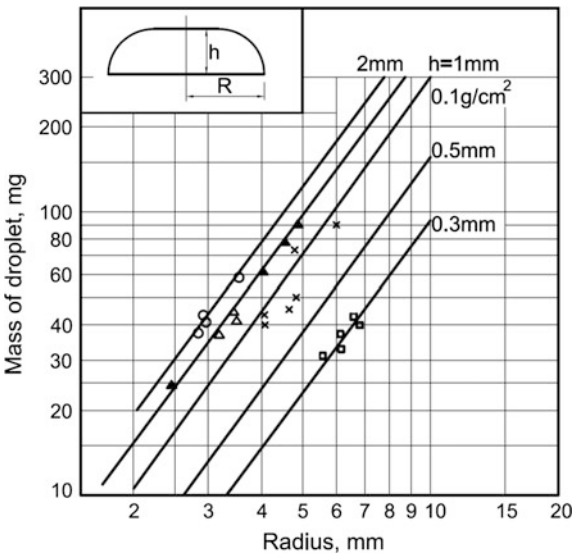

Fig. 2.22 Thickness evaluation on various surfaces. (□—glass; ×—planed wood; Δ—oil-treated wood; o—wax-treated wood)

A further proof for a possible interrelation between thickness and contact angle is given in Fig. 2.23, which represents the measured data as a function of cos Θ. The obtained relationship is a straight line (with good approximation) which corresponds to the theoretical curve according to Eq. (2.23).

Practical experience shows that thicker paint does not spread as well as thin paints, which is mainly due to the difference in their viscosities. At the same time, the effect of viscosity is never treated in spreading and contact angle problems. To study the possible influence of viscosity, measurements were carried out on the same surfaces as formerly, but using low fat (10 %) milk cream with a surface tension of 48 dyn/cm (65 % compared to water) and dynamic viscosity of 2.0 Ns/m^2 which is twice as high as that of water.

If viscosity had no influence on spreading, then a smaller surface tension should give better spreading. On a glass surface, the average thickness was 0.42 mm

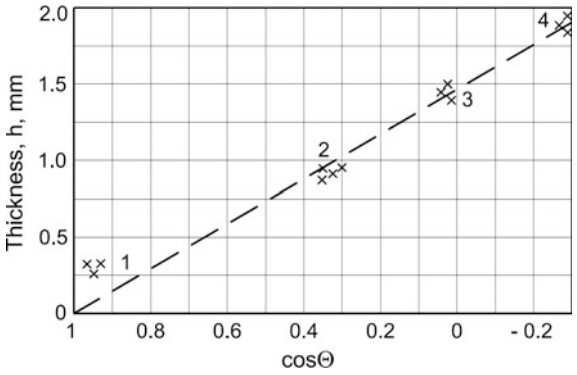

Fig. 2.23 Relationship between the average layer thickness and contact angle. *1*—glass; *2*—planed wood; *3*—oil-treated wood; *4*—wax-treated wood

(0.3 mm for water), and on planed wood surfaces, it was 1.0 mm (0.7–0.8 mm for water). On treated wood surfaces, the thickness was much the same as for water. From these results, we concluded that spreading is influenced by the viscosity to a given extent. Surface tension and viscosity have no definite connection with each other. For example, heating water from 20 to 100 °C, the viscosity decreases to 30 % and the surface tension only to 80 % compared to their initial values.

The following principles should be used in the adhesive joint process: A low surface tension γ_{LA} of the adhesive is preferable when applying adhesive onto a surface. The spreading is enhanced with high surface tension γ_{SA} and a low value of γ_{SL}. The assembly of the joint pairs, keeping in mind Eq. (2.22) for work of adhesion, will be enhanced by high values of γ_{SA} and γ_{LA}, and low value of γ_{SL}.

The optimum energy conditions for the overall adhesive joint process may be summarised as follows. The solid surface tension γ_{SA} should be as high as possible. The surface–liquid tension γ_{SL} should be as low as possible. Latter is equal to the statement that the adherend would possess affinity or interaction with the adherent. If we remember now the simplified Eqs. (2.22b) and (2.23b), we see that the energy of adhesion mostly depends even on γ_{SA} and the energy of spreading depends on γ_{SL}. The optimum surface tension of adhesive γ_{LA} may depend on different requirements. A good spreading requires lower values, while high joint strength needs higher surface tension. Furthermore, other factors such as the use of solvents and additives may influence or limit the optimum choice of surface tension γ_{LA}.

2.5 Photodegradation of Wood

2.5.1 Measurement Techniques for Studying Wood Degradation

The basic interaction during light and material contact is the interaction between one photon and one electron. The result of the interaction is highly determined by the energy (E) of the photon. This energy is in proportion to the frequency (v) of the proton.

$$E = hv \tag{2.29}$$

where h is the Planck constant ($h = 6.626 \times 10^{-34}$ Js). The UV photons of sunlight have enough high energy to break many of bonds in chemical components of wood. These alterations change the chemical and physical properties of the surface layer. These changes can be monitored by chemical and physical measurement techniques.

The most commonly used measurement techniques are the colour measurement, the infrared (IR) spectrum determination, and the roughness measurement. These tree techniques are discussed in this chapter. The electron microscopy is also a proper method in some special cases, and further chemical methods are available to clarify the details.

The degradation of wood appears mostly on the surface. The most sensitive surface parameter is the colour. The colour is mainly determined by the extractive content of wood. The colour change is created by the alteration of conjugated double-bond chemical systems. These systems are present originally in the lignin and in the extractives of wood. The degradation can split the chemical bonds followed by the oxidation of the radicals that were created. These processes can also create conjugated double-bond chemical systems. Typical example is the thermal degradation of hemicelluloses producing brown colour.

The objective colour measurement requires some rules. The colour of an object is highly determined by the emission spectra of the applied light source. The most preferable light source is the sun. The emission spectrum of the sun is changing slightly. That is why the International Commission on Illumination (CIE) defined the D_{65} standard illuminant. The D_{65} is intended to represent average daylight and has a correlated colour temperature of approximately 6500 K. The colour slightly depends on the direction from which it is observed. That is why the angle between illumination and observation must be the same for comparison. The most common angle is 10° for colour measurement of wood. The colour appearance of wood is usually inhomogeneous. Large test-window application is recommended for getting the average colour of the sample. There are available many systems to evaluate the colour and colour change of wood. The techniques of colour measurement for characterisation of photodegradation are described in Sects. 3.2 and 3.3.

The mostly used system is the CIELAB, three-dimensional rectangular coordinate system. This system is standardised in most countries. The L^*, a^* and b^* are the Descartes coordinates of the colour space in the CIELAB system (see more details in Sect. 3.2). The a^* and b^* coordinates are useful parameters to follow the chemical changes separately. However, for monitoring the visible colour change, the b^*/a^* quotient is the advantageous parameter.

The total colour change (ΔE^*), as a single number, is also often used. It represents the distance between two colour dots in the 3-dimensional colour space. It is usually applied to represent the colour change by one value. The ΔE^* is, however, not always reliable by itself. In some cases, ΔE^* values do not match to the visual observations. The individual colour coordinates (L^*, a^*, b^*, C^* and h) are more suitable to monitor the colour change caused by the photodegradation than the total colour change (see more information in Sect. 2.6.3).

Several papers try to present correlation between the total colour change and individual chemical changes. The real problem is that these researchers believe that they have found real correlation. However, total colour change is an extremely complex parameter since it is determined by the alterations of all three colour coordinates. Nevertheless, these colour coordinates are calculated by extremely complicated equations applying the tristimulus values. Furthermore, a^* and b^* encompass two independent tristimulus values calculated by integrals based on the reflection spectrum. (These integrals are not presented in this work.) The reflection spectrum carries information on the chemical changes through the absorption change of visible light. It is clear that the absorption change values undergo several mathematical manipulations to obtain the total colour change. As wood is a

chemically complex material, absorption changes are never created by a single chemical change. Thus, the total colour change is a result of extremely mixed individual absorption changes.

Finding correlation between the total colour change and increase of the IR absorption of the carbonyl groups during photodegradation is a common mistake. Nevertheless, authors can be happy because they are misled by the high value of the calculated coefficient of determination (R^2). Unfortunately, it is not well known that the high value of R^2 does not necessarily mean that the correlation exists. It only indicates how strong it is—providing the correlation exists at all. The origin of the mistake is that there is similar exponential time dependence of the total colour change and that of the absorption increase for carbonyl groups. However, it is not sufficient condition. A true correlation requires that the two phenomena are also physically connected to each other.

This artefact can be visualised easily. If someone measures the velocity of free fall body for some seconds and measures the same of an accelerating car and examines the correlation between the measured data, will be surprised. Calculating the R^2 value, it will be almost one unit. Hopefully, no one think that the free fall is determined by the accelerating car.

The change of surface roughness (see in Sect. 4.4 for details) is also a proper indicator to monitor the degradation of the surface. The roughness change is not as sensitive as the colour change, especially in case of short-term degradation.

The optical roughness measurement methods are usually more susceptible than the direct contact methods, but these are highly sensitive to the size of the measured area. A newly developed method utilises the fact that the light scattering depends on roughness. The increasing roughness produces greater scattering. The diffuse reflection spectrum of a sample integrates the absorption and the scattering as well. The absorption is characteristically wavelength dependent, while the scattering is slightly wavelength dependent and this correlation is close to linear. Looking at the reflection spectrum, the negative peaks represent the absorption in opposite format and the scattering produces the so-called baseline shift (Fig. 2.24). Quantifying the baseline shift, data can be created which correlates to the roughness. The baseline shift can be easily determined if there are minimum two wavenumbers (or wavelengths) where there are no absorption. The IR spectrum is usually presented as the function of wavenumber instead of wavelength. The wavenumber ($1/\lambda$) represents the number of waves located within one centimetre, and it is determined as follows:

$$\frac{1}{\lambda} = \frac{v}{c} \quad 1/\mathrm{cm} \tag{2.30}$$

where
λ is the wavelength,
v is the frequency and
c is the velocity of the light.

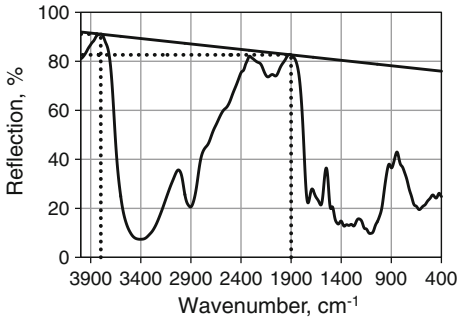

Fig. 2.24 The diffuse reflection infrared spectrum of Spruce wood indicating the baseline shift

Wood has no absorption at 1900 and 3800 cm^{-1} wavenumbers. It would mean the reflection should be 100 % at these places. But the reflection is less than 100 % because of the light scattering; this is called the baseline shift in IR spectroscopy (Fig. 2.24). Calculating the absorption spectrum, these reflection values are lifted up to 100 % (lifting up the whole spectrum) to eliminate the scattering effect. This is the baseline correction, which is regularly used in diffuse reflectance IR spectroscopy. The scattering depends on the roughness of the surface, and therefore, the baseline shift gives information about the surface roughness. Here, the baseline shift is given as the quotient of two reflection intensities at 3800 and 1900 cm^{-1} (Tolvaj et al. 2014a).

$$\text{Baseline shift} = R(3800)/R(1900) \tag{2.31}$$

where $R(3800)$ is the reflection intensity at 3800 cm^{-1} and $R(1900)$ is the same at 1900 cm^{-1}.

The IR reflection spectra of several wood species were recorded. After calculating the baseline shift parameters (2.31), the correlation between roughness and baseline shift was evaluated. The results are presented in Fig. 2.25 for Black locust and Scots pine species. The linear trend lines are parallel and are located close to each other. The high values of the R^2 show good correlation between roughness and baseline shift in all cases. This close correlation suggests that it is possible to

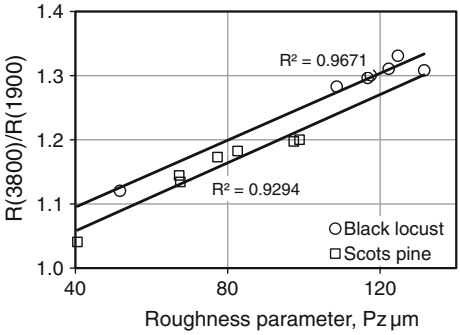

Fig. 2.25 Correlation between baseline shift and roughness of Black locust and Scots pine samples

monitor the roughness alteration effect of photodegradation by measuring the IR diffuse reflection infrared spectra and calculating the baseline shift (Eq. 2.31). It is highly important to note that exactly the same area of the sample must be used for all reflectance measurements; otherwise, the surface inhomogeneity overlaps the roughness change.

The infrared spectrum measurement is a widely used chemical method for determining the changes caused by different treatments. Moreover, it is a useful technique to determine the chemical composition of a material. The IR portion of the electromagnetic spectrum can be divided into three regions: the near-, middle- and far-infrared regions. These are named based on their relation to the visible spectrum. The middle region or analytical region, approximately 4000–400 cm^{-1} (2.5–25 μm), may be used to study the basic vibrations and associated rotational–vibrational structures. This region is the most frequently used for chemical analysis. Infrared spectroscopy utilises the fact that molecules absorb specific frequencies that are characteristic of their structure. The so-called fingerprint region is located within this analytical wavenumber range. Reflectance techniques are used mainly to measure the IR spectrum of wood. It is necessary to measure both the sample and a reference to take the infrared spectrum of a sample. As a usual measurement method, first the reference (background spectrum) must be measured and then replaced by the specimen, and the spectrum of the sample is measured. The proper material for the reference measurement must have bad mirror reflection and excellent diffuse reflectance. Instead of a good metal mirror, a rough surface is recommended with particles as small as possible. KBr powder is often used for this purpose. The KBr powder must be freshly dried, because this powder is strong water absorber. Water has many absorption peaks in the analytical IR region, and therefore, air humidity must be kept constant within the spectrophotometer and the sample compartment. The absorption spectrum is calculated in comparison with the reflected intensity data of the background material and that of the sample. High intensities in the background spectrum generate high intensities in the reflectance spectrum of the sample too. That is why the proper, good quality background spectrum is important for getting high-quality reflectance spectrum. It means that the reflection intensity data are repeatable only if the same material is used to measure the background spectrum (Tolvaj and Mitsui 2011). Fourier-transform infrared (FTIR) spectroscopy is used as a powerful technique nowadays. The equipment produces an interferogram by the interferometer. Then, the interferogram is Fourier-transformed to get the actual spectrum.

Since wood is not transparent for light, therefore, the traditional technique (measuring the light intensity before and after the sample) cannot be used to determine its absorption spectrum. Before creating the powerful FTIR technique, the only possibility was to pulp the non-transparent sample and press a small amount of the sample into KBr pellet. This pellet was transparent for IR light to determine the absorption spectrum of the non-transparent sample. The FTIR technique makes it possible to measure the diffuse reflectance spectrum. The reflectance spectrum contains the absorption and the scattering as well. Using the Kubelka–Munk (K-M) theory, the quotient of the absorption and scattering as the

function of the wavenumber can be calculated. The diffuse reflectance infrared Fourier-transformed (DRIFT) spectrum provides information about a thin surface layer. Using this method, the diffusely reflected light is collected, and the absorption is calculated by the Kubelka–Munk equation.

$$\frac{k}{s} = \frac{(1-R)^2}{2R} \tag{2.32}$$

where k, s and R are the absorption coefficient, the scattering coefficient and the reflectance of a thick enough layer, respectively. Fortunately, the scattering coefficient hardly depends on the wavenumber of the IR light, so the shape of K-M function is similar to the wavenumber dependence of the absorption coefficient. This K-M function is usually used as the IR absorption spectrum. The K-M theory is recommended for poorly absorbing materials. As wood is a strong IR light absorber in some wavenumber region (e.g. the absorption region of ether bands 1100–1200 cm^{-1}), the usage of K-M equation has limits to its validity (details will be discussed later).

Measuring the IR spectrum is a commonly used method to monitor the chemical changes of wood caused by different treatments. The treatment usually changes the roughness of the surface, and the increase in roughness results in the increase of light scattering. This phenomenon creates baseline shift. In this case, baseline correction must be done. The baseline correction is recommended to be done for reflectance spectrum before K-M transformation. There are two-point, three-point and multi-point baseline corrections. The computer supported IR spectrophotometers does the baseline correction automatically if the proper points are chosen. Basic points can be those wavenumbers where the sample does not have absorption. Neither of the wood species have any absorption at 1900 and 3800 cm^{-1} wavenumbers which means that two-point baseline correction can be applied for wood in all cases. Selecting a wavenumber with absorption, the spectrum may suffer dangerous alteration creating artificial changes!

Figure 2.26 shows the measured diffuse reflection spectrum of an Oak sample. The intensity of reflection should be 100 % at 1900 and 3800 cm^{-1} wavenumbers, but these intensities are less than 100 % because of the scattering apparently.

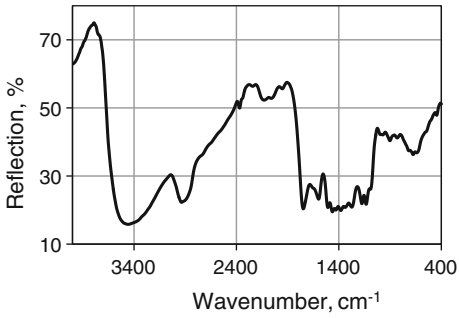

Fig. 2.26 The diffuse reflection spectrum of an Oak sample

Applying two-point baseline correction at 1900 and 3800 cm^{-1} wavenumbers, the spectrum of Fig. 2.26 will be converted as it is seen in Fig. 2.27. This process mostly eliminates the effect of scattering. This elimination is not perfect, however, because the wavenumber dependence of scattering is not precisely linear.

The K-M transformation (Eq. 2.32) converts the reflection spectrum into K-M spectrum which is similar to the absorption spectrum. The K-M conversion of Fig. 2.27 can be seen in Fig. 2.28 for Oak.

The left half of the spectrum consists of two broad bands. The higher peak belongs to the absorption of hydroxyl groups. Hydroxyl groups are located at various places in cellulose, hemicellulose and lignin. These diverse OH groups have absorption at different wavenumbers causing a rather wide absorption band. Water in the wood also results in absorption in this region. The second band represents the absorption of different methyl groups. The chemists created a list of absorption peaks of IR spectrum for identifying the absorbing chemical groups of the measured sample. This list is presented in Table 2.2 with the assignment of the bands. The list represents the maxima of the peaks. The place of the maxima slightly depends on the wood species. That is why intervals are given in Table 2.2. The intervals were determined by experimental data. Since the fingerprint region (between 800 and 1800 cm^{-1}) consists of several overlapping bands, some of the peak maxima are not

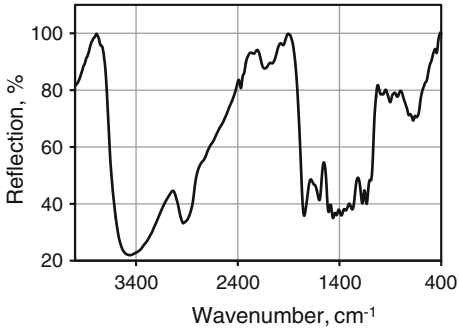

Fig. 2.27 The baseline corrected diffuse reflection spectrum of an Oak sample

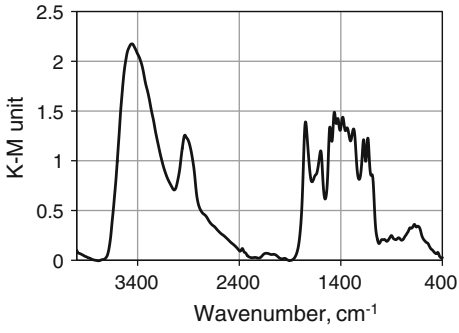

Fig. 2.28 The K-M spectrum of an Oak sample

Table 2.2 Characteristic IR bands of wood (place of maximum) and band assignments (Tolvaj and Faix 1995; Calienno et al. 2014; Huang et al. 2008)

Wavenumber (cm^{-1})	Wavelength (nm)	Assignment
3600–3550	2778–2817	Intramolecular hydrogen bond in a phenolic group (in lignin) and weakly bounded absorbed water
3360–3310	2976–3021	O(3)H..O(5) intramolecular hydrogen bonds in cellulose
2928	3415	CH_2 stretching asymmetric
2854	3504	Symmetric CH_2 stretching
1770–1757	5650–5692	C=O stretching vibration of non-conjugated ketones and γ lactones
1736–1705	5760–5865	C=O stretching vibration of carboxyl groups and acetyl groups in hemicelluloses (xyloglucan)
1660–1653	6024–6050	Conjugated C–O in quinines coupled with C=O stretching of various groups (flavones)
1628–1618	6143–6180	C=O stretching in flavones
1604–1594	6234–6274	Aromatic skeletal breathing with CO stretching (syringil lignin)
1512–1505	6614–6645	Aromatic skeletal (guaiacyl lignin)
1478–1476	6766–6775	C–H deformation in lignin
1465–1457	6826–6863	C–H deformation in xylan
1435	6969	C–H deformation in lignin and carbohydrates
1390–1380	7194–7246	C–H deformation in cellulose and hemicellulose
1369–1366	7305–7321	Aliphatic C–H stretching in methyl and phenol OH
1333–1342	7502–7452	C–H deformation, C-OH stretching, syringyl ring
1319	7582	C–H_2 wagging, C–H deformation (conifers)
1285	7782	C–H bending mode in cellulose
1285–1275	7782–7843	C_{aryl}-O, guaiacyl ring breathing with CO stretching
1240–1230	8065–8130	C–O linkage in guaiacyl aromatic methoxyl groups and acetyl groups in xyloglucan
1183–1175	8453–8511	C–O–C stretching (asymm.) in cellulose and hemicelluloses
1158–1156	8636–8726	C–O–C stretching in pyranose rings, C=O stretching in aliphatic groups
1138–1131	8787–8842	C–O–C stretching (symm.), arom. C–H i.p. deformation, glucose ring vibration
1108–1106	9025–9042	C–O–C stretching
1078–1076	9276–9294	C–O stretching mainly from C(3)–O(3)H in cellulose I
1050–1045	9524–9569	C–O and C–C stretching in cellulose and hemicelluloses
898	11,136	C–H deformation of cellulose

real ones because of the superposition of two or more individual bands. The places of maxima are not exactly overlap with the maxima in Fig. 2.28. Therefore, the difference spectra were used to determine the places of maxima.

The "fingerprint" region is about 1000 cm^{-1} wide interval and slightly depends on the complexity of the material. The usual interval is between 500 and 1500 cm^{-1}. In case of wood, the fingerprint region is located between 800 and 1800 cm^{-1}. The difference spectrum method helps to identify the changes. After creating the difference spectrum (irradiated minus initial), only those absorption bands appear where changes occurred. The increase in absorption is represented by positive band, while negative band represents the absorption decrease. The differences are usually small compared to the intensities of the original spectrum. That is why the disturbing effects must be minimalized. These effects for wood are inhomogeneity and anisotropy of the sample and the roughness change during treatment. The same area of the sample must be measured before and after the treatment. The grain direction, the angle between the fibre direction and the incident IR light must be identical for all measurement (Zavarin et al. 1990; Tolvaj and Mitsui 2004).

The increase of the surface roughness during treatment may cause difficulty if the reflection intensity is low. It happens if the absorption or the scattering are strong. The K-M equation determines the quotient of absorption and scattering. This quotient is something like the hyperbolic function of the reflection intensity (Eq. 2.32). The rough surface elevates the light scattering and decreases the collected light intensity. The K-M intensities increase enormously due to the increasing scattering and not because of increase in absorption (Tolvaj and Mitsui 2011). This phenomenon is visible in Fig. 2.29. The increase at 1740 cm^{-1} is not surprising since it is the absorption place of non-conjugated carbonyl groups and the number of these groups is increasing during UV irradiation. However, most part of the fingerprint region reflects the lifting effect of the increasing scattering. The low absorption interval between 1450 and 1650 cm^{-1} is not affected by the lifting and the absorption decrease at 1507 cm^{-1} is well visible. The lifted lines contain the absorption changes as well, but it is difficult to find them.

The difference spectra clearly show the superposition of the absorption change and the lifting effect (Fig. 2.30). The usual changes are visible after one-day treatment. There are clear absorption decreases at 1600 and 1508 cm^{-1} indicating the degradation of lignin. The ether band splitting is also visible between 1130 and 1180 cm^{-1}. Two positive peaks emerged at 1705 and 1763 cm^{-1}. A small lifting

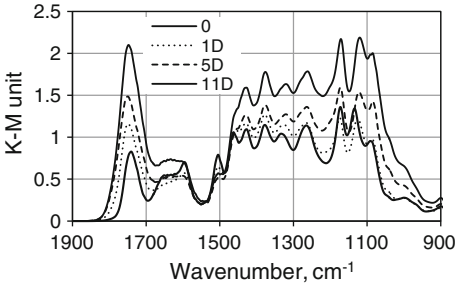

Fig. 2.29 The K-M (absorption) spectra of Beech after 1, 5 and 11 days (D) of UV irradiation

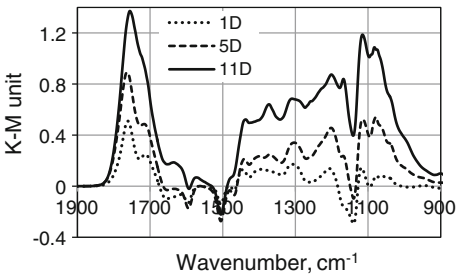

Fig. 2.30 The difference spectra of Beech after 1, 5 and 11 days (D) of UV irradiation without normalisation

effect is visible between 1000 and 1450 cm^{-1} caused by 1-day treatment. The increasing treatment time amplifies the lifting effect, and it becomes more and more visible. After 11 days of irradiation, almost the whole difference spectrum was lifted up. The negative peaks of ether bond degradation seem to be a valley between two positive peaks after 11 days of irradiation.

In similar cases, the spectrum normalisation can help to obtain a more correct difference spectrum. The normalisation can be applied properly if there is a peak not affected by the applied treatment. The band maximum around 1375 cm^{-1} can be the proper normalisation peak for wood during the photodegradation. This C-H band of cellulose is often used as internal standard because of its high intensity and central position. This peak can only be used for normalisation if the examined treatment does not influence this cellulose band. During the normalisation process, the absorption intensities of the treated sample are multiplied to get the same intensity at the normalising place as the spectrum of the untreated sample. The other possibility is to multiply both spectra to get the unity (1.0) at the normalising place. This second normalisation can be recommended if more than two changes are compared. The difference spectra of Fig. 2.29 are seen in Fig. 2.31 after normalisation at 1375 cm^{-1}. Most parts of these difference spectra represent the absorption changes correctly. A moderate lifting effect is visible only between 900 and 1320 cm^{-1}.

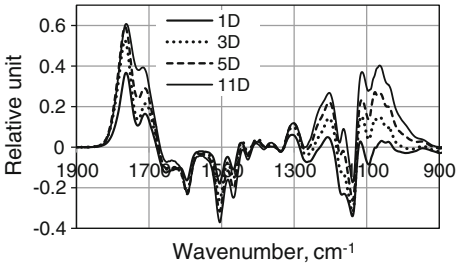

Fig. 2.31 The difference spectra of Beech (calculated using the normalised spectra) after 1, 3, 5 and 11 days (D) of UV irradiation

Comparing Figs. 2.30 and 2.31, the beneficial effect of normalisation is obvious. The remained lifting effect must be taken into consideration during the difference spectrum evaluation in this highly absorbing region.

Beside the diffuse reflectance technique, the IR absorption spectrum of non-transparent materials can be determined with the attenuated total reflectance (ATR) method. The total reflection works if the crystal is made of an optical material with a higher refractive index than the sample being studied. In that case, the light does not cross deeply the boundary of the crystal but will be totally reflected if the incident angle is large enough. During this reflection, the light slightly penetrates the second material (examined sample) and suffers minor absorption. There must be close contact between the crystal and the sample. The sample surface must be as flat as possible, and it must be pressed to the surface of the crystal to ensure as strong contact as possible. The ATR measurement is only partly applicable for the examination of wood because of its high porosity. It follows that the real contact area between the crystal and the wood material is always smaller than the actual surface despite of the press. Most of the applied crystals could not tolerate the pressure that the wood would require, except the diamond, but it shows strong absorption in the absorption region of non-conjugated carbonyl groups, highly reducing the sensitivity in this region.

The third possible method to determine the IR spectrum of wood is the photoacoustic method. The sample is irradiated by IR light rapidly interrupted with a rotating slotted disc. The absorbed energy from the light causes the local heating of the sample, and the generated thermal expansion of the surrounding gas produces pressure wave. This pressure wave is detected by a microphone. The wave intensity correlates to the absorbed energy, and the computer creates the absorption spectrum of the sample using the amplified microphone signal. This method does not need any special sample preparation.

2.5.2 Mechanism of Photodegradation

As the energy of photon increases proportionately with its frequency, the blue light and the UV radiation can be effective to produce degradation. Photodegradation is usually the first step for decomposition of outdoor wooden applications. The UV part of the sun radiation splits some chemical bonds producing free radicals due to the dehydrogenation, dehydroxylation and demethoxylation and generates chain scissions in cellulose and hemicellulose. The free radicals react with oxygen forming hydroperoxides. The lignin and the extractives are good light absorbers, and these components suffer the major degradation during UV radiation. The consequence of this photodegradation is embodied in drastic changes in the appearance of wood showing discolouration, lightness decrease (darkening), loss of gloss, roughening and checking of the surface. Then, the rain can leach out the products of degradation, making room for further degradation. These processes cause the destruction of mechanical and physical properties of the surface layer.

Wood is not transparent for light because of the wide range of chromophoric groups or systems distributed in surface components of wood. The measured depth of light penetration depends partly on the measuring method. The infrared absorption change can be used as an indicator. The absorption decrease directly shows the cleavage of chemical bounds caused by light absorption. The absorption increase indicates the newly created chemical groups. This is a secondary process, and in most cases, the degradation process is followed by oxidation. It may affect deeper layer than that reached by light. Kataoka et al. (2005) found that there is an inversely proportional relationship between the maximum depth of photodegradation and wood density which explains why low-density earlywood erodes more rapidly than denser latewood. There is a similar relationship between the different density of wood species and their rate of erosion during photodegradation. The penetration depth of light into wood depends on the wavelength of light as well. The wavelength dependence of light penetration was tested by the intensity of the IR band at 1730 cm^{-1} (Kataoka et al. 2007). Significant changes in the carbonyl band at 1730 cm^{-1} were detected at depths of up to 70, 100, 150, 250, 300 and 500 μm, respectively, for specimens irradiated with light of wavelengths of 278, 310, 341, 372, 403 and 434 nm, respectively. Light above 434 nm did not affect the intensity of this carbonyl band.

The most sensitive detector of the photodegradation is the colour change. The colour of wood is determined by the conjugated double-bond systems. These types of chromophoric groups are located in lignin and mostly in extractives. The colour change indicates the degradation of conjugated double-bond systems and the creation of such systems.

For investigating the colour change of wood, strong UV light emitter, mercury vapour lamp was used to irradiate specimens. The total electric power of the applied double mercury lamps was 800 Watt, and the samples were located 64 cm from the lamps. The emission spectrum of mercury lamp (supplied by the producer of the lamp) is located mainly in the UV region (80 %). It contains 31 % UV-A (380–315 nm), 24 % UV-B (315–280 nm) and 25 % UV-C (280–240 nm) radiation. The photons of UV-C range have sufficient energy to split almost all chemical bonds in wood. The temperature was constant 30 °C in the irradiation chamber avoiding thermal degradations. A previous study demonstrated the importance of the temperature during the artificial photodegradation (Persze and Tolvaj 2012). Hardwood and sapwood species were chosen with different extractive types and contents. The investigated hardwood samples were as follows: Ash (*Fraximus excelsior* L.), Black locust (*Robinia pseudoacacia* L.), Oak (*Quercus petraea*) and Poplar (*Populus x euramericana Pannonia*); the softwood samples were as follows: Larch (*Larix decidua* L.), Scots pine (*Pinus sylvestris* L.) and Spruce (*Picea abies* Karst.). Radial surfaces were prepared to determine the average changes in colour of earlywood and latewood. The colour of the wood specimens was measured before and after irradiations. The exposures were interrupted after 8, 20, 40, 90 and 200 h to measure the colour data.

The colour change was notable and visible even with the naked eye after two hours of irradiation for Black locust. In contrast, Poplar and Larch hardly suffered

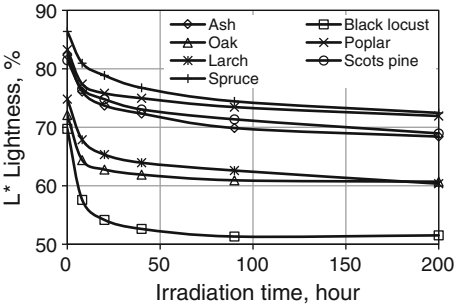

Fig. 2.32 The lightness change of the samples due to mercury lamp irradiation

any visible colour change during the same period of time. The lightness decreased rapidly during the first 10 h of irradiation (Fig. 2.32). After 20 h, the lightness change was moderate and almost linear. The Black locust suffered the greatest (18 units) and Oak and Poplar the smallest (11 units) lightness change during the 200 h of irradiation. The rapid change of lightness in the first 8 h (4 % of the total irradiation time) accounted for 67 % of the total change in Black locust and in Oak, 52 % in Poplar, 48 % in Larch, 45 % in Ash and 39 % in Scots pine and in Spruce. The lightness of Black locust and Oak did not change during the last 110 h of irradiation. The other samples produced slight, but continuous lightness decrease during this period.

The redness change (the alteration of a^* coordinate) showed much greater diversities among the species than the lightness change (Fig. 2.33). The redness increased continuously during the irradiation in all cases. The increase was slow and almost linear for all conifers. The Black locust and the Oak samples showed changes with great differences in intensity. The hardwood samples undergo a rapid increase during the first 8 h, and it was 67 % of the total change for Black locust, 33 % for Oak, 26 % for Ash and 20 % for Poplar. These data for conifers were between 6 and 13 %. Among the hardwoods, Poplar has less extractive content and it produced the smallest redness increase. The initial redness of Larch is higher than the same parameter for the other species and Larch generated the smallest change (3.7 units) during the 200-h treatment. It is thought that the dark coloured extractives are responsible for the high durability of Larch wood.

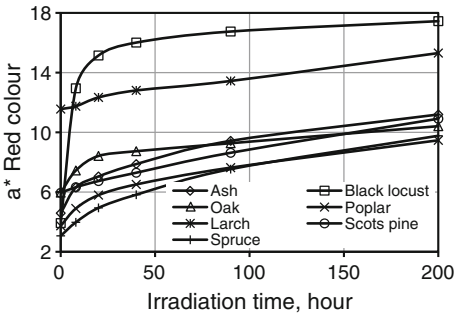

Fig. 2.33 The red colour change of the samples due to mercury lamp irradiation

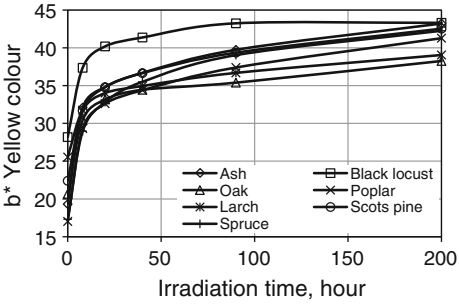

Fig. 2.34 The yellow colour change of the samples due to mercury lamp irradiation

The chromophoric groups in wood are located in the lignin, in the extractives and in their derivatives. Lignin derivatives play the main role mostly in yellowing. This phenomenon was widely investigated in terms of the yellowing of paper containing lignin. The degradation products of extractives mainly determine the alteration of red colour coordinate during photodegradation (Persze and Tolvaj 2012). Similar result was found related to the colour alteration by steaming as well. The Black locust wood has much higher extractive content than the other investigated species, and it contains robinetin-type extractives as well. The degradation products of robinetin produce an intensive increase in redness during steaming of Black locust (Tolvaj et al. 2010). That is why Black locust produced much greater increases of redness during photodegradation than the other species.

The yellow colour coordinate showed similar changes for all examined species (Fig. 2.34). The yellowness increased rapidly during the first 10 h of irradiation. After 20 h, the yellowing was moderate and the alteration was close to linear. The Black locust was an exception again. Its initial colour is more yellow (28 units) than the colour of the other species. Beside the high yellowness, it has almost no redness. That is why the natural appearance of Black locust wood is not attractive for most people. The initial yellowness of Larch (25.5 units) is also high, but it is accompanied by high red coordinate creating a pleasant warm brownish colour. The yellow colour coordinate of Black locust remained constant during the last 110 h of irradiation. The increase of yellow coordinate of Oak and Larch was less intensive than that of the other species during the last 180 h of irradiation (except Black locust). Poplar and Spruce suffered the greatest yellow colour change (24.5 units) during the 200 h of irradiation.

The uniform yellowing can be explained mainly with the photodegradation of lignin. The yellowing differences were generated by the protecting effect of the extractives and their derivatives.

The extraordinary behaviour of Black locust can be explained by its high extractive content. The UV light degrades the extractives followed by the rapid oxidation of the degradation products. This results in a rapid increase in redness. The modified chromophores act as a kind of energy trap which slow down the photodegradation of the main wood components, mainly lignin. Probably similar protection is provided by the originally existing chromophoric units of Larch wood.

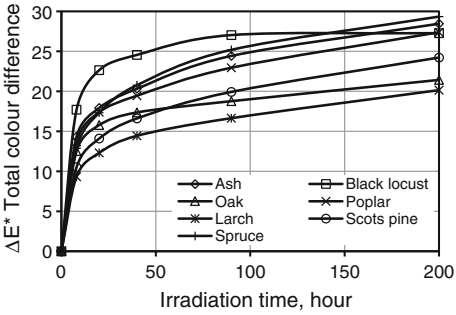

Fig. 2.35 The total colour change of the samples due to mercury lamp irradiation

Poplar and Spruce have low concentration of extractives. That is why these species produced the greatest yellow shift.

The total colour change as a complex parameter shows the summed colour alteration (Fig. 2.35). The trend lines show rapid colour alteration at the beginning of the treatment followed by moderate but continuous increase. The Black locust suffered greater colour change than the other species at the beginning of the treatment. During the second half of the treatment, Black locust did not show any colour change. The colour alteration of Oak was between Black locust and the other species during the second half of irradiation. The total colour difference data do not give additional information compared to the individual colour coordinates.

The alterations of the colour coordinates are sensitive indicators of the photodegradation but do not give exact information about the chemical changes. More detailed information can be obtained if the IR absorption spectrum is measured before and after treatment. The different chemical groups have individual absorption bands. An absorption increase indicates the increasing number of absorbing groups, while the absorption decrease represents the splitting of the chemical bounds. Wood is not transparent to light, so the direct measurement of absorption is not possible. During reflection, the light penetrates slightly into the wood surface with a little absorption and scattering. The diffusely reflected light provides information about the absorption.

Using this method, the diffusely reflected light is collected and its absorption is calculated by the K-M equation (Eq. 2.32). Fortunately, the scattering coefficient hardly depends on the wavenumber of the IR light; thus, the shape of K-M function is similar to the wavenumber dependence of the absorption coefficient. This K-M function is usually used as the IR absorption spectrum.

The infrared spectroscopy is an excellent tool to determine the chemical changes caused by the light irradiation. It provides information from the surface layer affected by the irradiation. The fingerprint region contains the highly overlapped absorption bands of cellulose, hemicelluloses and lignin. Figure 2.36 represents the absorption spectra (calculated by the K-M theory) of Beech sample before and after 24-h irradiation by mercury lamp at 70 °C. The carbonyl band between 1680 and 1820 cm^{-1} increased, while the peaks of the aromatic ring vibrations arising from lignin (at 1508, 1460 and 1425 cm^{-1}) decreased during the irradiation. The band for

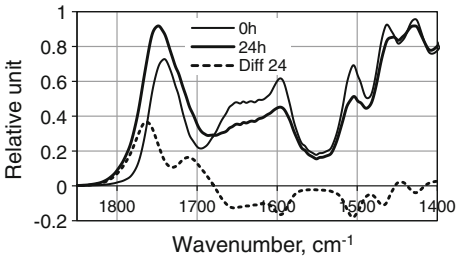

Fig. 2.36 Absorption spectra of Beech before treatment and after 24-h UV treatment and the difference spectrum

the aromatic skeletal vibration at 1596 cm^{-1} also decreased, but it can be observed in the case of hardwoods only. This peak does not exist in the case of softwoods because it belongs to the so-called syringyl lignin found mostly in hardwood. Bands at 1596, 1504, 1455 and 1430 cm^{-1} have similar width, but the carbonyl band at 1741 cm^{-1} is much wider than the others. It suggests that this carbonyl band is the superposition of some individual bands. Hence, most publications treat the band of unconjugated carbonyls as a single absorption band with a maximum around 1740 cm^{-1}.

If we have a closer look at the absorption change of the unconjugated carbonyl band (Fig. 2.36), the shift of the band towards higher wavenumbers is visible. The maximum moves to 1748 cm^{-1}. Moreover, the greatest difference between treated and initial spectra appears not at the maximum but at the left side of the band. The difference at the maximum (1740 cm^{-1}) is 0.14, and at 1763 cm^{-1}, it is 0.37 units, which is more than double. These findings highlight the disadvantage of the simple comparison method where the initial and the treated spectra are presented on top of each other.

The difference spectrum method solves this problem. Creating the difference spectrum (irradiated minus initial), only those absorption bands appear where change has happened. The absorption increase is represented by positive band, while negative band represents the absorption decrease. The changes are clearly visible by calculating the difference spectrum of Beech sample irradiated for 24 h (Fig. 2.36 dotted line).

The difference spectrum of Beech consists of two positive bands at 1765 and at 1705 cm^{-1}. This result is strengthened by 2D IR spectroscopy (Calienno et al. 2014). The band at 1763 cm^{-1} represents the absorption of CO stretching for unconjugated ketones and γ lactones generated by the oxidation after the splitting of the aromatic ring. The band at 1705 cm^{-1} represents the absorption of aliphatic carboxyl groups (Tolvaj et al. 2013). Between 1600 and 1690 cm^{-1}, the conjugated carbonyls in lignin and in phenolic molecules and quinone carbonyl groups are absorbed, and the absorption of OH groups in water is also present. In this region, Beech shows a broad decrease with two minimums at 1655 and at 1596 cm^{-1}.The absorption decrease at 1596 cm^{-1} indicates the degradation of aromatic ring in

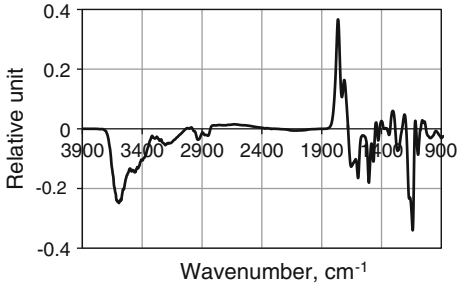

Fig. 2.37 Difference spectrum of Beech caused by 24-h UV treatment

syringyl lignin. The negative peak at 1508 cm^{-1} belongs to the aromatic skeletal vibration of guaiacyl lignin. This negative peak is detectable together with the absorption decrease of the aromatic C-H deformation at 1469 and 1428 cm^{-1} and with the absorption decrease of the guaiacyl ring breathing at 1270 cm^{-1} (Fig. 2.37). The degradation of the aromatic ring for lignin is demonstrated by these absorption decreases. The absorption changes of Beech wood are presented in Fig. 2.37 within the whole examined region. The greatest absorption decrease is visible at 1174 and 1139 cm^{-1}. The first decrease belongs to the asymmetric stretching of ether bond in cellulose. The second decrease belongs to the symmetric stretching of ether bond, the aromatic C-H deformation and to the glucose ring vibration. These absorption decreases indicate the ether splitting and the depolymerisation of cellulose (Tolvaj et al. 2013).

There are 4 small positive bands in the 1100–1450 cm^{-1} wavenumber range. The accuracy of these peaks (at 1445, 1309, 1211 and 1119 cm^{-1}) is questionable. They may be created by the K-M transformation (Tolvaj and Mitsui 2011).

There are absorption decreases in the OH absorption region (3000–3700 cm^{-1}). This is a wide band as a result of the superposition of many individual absorption changes belonging to the OH groups located in different positions. The minimum of the absorption decrease is at 3600 cm^{-1}. The broad band at 3600 cm^{-1} presents the absorption decrease of the intramolecular hydrogen bond in the phenolic group in lignin. This absorption decrease can be partly the effect of drying, i.e. the elimination of the water from the wood. This intensity loss can also be interpreted as the rupture of intramolecular OH bonds of cellulose, comparable to that of the ether bridge. The absorption decrease in OH region can also be interpreted by the loss of OH groups followed by dehydration after UV irradiation. Dehydration belongs to the plausible reaction, during which double bonds—responsible for coloured compounds—are formed. The formation of esters and lactone rings, also common features of photodegradation, occurs via water loss and OH group consumption (Tolvaj and Faix 1995).

There are two small absorption decreases at 2846 and 2936 cm^{-1} belonging to the symmetric and asymmetric methoxyl stretching. These small decreases are thought to be triggered by the demethylation, elimination of CH_2OH groups both from lignin and polysaccharides.

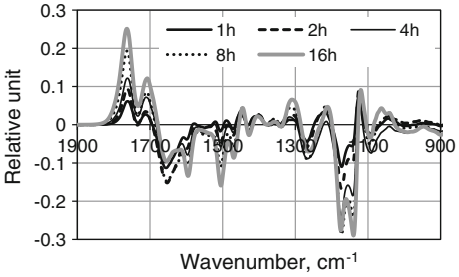

Fig. 2.38 Difference spectra of Beech after 1, 2, 4, 8 and 16 h of UV irradiation by mercury lamp

The time dependence of photodegradation can be monitored by the difference spectrum method. Figure 2.38 represents the difference spectra of Beech after 1, 2, 4, 8 and 16 h of UV irradiation by mercury lamp. The lignin degradation was continuously demonstrated by the absorption decrease at 1506 and 1596 cm^{-1}. The negative peak at 1654 cm^{-1} first decreased than remained constant. The two carbonyl peaks around 1707 and 1763 cm^{-1} increased parallel. The growing of the peak at 1763 cm^{-1} was a little faster than the growing of the nearby peak. The most remarkable change happened at 1174 and 1139 cm^{-1}, respectively. The decrease of the peak at 1174 cm^{-1} was faster at the beginning, but it slowed down after 4 h. The other peak at 1139 cm^{-1} decreased continuously and has overtaken its neighbour before 16 h of irradiation. The difference between the two peaks increased forth after 24 h of irradiation (see also Fig. 2.37).

There are differences in the course of photodegradation depending on the wood species. Figure 2.39 represents the IR absorption changes of Beech, Spruce and Oak earlywood caused by irradiation for 8 h at 30 °C by mercury lamp. The absorption decrease of guaiacyl lignin at 1508 cm^{-1} is similar for all species. However, the absorption decrease of syringyl lignin at 1596 cm^{-1} is missing in case of conifers. The reason is that conifers have hardly any syringyl lignin. The absorption increase in the region of carbonyl groups (1670–1810 cm^{-1}) is mostly originates from the degradation products of lignin. Therefore, there are differences between conifers

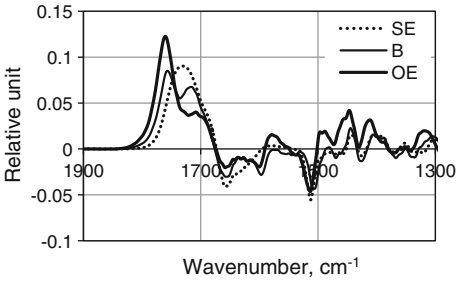

Fig. 2.39 Difference spectra of Beech (*B*), Spruce (*S*), Oak (*O*) and earlywood (*E*) after 8-h UV irradiation

and deciduous species in the carbonyl region as well. Beech has two separate maxima at 1710 and 1760 cm^{-1}. Oak earlywood has also two maxima similar to Beech, but the intensities are different. The peak at 1760 cm^{-1} is much higher than the other. Probably, Spruce earlywood has two positive bands, but only one at 1710 cm^{-1} is the same for all three species. The other peak moved closer, creating a visually integrated band at 1730 cm^{-1} for Spruce. The situation is the same for all conifers. The width of this band confirms that it is the superposition of two absorption increase. These results suggest that the absorption increase at 1710 cm^{-1} is created mainly by the degradation products of guaiacyl lignin and the other absorption increase at 1760 cm^{-1} is created mainly by the degradation products of syringyl lignin. There must be a third peak arising between the two previous ones. These suggestions, however, need further chemical investigations.

There are differences in sensibilities of earlywood and latewood to the photodegradation. The latewood has usually more protecting ability than the earlywood. It is well demonstrated in Figs. 2.40 and 2.41. Figure 2.40 demonstrates the absorption change difference between Poplar earlywood and latewood. The lignin in earlywood is more degradable than that in the latewood. The absorption decrease of both syringyl (at 1595 cm^{-1}) and guaiacyl (at 1505 cm^{-1}) lignin is smaller in latewood than that in earlywood. As a consequence, the absorption increase of carbonyl groups is smaller in latewood than that in earlywood. The difference is greater at the peak of 1706 cm^{-1} than that at 1760 cm^{-1}. There is one place where the latewood suffered greater changes than the earlywood, namely in the absorption band of the asymmetric stretching of ether bridge at 1172 cm^{-1}.

Conifers have somewhat different photodegradation behaviour than deciduous species (see Fig. 2.39). Figure 2.41 shows the changes in absorption differences of Spruce earlywood and latewood. The conjugated carbonyls (around 1660 cm^{-1}) in latewood suffered greater degradation than the same groups in earlywood. This broad negative peak pulled down the partly overlapped positive peak at 1706 cm^{-1}. There is a small negative baseline shift for latewood in this region as well. The earlywood was less stable than the latewood indicated by the absorption decrease at 1507 cm^{-1}. The small positive peak at 1490 cm^{-1} pushed the negative peak towards

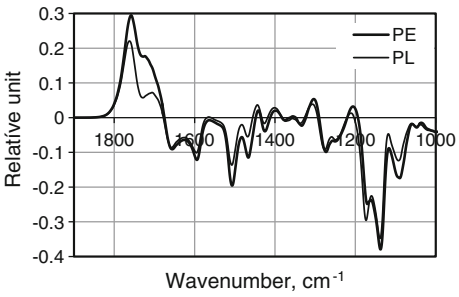

Fig. 2.40 Absorption change of earlywood (*E*) and latewood (*L*) for Poplar (*P*) caused by 16-h UV treatment

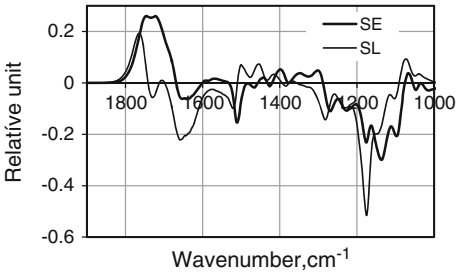

Fig. 2.41 Absorption change of earlywood (*E*) and latewood (*L*) for Spruce (*S*) caused by 24-h UV irradiation

higher wavenumbers for latewood. The latewood produced smaller absorption increase in the non-conjugated carbonyl region than the earlywood. Both peak intensities (at 1713 and 1736 cm^{-1}) are the same for earlywood. There is a hardly visible shoulder at 1680 cm^{-1} representing the third absorption increase caused by UV irradiation. However, for latewood, the peak at shorter wavenumber is much smaller than the other at greater wavenumber. This behaviour of spruce is similar to Poplar (see Fig. 2.40). The peak where the latewood suffered greater change than earlywood is located at 1175 cm^{-1}. The situation is similar for Poplar as well.

Examining wood species having heartwood and sapwood, it was realised that the heartwood production does not influence the photodegradation behaviour of earlywood and latewood. There was no remarkable difference in the photodegradation of earlywood sapwood and heartwood. The same was found for latewood.

The photodegradation increases the surface roughness of wood. The roughness was measured with two methods: optical and contact surface roughness measurement. The unfiltered P profile was computed from the traced profile (EN ISO 3274). The surface roughness parameters (Pz; Pt; Pa; Pmax) can be used also for this profile. The roughness parameters were recorded after five days of UV light irradiation, which was followed by two-day intervals. There was a total of 6 irradiation periods. The necessary parameters were measured right after subjecting the samples to light irradiation. The roughness parameters increased continuously during UV irradiation for all examined species. Figure 2.42 shows the results for Poplar measured on radial surfaces. The roughness increase was linear, and similar results were found for Spruce and Scots pine as well. For Black locust, the increase was a little higher during the first 5 days compared to the later period (Tolvaj et al. 2014a). The optical method produced similar results.

The baseline shift (Eq. 2.31) of earlywood and latewood for Poplar was measured. These baseline shift data are presented in Fig. 2.43. The optical roughness measurement also showed increasing roughness due to the UV irradiation. The increase was continuous and linear with increasing treatment time. This change was in good correlation with the results of contact roughness measurement. Figure 2.43 represents the high sensitivity of the optical roughness measurement. The latewood became less rough than the earlywood. This figure shows clearly that earlywood is

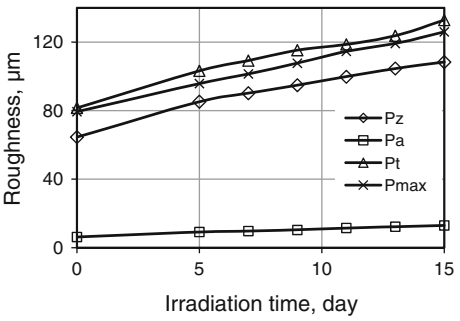

Fig. 2.42 Selected roughness parameters of UV-treated Poplar wood

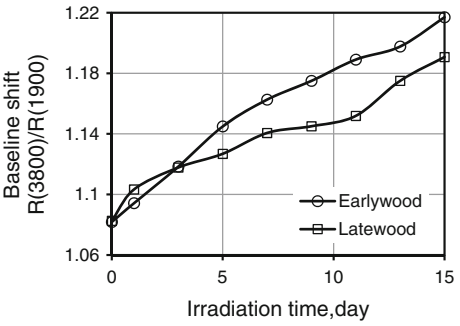

Fig. 2.43 IR baseline shift of Poplar caused by UV irradiation

more sensitive to the UV irradiation than the latewood. This finding is in good correspondence to the results of IR changes presented in Fig. 2.40. The IR absorption measurement also indicated that earlywood suffered greater chemical changes during UV irradiation than the latewood. Figure 2.43 shows that the applied optical roughness measurement is highly sensitive to represent the roughening effect of photodegradation.

2.5.3 Photodegradation of Thermally Modified Wood

There are two main types of thermal treatment. One is the treatment at low temperature (80–130 °C) under wet condition. It is called steaming, and the steam must be saturated. If the steam is not saturated (overheated steam), the wood will dry rapidly. The other possibility is the dry thermal treatment where the temperature must be higher than for steaming. The dry thermal treatment causes considerable changes if the temperature is above 150 °C. Below this temperature, the chemical changes are slow according to the Arrhenius law (2.33). Thus, it would take a long time to get the proper dark colour under dry condition. The cost is a disadvantage of low temperature for industrial use. However, chemical changes become faster with rising temperature. This increase is exponential according to the Arrhenius law.

The chemical decomposition of wood is highly intensive above 220 °C, and it causes rapid decrease of the excellent mechanical properties of wood. Therefore, industrial thermal treatments apply temperatures below 220 °C. The wood material treated under dry thermal condition is usually called thermowood. The colour of a material is created by the conjugated double-bond (chromophore) chemical systems. Lignin and certain extractives consist of such chromophores in the natural wood. Thermowood contains additional chromophores produced during the degradation of the hemicelluloses.

To determine the short-term photodegradation behaviour of thermowood samples, two hardwood and two softwood species were utilised. The hardwood species were Black locust heartwood (*Robinia pseudoacacia* L.) and Poplar (*Populus x euramericana Pannonia*). The softwood species were Larch heartwood (*Larix decidua* L.) and Spruce (*Picea abies* Karst.). The initial moisture content of the samples was between 8 and 10 %. The dry thermal treatment was carried out in a laboratory scale drying chamber at 160 and 200 °C in the presence of air and ventilation (open system). The preheating time was 30 min. The duration of the effective thermal treatment time was 2, 4 and 6 h. The 2-h treatment time at 160 °C produced only a minor colour change; therefore, these samples were not used for further investigation. The thermally treated samples along with untreated control samples were then artificially photodegraded. A strong UV light emitter, mercury vapour lamp provided the light irradiation. The L^*, a^* and b^* colour coordinates were measured and calculated based on the D_{65} illuminant and 10° standard observer with a test-window diameter of 8 mm (Tolvaj et al. 2014b).

The samples underwent considerable colour change during thermal treatments, as shown in Figs. 2.44, 2.45, 2.46, 2.47 and 2.48. These data are presented in the figures at zero irradiation time. The lightness of all species decreased compared to the untreated samples. The magnitude of change followed the intensity of the thermal treatment. In other words, higher temperature and longer treatment time produced greater decrease in lightness. The selected thermal treatment parameters resulted in a large variety of lightness (see the first dots in Fig. 2.48). The redness of all species increased with heating, and the order of the change followed the intensity of the thermal treatment (see Fig. 2.44). Higher temperature and longer treatment time produced a greater increase in redness. Spruce was highly sensitive to both thermal treatment temperature and duration of exposure. Poplar was also highly sensitive to the temperature of the thermal treatment, but not sensitive to the thermal treatment time. The yellow colour of Larch, Poplar and Spruce increased following the tendency of red colour change (Fig. 2.46). The only exception was the Black locust (Fig. 2.45). Its originally high yellow colour decreased due to the thermal treatment following the same tendency as the lightness change.

The photodegradation due to UV irradiation caused the most detailed differences in the redness change. The red colour changes are represented in Figs. 2.44. Trend lines showing the red coordinate shift were convergent for the low extractive content species (Poplar and Spruce), but they were first rapidly convergent and later divergent for the high extractive content species (Black locust and Larch). Black locust and Larch samples produced rapid change in redness during the first 3 h of

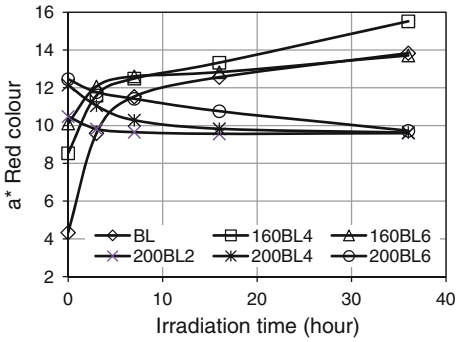

Fig. 2.44 Redness change of Black locust caused by light irradiation (*abbreviation* thermal treatment temperature/sample name/thermal treatment time in hour)

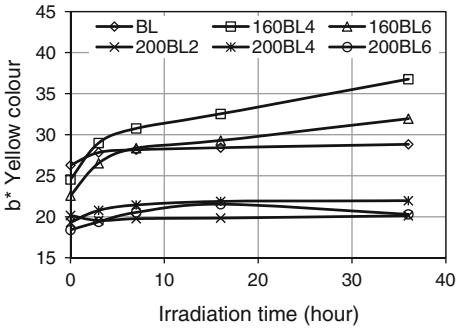

Fig. 2.45 Yellow coordinate shifts of Black locust samples caused by light irradiation (*abbreviation* thermal treatment temperature/sample name/thermal treatment time in hour)

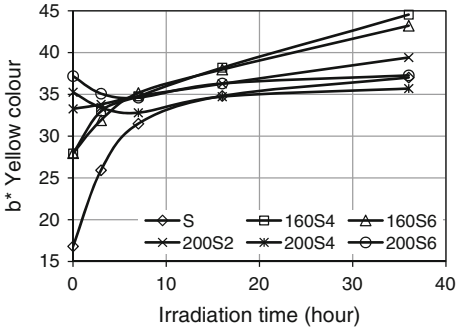

Fig. 2.46 Yellow coordinate shifts of Spruce samples caused by light irradiation (*abbreviation* thermal treatment temperature/sample name/thermal treatment time in hour)

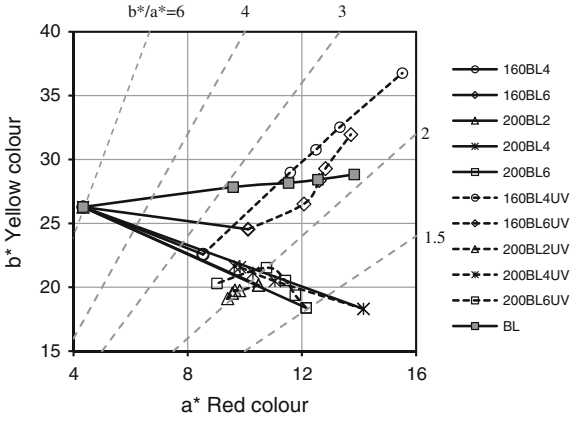

Fig. 2.47 Redness and yellowness change of Black locust (BL) during dry thermal treatment and UV irradiation (*abbreviation* thermal treatment temperature/sample name/thermal treatment time in hour). The duration of UV irradiation was 6, 16, 36 and 72 h

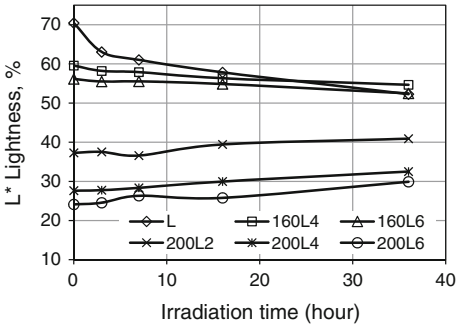

Fig. 2.48 Lightness change of the Larch samples caused by light irradiation (*abbreviation* thermal treatment temperature/sample name/thermal treatment time in hour)

exposure. In comparison, the other two species showed moderate redness change during this period.

After 7 h of treatment, the trend lines became straight, showing a slow increase or remained constant. The thermally treated samples showed different changes depending on the treatment temperature. Red coordinate shift of samples treated at 160 °C followed the tendency observed in natural wood (thermally untreated) samples. This allows us to conclude that the thermal treatment at 160 °C did not affect the redness change behaviour of wood.

However, the samples thermally treated at 200 °C changed their redness in a different way than untreated wood. After moderate decrease in redness during the first 7 h of light irradiation, these treated samples kept a nearly constant redness value during the examined period. The samples treated at 200 °C for 2 h showed the

most stable redness values during photodegradation. The redness change is mainly determined by the chemical changes of extractives and by the chromophore products of the thermally degraded hemicelluloses. It can be concluded that at 200 °C thermally modified extractives and the chromophore products of hemicelluloses are fairly stable during light irradiation.

The yellow colour changes of the examined species are presented in Figs. 2.45 and 2.46. Two graphs are presented here because the changing tendencies and values of Poplar were the same as those of Spruce and similar to Larch. Larch samples showed similar behaviour as Spruce samples; only the intensity of the changes was a little stronger for Larch during the first 3 h of light exposure. The yellow colour of Black locust is naturally different compared to the other European species. This deviation is caused by its high robinetin content. A previous study demonstrated that the high extractive content of Black locust partly protects its lignin content during light irradiation (Tolvaj and Varga 2012).

The same finding is partly demonstrated here as well. The untreated Black locust produced the least yellowing compared to the other examined untreated samples. Some of the extractives of Black locust underwent thermal degradation, represented by the increasing values of a^* and b^* coordinates. The extractives modified during the thermal treatment at 160 °C were not able to protect the lignin of Black locust, as it is visible on Fig. 2.45. The yellow colour increase of the Black locust samples treated at 160 °C was much greater than that of the untreated samples. The degradation behaviour of thermally modified Black locust at 160 °C was similar to the degradation of the other species that do not contain protective extractives. Black locust samples treated at 200 °C did not produce remarkable yellowness changes. The other samples showed a slight yellow colour decline during the first 7 h of light irradiation. After this time period, the yellowing of the samples treated at 200 °C followed the slow yellow coordinate increase of the untreated samples. The yellow colour change of the samples treated at 200 °C for 2 h seemed to be the most stable, as discussed in the case of red colour change. The yellow colour change of the investigated samples showed that the lignin of thermally modified wood underwent a similar photodegradation as that of the untreated natural wood. This was found in a previous study (Srinivas and Pandey 2012).

There is another possibility to represent the colour alteration on the a^*- b^* plane (Fig. 2.47). The equal b^*/a^* lines (constant hue) are also represented in this figure. The thermal treatment (solid line) generated moderate decrease in yellowness and great increase in redness for Black locust. The UV treatment generated considerable colour saturation for the samples pretreated at 160 °C. The samples pretreated at 200 °C did not change the saturation, but the hue returned to those samples which were pretreated at 160 °C. The colour hue was in a narrow interval between 2 and 2.5 during the UV treatment. The thermal treatment at 200 °C pushed the value of hue below 2, but the UV irradiation raised back this value above 2. The effect of the two type of pretreatments was opposite for the effect of UV treatment. The other wood species produced similar colour changes during the UV irradiation; only the redness change was much less and the yellowness change was positive during the thermal pretreatment.

The lightness of the investigated samples decreased considerably during the dry thermal treatment (Fig. 2.48). This decrease was 83, 66, 62, and 56 % for Black locust, Larch, Poplar and Spruce, respectively.

There were only minor differences among the species during the light irradiation. That is why only the data of Larch are presented here. Poplar and Spruce showed the same changing behaviours, and this pattern of change was also similar to that of the Larch samples. Untreated wood samples suffered rapid lightness decrease during the first 10 h of light irradiation, followed by moderate decrease. The originally dark thermally treated samples exhibited slow but continuous changes. The values of these changes were considerably less than those of the untreated samples. The direction of change was determined by their initial lightness value. Samples having initial lightness values higher than 40 units showed decreasing lightness, while those with initial L^* values less than 40 units showed lightening during irradiation. These results suggest that thermal treatment slightly reduced the lightness change effect of photodegradation (Tolvaj et al. 2014b).

The short-term photodegradation behaviour of thermowood is valuable for the scientist, but in practice, the long-term effects are even more important. Some researcher found that dry thermal treatment increases the weathering stability of wood, while others stated that thermowood undergoes the same photodegradation as natural wood. Some results are presented here.

Ayadi et al. (2003) tested the colour stability of heat-treated wood samples. The heat treatment was performed at 240 °C for 2 h in nitrogen atmosphere. Heat-treated samples of Ash, Maritime pine and Poplar heartwood were exposed to UV light for 835 h. The total colour change was determined as a complex parameter representing the changes. The experiments showed that the colour stability of the heat-treated wood was better after the 835 h of exposure when compared to untreated wood. The difference in degradation between thermally treated and untreated wood increased rapidly during the first 36 h of UV light exposure. After this period, the trend lines of total colour change were close to parallel.

Huang et al. (2012) investigated the photodegradation of heat-treated (190–115 °C) Jack pine (*P. banksiana*), Aspen (*P. tremuloides*) and Birch (*B. papyrifera*) samples. There was a major increase in yellow and red colour coordinates with corresponding decreases in the reflectance (L^*) for all the three species during heat treatment. Heat-treated woods had better colour stability during the early times of weathering, while the colours of heat-treated woods and untreated woods were very similar after the specimens have been subjected to long-term artificial weathering. They found that degradation of hemicelluloses can consequently cause an increase in the amount of lignin component of Birch wood. This increase becomes more important as the treatment temperature increases. It was also found that the heat treatment increases the crystallised cellulose content. The increased lignin and crystallised cellulose content brought about by heat treatment protects heat-treated birch against degradation taking place during weathering (Huang et al. 2013).

Yildiz et al. (2011) investigated the outdoor weathering properties of heat-treated Alder wood. The treatment parameters were as follows: 150, 180 and 200 °C,

for periods of 2, 6 and 10 h, respectively. The samples were outside for 3 years in Turkey. It was found that heat treatments delayed and decreased the rate of colour change caused by the weathering but did not completely prevent it. The most advantageous treatment condition was at 200 °C for 10 h. The photodegradation behaviour of thermally treated Rubber wood (*Hevea brasiliensis*) was investigated by Srinivas and Pandey (2012). Oven-dried samples were kept in a glass tray and were heat treated in a preheated vacuum oven at 225 °C for 2, 4 and 6 h under 400 mm (Hg) of vacuum to obtain three different levels of thermally modified wood specimens. Results of colour changes and FTIR spectroscopy revealed that thermal modification of wood does not induce resistance against UV radiation.

Pannonia poplar (*Populus x euramericana Pannónia*) samples were thermally treated in vegetable oil at 160 and 200 °C (Bak et al. 2012, 2014). After thermal treatment, the samples underwent outdoor weathering during a year. It was concluded that wood samples treated at lower (160 °C) temperature underwent more severe total colour changes compared to the samples thermally treated at higher temperature (200 °C). It means that the colour stability of the thermally treated wood depends mainly on the temperature.

2.6 Weathering Processes of Wood

Outdoor weathering processes of wood can be divided into two main groups: biotic and abiotic degradations. The biotic degradation is mainly caused by fungi and insects attack. Biotic degradations will not be discussed in this book.

The main factor of the abiotic degradation is the sunlight. Within the sunlight, the UV radiation is the most harmful for biomaterials. The results of UV radiation for wood were discussed above. The effectiveness of UV radiation is partly influenced by the temperature of the wood. This effect was neglected earlier, but nowadays some publications highlight its importance. In addition, rain leaches out the water soluble extractives and degradation products from the surface of the outdoor wood.

The colour of individual wood species is mainly defined by its extractive content. The degradation of these extractives partly determines the colour alteration during photodegradation. Pandey (2005b) compared the photodiscolouration of natural and extractive free wood samples. He demonstrated that the extractive free specimens exhibited a steady increase in colour change with increasing irradiation time. Unextracted wood surfaces showed rapid colour changes during the initial period of exposure, which decreased upon prolonged exposure time. Chang et al. (2010) found that the rate of wood degradation was lessened by the presence of extractives, when they examined the photodegradation of Japanese cedar and Taiwan acacia.

2.6.1 Photodegradation Due to Sun Radiation

The direct investigation of photodegradation caused by sunlight is difficult. Exposure to direct sunlight is not repeatable under the same conditions. Rainfall, air humidity and alteration of the temperature are uncontrollable parameters that are able to modify the effect of sunlight. The other problem is the changing intensity of the sun radiation during the day and over the year. Clouds sometimes partly or fully cover the sun. These periods should be subtracted from the total treatment time, but it would be extremely difficult. It means that the irradiation time and intensity (the most important parameters) are not exactly known during outdoor solar radiation. Therefore, the effect of light irradiation is mostly investigated using artificial light sources.

In our experiments, the samples were exposed to sunlight exposure only on sunny days to determine the effect of the sunlight alone (Tolvaj and Mitsui 2005). That type of outdoor irradiation was not found in the literature at all. The aim of the study was to investigate the pure photodegradation effect of sunlight. The other aim was to determine whether artificial light sources are able to properly imitate the photodegradation of wood caused by sunlight. The similarities and the differences in the effects caused by natural and artificial light (xenon and mercury lamps) on wood were examined, to determine which type of radiation simulates the effects of sunlight. The air temperature varied from 16 to 41 °C. The max. r.h. was 80 %, and the daily average of total solar power density was between 436 and 459 W/m^2. The SX-75 Suga Test Instrument was equipped with a xenon lamp. The power density of the lamp was 180 W/m^2 within the range of 300–400 nm, at 63 °C (black panel) and 50 % r.h. As the intensity of sunlight changes continuously during the day and during the year, the comparison was made on the basis of irradiation time, not on the irradiated energy. Total irradiation time was 200 h for both sunlight and xenon light.

During the first 30 h of light irradiation by sun and xenon lamp, the colour change was rapid, as it is shown in Figs. 2.49, 2.50, 2.51 and 2.52. Changes in lightness were particularly pronounced (Fig. 2.49). The first 30 h of sunlight accounted for ca. 60 % of the total change of lightness in hardwoods and 40–50 %

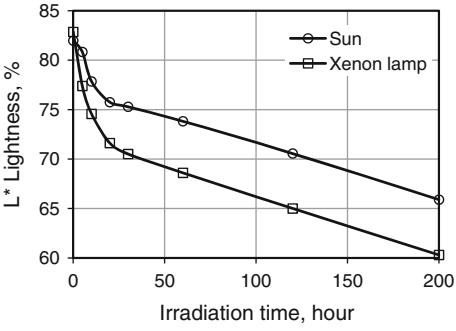

Fig. 2.49 Lightness change of Spruce due to irradiation by different light sources

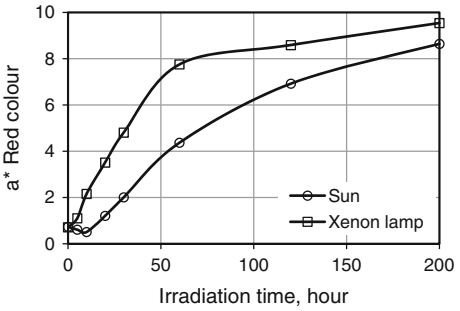

Fig. 2.50 Red colour change of Spruce due to irradiation by different light sources

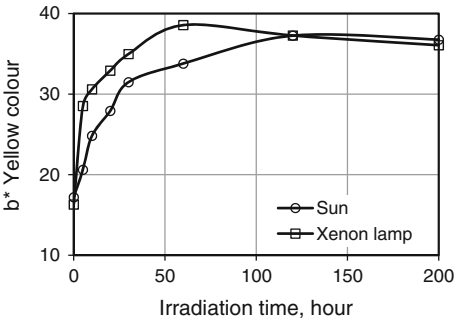

Fig. 2.51 Yellow colour change of Spruce due to irradiation by different light sources

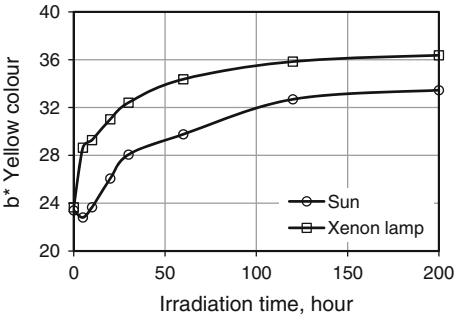

Fig. 2.52 Yellow colour change of Poplar due to irradiation by different light sources

of that in softwoods. Artificial light sources caused even faster changes in lightness than sunlight during the first 30 h of exposure. After 30 h of irradiation, the trend changed and the trend lines became parallel.

The *a** coordinate represented in Fig. 2.50 for Spruce did not change significantly during the first hours of exposure to sunlight. Even in the first 10 h of irradiation, sunlight produced only a minor redness decrease in Spruce just as in the other conifers. Only Black locust became redder intensively during the first hours of sunlight exposure. In contrast, samples exposed to xenon light became redder already in the first hours of irradiation. Black locust produced half of the total

change in redness during the first 10 h. The extraordinary behaviour of Black locust may be the evidence of its high extractive content. The robinetin content of this species was especially sensitive to UV light exposure. The xenon lamp created greater increase in redness up to 60 h of irradiation than sunlight. After this period, the difference decreased continuously.

The third colour coordinate b^* for Spruce shows even faster alteration than a^* if sunlight and xenon light exposure are compared (Figs. 2.51 and 2.52). Yellowing of the samples caused by xenon light was concentrated in the first 5 h of irradiation. The yellowing during this period accounts for 61 % of the total yellowing of Spruce sample induced by xenon lamp. The same change caused by sunlight accounts only 17 %. After 60 h of irradiation, the intensity of change decreased or stopped and the trend lines converged or became parallel (Tolvaj and Mitsui 2005). Poplar showed less yellowing than the Spruce sample independently of the light source. The yellowing is produced mostly by the oxidation products of lignin degradation. The lignin decay and the resulting quinone formation are related to the photoyellowing (Müller et al. 2003). These newly created quinones are also sensitive to light irradiation and undergo further degradation. In the first period of irradiation, the quinone production is dominant and slow down later on. On the other hand, the degradation procedure of quinone structures is slow at the beginning (there are only a few) but will become more intensive later on. The result of these two processes produces a maximum. After reaching the maximum, the creation of quinone structures is slower than their degradation. For Spruce, this maximum is located at 60 and 120 h of exposure created by xenon lamp and sun irradiation, respectively. For Poplar, these maxima are located out of the examined time range.

The xenon lamp irradiation simulates the colour change caused by sunlight only when wood is subjected to a long-term exposure. Short-term exposure to xenon light causes a more rapid colour change, mainly yellowing, than sunlight.

Infrared spectroscopy was used for studying the chemical changes in wood caused by light irradiation. The differences in the change of IR spectra caused by the two types of irradiation (sun and xenon lamp) are qualitative rather than quantitative. The difference IR spectra were calculated to clearly present the changes. Deviation was found between hardwoods and softwoods represented here by the spectra of Spruce and Black locust in Figs. 2.53, 2.54 and 2.55, respectively. Only the fingerprint area is displayed because the main differences were found in this region. The band assignment can be found in Table 2.2.

After irradiation, the carbonyl band between 1680 and 1900 cm^{-1} increased. There was a typical negative peak at 1508 cm^{-1} belonging to the aromatic skeletal vibration of guaiacyl lignin. This negative peak is visible together with the absorption decrease of the aromatic C–H deformation at 1469 and 1428 cm^{-1} and with the absorption decrease of the guaiacyl ring breathing at 1265 cm^{-1}. The band for the aromatic skeletal vibration at 1600 cm^{-1} (syringil lignin) also decreased in the case of hardwoods. Two great absorption decreases are visible at 1174 and 1139 cm^{-1}. The first decrease belongs to the asymmetric stretching of ether bond, while the second belongs to the symmetric stretching of ether bond, the aromatic C-H deformation and to the glucose ring vibration. These absorption decreases

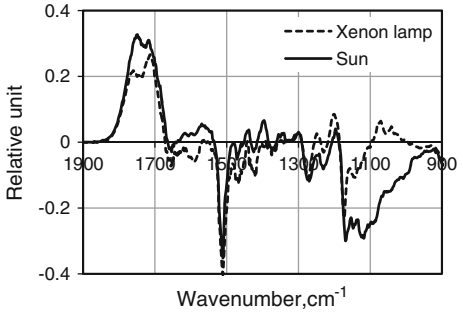

Fig. 2.53 Difference IR spectra of Spruce caused by 120-h light irradiation

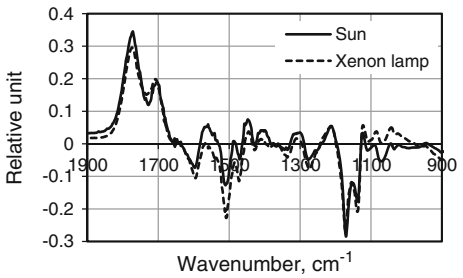

Fig. 2.54 Difference IR spectra of Black locust caused by 200-h light irradiation

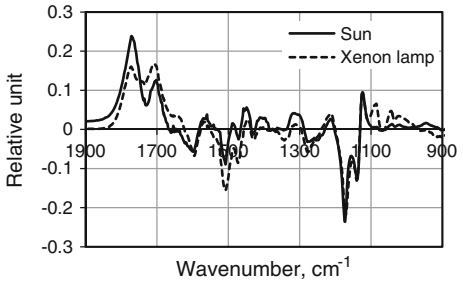

Fig. 2.55 Difference IR spectra of Black locust caused by 60-h light irradiation

indicate the ether splitting and the degradation of cellulose. (There is baseline difference between the difference spectra created by sunlight and xenon lamp in the 1400–1600 cm^{-1} wavenumber region.) The effect of the two irradiation types (sun and xenon lamp) differed in peaks of the 1680–1900 cm^{-1} wavenumber region. Usually, two peaks are developed in this region during the exposure of wood to UV radiation. In softwoods, these peaks are close to each other (Fig. 2.53); thus, the highly overlapped bands are sometimes visible as one broad band if the irradiation is strong enough or prolonged. For hardwoods, these bands are usually more separated (Figs. 2.54 and 2.55).

The absorption wavenumbers of the CO stretching in unconjugated ketones, carboxyl groups and lactones are between 1730 cm^{-1} and 1780 cm^{-1}, and the non-conjugated aliphatic carbonyls are absorbed between 1700 cm^{-1} and 1750 cm^{-1}.

The xenon light caused greater increase in the peak at 1716 cm^{-1} wavenumber than at 1748 cm^{-1} for Spruce. Sunlight produced similar change at 1716 cm^{-1} than xenon light for both hardwoods and softwoods, but some differences were found at higher wavenumbers. The xenon lamp irradiation produced smaller absorption increase here than the sunlight. These two bands are located at 1706 and 1770 cm^{-1} for Black locust. The increase of the two carbonyl bands had distinctive time dependence. The xenon lamp caused faster increase of the band around 1710 cm^{-1} than for the other band at higher wavenumber at the beginning of the treatment. The height of these two bands was close to each other after 200 h of irradiation for Spruce wood.

The change was similar for Back locust as well, but the height of the peaks occurred equal earlier, after 60 h of irradiation (Fig. 2.55). The difference between the effect of sunlight and xenon light decreased after this period. The effect of xenon light proved to be equal to the effect of sunlight after 200 h of irradiation on Black locust (Fig. 2.54). These findings strengthen our conclusion suggested by colour measurements that the xenon light irradiation can simulate the effects of sunlight only in a long-term irradiation (Tolvaj and Mitsui 2005).

2.6.2 Temperature Dependence of Photodegradation

The superposition effects of two or more influential parameters were hardly examined for degradation of wood. Matsuo et al. (2010), Matsuo et al. (2014) investigated the time–temperature superposition during thermal degradation of wood in the temperature range 90–180 °C. The effect of elevated temperature during photoirradiation (the superposition of light irradiation and thermal treatment) is also a phenomenon which is rarely investigated, even though the surface temperature of wood rises considerably during light irradiation. Persze and Tolvaj (2012) irradiated wood samples using mercury vapour lamp at 80 °C and at 30 °C to screen out the effect of thermal decomposition during photodegradation. Their results demonstrated that the same light irradiation resulted in considerably greater redness increase at 80 °C than at 30 °C. It was found that the extractive content has an important role in thermal decomposition during photodegradation.

The effects of consecutive photodegradation and thermal degradation (photoirradiation followed by thermal treatment or thermal treatment followed by photoirradiation) are widely investigated. Mitsui and his co-workers (Mitsui et al. 2001, 2004, 2005; Mitsui 2004) found that the combination of light and heat treatment (light irradiation was followed by heat treatment) creates even more discolourations than the separate light and heat exposures do. The colour change caused by heat treatment was much greater after light irradiation than without it. In these studies, the light irradiation was followed by dry and wet thermal treatment. The light irradiation produced small redness increase in dry condition, but the following thermal treatment created 8 times greater redness increase. The applied temperature was high (120–160 °C) in Mitsui's study. The change of IR spectrum showed

different alterations. The intensity of carbonyl groups (that increased with light irradiation) decreased with wet heat treatment. The increment of two carbonyl sub-bands by light irradiation was similar, but the decrement of the carbonyl band at 1756 cm^{-1} was greater than at 1716 cm^{-1}, with heat treatment after light irradiation.

The other possibility, the photodegradation of previously thermally treated wood, was also investigated by several authors. Some papers explained that thermally treated wood had greater resistivity to photodegradation than non-treated ones. But others found that thermally treated wood undergoes the same photodegradation as untreated wood. More details can be found in Sect. 2.5.3.

The effect of low temperature was also investigated. Mitsui and Tsuchikawa (Mitsui and Tsuchikawa 2005) irradiated wood samples that were kept in a conditioning chamber set for −40 °C. They concluded that the measured degradation was much smaller at −40 °C than under usual laboratory condition.

In order to clarify the superposition effect of elevated temperatures during photodegradation of hardwood and softwood, samples were irradiated by mercury lamp at elevated temperatures (Tolvaj et al. in print). The investigated hardwood samples were as follows: Ash (*Fraxinus excelsior* L.) and Poplar (*Populus x euramericana Pannonia*), and the softwood samples were as follows: Scots pine (*P. sylvestris* L.) and Spruce (*P. abies* Karst.). The UV radiation of mercury vapour lamp was 80 % of the total (UV and visible) light emission (31 % UV-A, 24 % UV-B and 25 % UV-C). The total electric power of the applied double mercury lamps was 800 W, and the samples were located 64 cm from the lamps. Four different air temperatures 30, 80, 120 and 160 °C were used in the irradiation chamber. A series of samples was treated in the same chamber set for 30, 80, 120 and 160 °C but without light irradiation. The effect of pure thermal degradation was determined by this experiment. Total treatment time was 36 h in all cases. The colour of the wood specimens was measured before and after treatments. The exposures were interrupted after 6, 11, 16 and 36 h to measure the colour data. Measurements were carried out with a colorimeter (Konica-Minolta 2600d). The CIE L^* (lightness), a^* (redness) and b^* (yellowness) colour space data were calculated based on the D_{65} illuminant and 10° standard observer with a test-window diameter of 8 mm.

Figure 2.56 represents the superposition effects of photodegradation and thermal treatment, using simultaneous light irradiation and heat treatment. The temperature within the irradiation chamber including the samples was altered (30, 80, 120 and 160 °C), but the light irradiation always remained the same. The lightness value was increased at higher temperatures, but its effect between 30 and 120 °C was moderate. Moreover, the thermal effect of 30 °C is so small that it can be neglected and this circumstance allows the determination of the colour change caused by pure light irradiation (which is UV 30 °C in Fig. 2.56).

The only exception was the Scots pine having great lightness change (more than doubled) between 80 and 120 °C. The other 3 species also doubled the lightness change between 120 and 160 °C. There were no consequent differences in the lightness change among the species. Only Ash was a little more sensitive to the treatment than the others. It seems that the darkening increased exponentially by

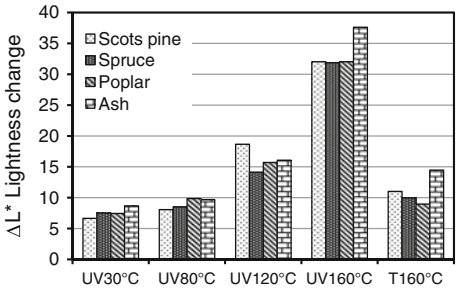

Fig. 2.56 Decrease of lightness (L^*) for the investigated wood species due to UV irradiation at different temperatures (*UV*) and only thermal treatment (*T*) at 160 °C. The duration of all treatments was 16 h

increasing temperature according to the Arrhenius law. (This statement will be clarified later.) The samples in the totally dark chamber showed considerably less darkening at 160 °C (last columns in Fig. 2.56) than the light irradiated samples at 160 °C.

The representation in Fig. 2.56 does not allow deeper insight into the lightness and colour hue variations as a function of influencing factors. Due to the simultaneous action of light irradiation and heat, it is interesting to examine first their separate effects.

The lightness and colour hue (b^*/a^*) variation of the investigated wood species due to pure light irradiation at ambient (30 °C) temperature are seen in Fig. 2.57. (Measurements showed that this low temperature did not cause any colour change during the 16 h in total darkness.) It is striking that in the first part of the treatment, all species became greyer and later, after 6 h treatment, the direction of change turned and the rate of change slowed. In 36 h of irradiation, the samples did not get back their initial colour hue.

The pure heat treatment has shown also remarkable anomalies at 120 and 160 °C temperatures (Fig. 2.58). At air temperatures of 120 °C, all samples moved towards

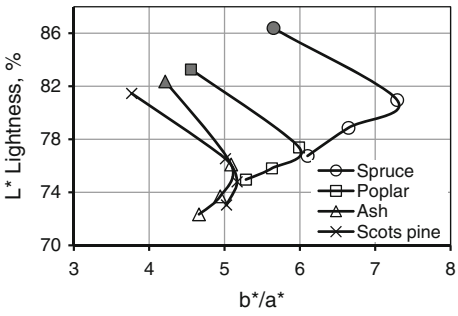

Fig. 2.57 Change of lightness and colour hue due to UV irradiation at 30 °C (*filled marks* means nonirradiated, followed by 6-, 16- and 36-h irradiations)

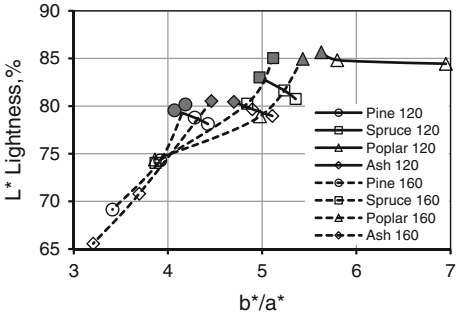

Fig. 2.58 Interaction between lightness and colour hue at heat treatment with different temperatures (*filled marks* means non-treated, followed by 6- and 16-h thermal treatments)

the grey colour hue, although the range of movement was different. Poplar produced the greatest hue change. The change in lightness was moderate in all cases. At 160 °C temperature, however, all samples became more brownish accompanied by high rate of lightness decrease. From these results, it follows that the temperature level, if it is acting alone, plays a definite role in the chemical reactions taking place during heat treatment. The IR measurement demonstrated that lignin did not suffer degradation during pure heat treatment. The thermal degradation of extractives has happened, and it was followed by the creation of quinones generating brown colour. The created brownish colour may partly be originated by the "caramellisation" of the sugar units produced by the degradation of the hemicelluloses as well.

The combined and simultaneous effects of light irradiation and heat treatment are demonstrated in Fig. 2.59. The measurement results show here, more or less, the usual picture; the samples became always more brownish and their lightness reduction is remarkable. An interesting feature is that the course of changes is always the same but naturally temperature dependent. The 160 °C generated much greater lightness and hue change than the 120 °C temperature.

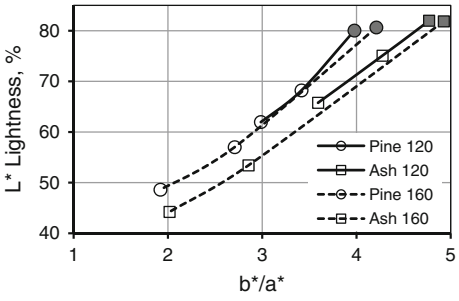

Fig. 2.59 Lightness and colour hue changes at simultaneous UV irradiation and heat treatment (*filled marks* means nonirradiated, followed by 6- and 16-h irradiations)

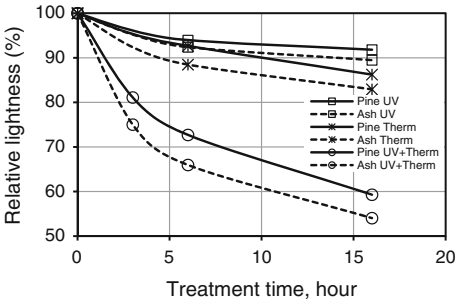

Fig. 2.60 Relative lightness and its components as a function of treatment duration for Pine and Ash (UV at 30 °C, Therm at 160 °C, UV+Therm at 160 °C)

In the following, it is interesting to examine the difference between the separate and simultaneous influences of light irradiation and heat treatment on lightness and colour hue. Knowing the separate effects from Figs. 2.57 and 2.58, they can be compared to those given in Fig. 2.59.

A more illustrative representation of the components and resultant of lightness variations is possible as a function of treatment duration (Fig. 2.60). It can clearly be seen that the sum of components is much less than the resultant due to the simultaneous effects. The simultaneous action of light irradiation and heat strengthen each other and a magnifying factor can be defined as follows:

$$M = \frac{\Delta L_{1+2}}{\Delta L_1 + \Delta L_2}$$

where .

ΔL_{1+2} is the lightness reduction due to combined actions of light irradiation and heat,

ΔL_1 is the lightness reduction due to light irradiation and

ΔL_2 is the lightness reduction due to heat treatment

This relationship is given in Fig. 2.61 for Pine and Ash at two different temperatures. The magnifying is slightly decreasing as a function of treatment duration, and its value fluctuates around two. Probably, the magnifying factor has a maximum somewhere as a function of temperature, for a given irradiation wavelength and intensity. Namely, if one of influencing factors dominates, then its prevailing action governs the lightness reduction and the magnifying factor tends to one. From these experiments, the accurate position of maximum cannot be given, but it is, with high probability, between 120 and 160 °C and nearer to 120 °C than to 160 °C (see the relative position of curves).

A comparison of colour hue is more complicated. The colour hue and its coordinates have a very complicated superposition law which is not known for the mixed colour of wood species. For example, the pure light irradiation and heat

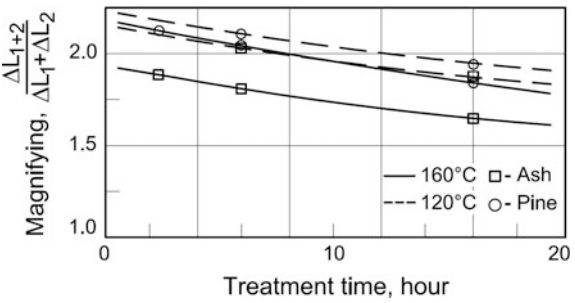

Fig. 2.61 Factor of magnifying as a function of treatment duration for two different temperatures

treatment at 120 °C both produce greyer colour hues, but their combined effect results in browner colour hues (see Figs. 2.57, 2.58 and 2.59).

A rough comparison for heat treatment and combined treatment at 160 °C is possible which is represented in Fig. 2.62. Keeping in mind the initial values and possible final values, the relationship is parabolic. Depending on the colouring materials in wood species, the correlation curves are slightly shifted to each other.

The redness change showed even greater differences between the sum of pure light and heat treatments and the simultaneous light and heat treatment than the lightness change (Fig. 2.63). Publications reported the softening and the condensation of lignin during thermal treatment above 100 °C (Popescu et al. 2013; Hill et al. 2006). It seems that the UV light irradiation is able to create much more quinones during the redistribution and condensation of lignin at 160 °C than at ambient temperatures. These quinone structures are partly responsible for the redness increase.

The yellow colour shift proved to be different compared to the change of lightness and redness. Figure 2.64 shows that there was a significant yellow coordinate increase even at 30 °C. This increase was 91 % for Poplar. (For comparison, the lightness decrease was 9 % and the redness increase was 55 % for Poplar at 30 °C.) The light irradiation at 80 °C produced similar yellowing as at 30 °C. The increase in yellowness is created mostly by the light degradation products of lignin. It means

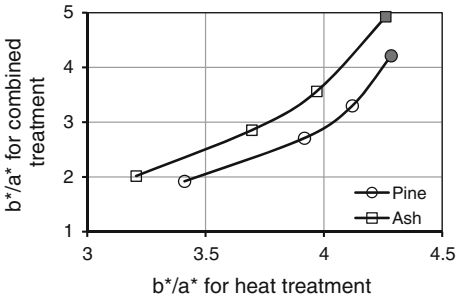

Fig. 2.62 A possible correlation between heat and combined treatments at 160 °C temperature (*filled marks* means non-treated, followed by 2-, 6- and 16-h treatments)

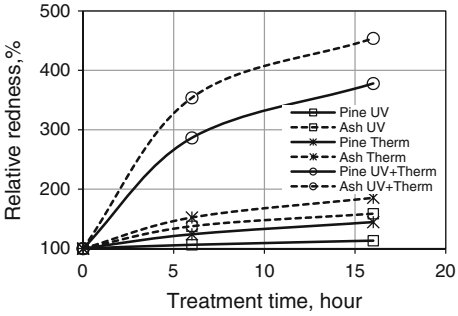

Fig. 2.63 Relative redness and its components as a function of treatment duration for Pine and Ash (UV at 30 °C, Therm at 160 °C, UV+Therm at 160 °C)

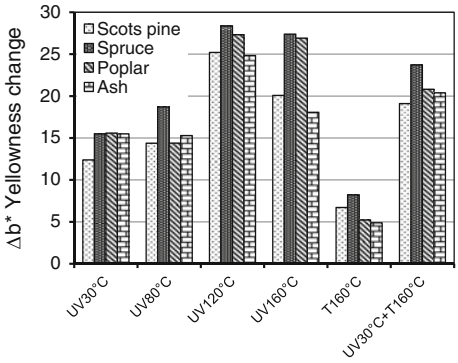

Fig. 2.64 Yellowness (b^*) change of the investigated wood species due to UV irradiation at different temperatures (*UV*) and only thermal treatment (*T*) at 160 °C. The duration of all treatments was 16 h

that the lignin degradation is not temperature dependent within the 30–80 °C temperature range. The only exception was the Spruce, producing considerably greater yellowing at 80 °C than at 30 °C. Spruce was more sensitive to yellowing at all applied treatments than the other species. It seems that the light degradation products of lignin are not enough stable at 160 °C. This high temperature can degrade the newly created chromophore compounds resulting in yellowness decrease. The pure thermal treatment at 160 °C produced much smaller yellowness change than the UV irradiation at the same temperature. Furthermore, this yellowness increase caused by the pure thermal treatment at 160 °C was much smaller than the yellowness increase created by the photodegradation at 30 and 80 °C. In contrast, the redness change was similar caused by both the photodegradation at 80 °C and the pure thermal treatment at 160 °C. These findings strengthen the fact that the red coordinate shift is created mostly by the degradation products of the extractives, while the yellowing is mostly due to the degradation products of lignin.

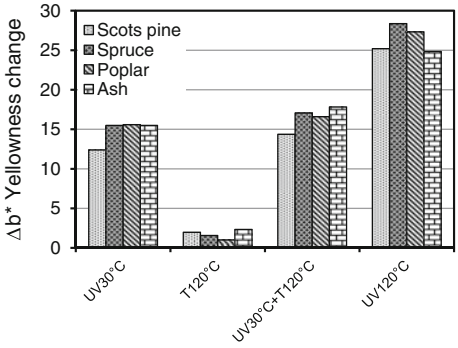

Fig. 2.65 Yellowness change of the investigated wood species due to UV irradiation at different temperatures (*UV*) and only thermal treatment (*T*) at 120 °C. The duration of all treatments was 16 h

The sum of the yellowness changes caused by two independent treatments (UV30 °C + T160 °C) was similar to the yellowness change caused by the simultaneous light irradiation and thermal treatment (UV160 °C). The small difference was positive for Spruce and Poplar and negative for Ash. This similarity does not mean that there is no multiplication effect from simultaneous treatments. Figure 2.64 clearly shows that there is a third effect at 160 °C as well. (The effect of 120 °C is greater than the effect of 160 °C.) Namely, this temperature is high enough to degrade new chemical products of photodegradation. This secondary degradation causes the decrease of yellowness at 160 °C.

At 120 °C, this secondary degradation probably does not occur, or its effect is small. The effects of 120 °C are visible in Fig. 2.65 showing the yellowness change of each wood species. The pure thermal treatment at 120 °C caused only a minor yellowness increase. It is much less than at 160 °C (see Fig. 2.64). The sum of the yellowness changes caused by the two separate treatments (UV30 °C + T120 °C) was considerably smaller than the yellowness change caused by the simultaneous light irradiation and heat treatment (UV120 °C).

The Arrhenius equation (2.33) relates the rate of a chemical reaction k to temperature T, and it includes the activation energy. The equation is simple if the activation energy (E_a) is constant. The Arrhenius equation can be given in the form:

$$k = A\mathrm{e}^{-E_a/(RT)} \tag{2.33}$$

where R is the universal gas constant.

The former form can be written equivalently taking logarithm natural as follows:

$$\ln k = \frac{-E_a}{R}\frac{1}{T} + \ln A$$

An Arrhenius plot displays the logarithm of a kinetic constant (k, ordinate) plotted against inverse temperature ($1/T$, abscissa). Arrhenius plots are often used to analyse the effect of temperature on the rates of chemical reactions. For a single rate-limited thermally activated process, an Arrhenius plot gives a straight line, from which the activation energy (E_a) and the pre-exponential factor (A) can both be determined.

The Arrhenius plots for lightness, redness and yellowness are presented in Figs. 2.66, 2.67 and 2.68, respectively. The data of one selected species are presented in all cases, because the other examined species showed similar behaviours. All Arrhenius plots have a breaking point close to 100 °C. The logarithm of lightness decreased with increasing temperature (Fig. 2.66) shown here by the data of Ash. The tendency of decrease was similar for both dry thermal treatment and combined UV and thermal treatment as well. The intensity of decrease was much greater for combined UV and thermal treatment than for dry thermal treatment. The trend lines show a breaking point. It means that the lightness change is determined by more than one temperature-dependent chemical changes above 100 °C. The hemicelluloses are the most temperature sensitive molecules among the main substance molecules of wood. The thermal degradation of hemicelluloses can be one of the additional chemical changes above 100 °C. The other effect can be the creation of quinones during photodegradation at elevated temperatures. Popescu et al. (2013) reported the softening and the condensation of lignin during thermal treatment at 140 °C. Probably, the UV light irradiation is able to create many more quinones during the redistribution and condensation of lignin at 160 °C than at ambient temperatures. Kubovsky and Kacík (2014) irradiated wood samples by infrared light which was produced by CO_2 laser. They found that the high input of energy accelerates the interaction of the functional groups resulting in the subsequent condensation of lignin. Condensation occurs at the α-carbon to form condensed structures, mainly of the diphenylmethane type. This type of structures oxidises easily and forms quinones which form strong hydrogen bonds with hydroquinone and phenol. Similar quinone structures can be created by UV light at elevated temperature above 100 °C. These quinone structures can be partly responsible for the increase in darkening and for the increase in redness.

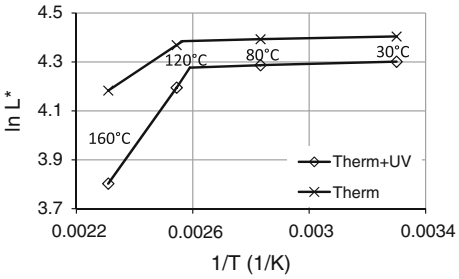

Fig. 2.66 The Arrhenius plots of lightness for Ash samples obtained by UV irradiation (*Therm +UV*) and dry thermal treatment (*Therm*) at the indicated temperatures

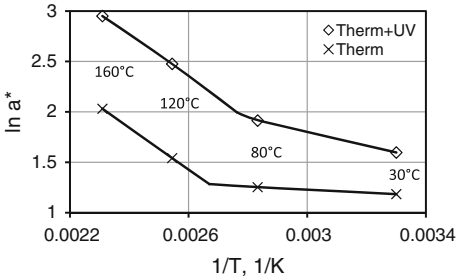

Fig. 2.67 The Arrhenius plots of redness for Spruce samples obtained by UV irradiation (*Therm +UV*) and dry thermal treatment (*Therm*) at the indicated temperatures

The Arrhenius plots of redness are shown in Fig. 2.67 presented here by the data of Spruce. The logarithm of redness increased with rising temperature. The increase was more rapid for combined UV and thermal treatment than for pure dry thermal treatment. The Arrhenius plots are close to linear in both cases. This is because the redness change is determined mostly by the degradation products of the extractives. Having a closer look at the data of Fig. 2.67, a breaking point can be observed between 90 and 100 °C. Below this point, the redness increase was slightly slower for both type of treatment than above this point. This breaking point is located at 95 °C in case of Black locust for the colour modification caused by steaming. The breaking point represents the complexity of the process. The degradation of hemicelluloses becomes visible above this temperature beside the degradation of the extractives. The quinone structures can be partly responsible for the redness increase.

The Arrhenius equation indicates that at any temperature, there will always be some reaction, though it may be immeasurably slow if the temperature is low enough. Even this slow change becomes visible if the time period is long enough. This phenomenon is visible on indoor claddings made of Spruce. The originally yellowish surface becomes more and more reddish during the years even at 20–25 °C.

The Arrhenius plots of yellowness are shown in Fig. 2.68 presented by the data of Scots pine. The logarithm of yellowness increased with rising temperature. The tendency of change was completely different for combined UV and thermal

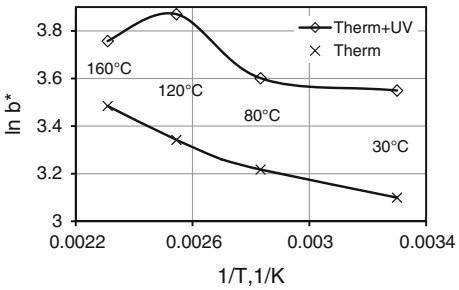

Fig. 2.68 The Arrhenius plots of yellowness for Scots pine samples obtained by UV irradiation (*Therm+UV*) and dry thermal treatment (*Therm*) at the indicated temperatures

treatment compared with pure dry thermal treatment. The pure thermal treatment created continuous, almost linear change with rising temperature. It represents that the thermal degradation of extractives follows the Arrhenius law. There is a hardly visible breaking point here as well, as in Fig. 2.67. The photodegradation of wood at elevated temperature is a highly complex process. That is why the Arrhenius plot is not a straight line. The yellowness change caused by the photodegradation is created mainly by the degradation products of lignin. The lignin degradation is not temperature dependent below 80 °C as clearly shown in Fig. 2.64. Only a small yellowness decrease was detected for Poplar and Ash and a little increase for the conifers between 30 and 80 °C. Above 80 °C, the yellowness increase was rapid, but it is visible only up to 120 °C. Above 120 °C, the degradation products of lignin undergo further thermal degradation reducing the yellowness.

It can be concluded that UV light irradiation produces much greater colour change at elevated temperatures above 80 °C than at ambient temperature. All 3 colour parameters (L^*, a^*, b^*) have shown this magnification effect for elevated temperatures. The colour change caused by UV light irradiation at 30 °C (effect of UV light) was added to the colour change caused by pure thermal treatment at 160 °C. The sum of the colour changes caused by these two separate treatments was considerably smaller than the colour change caused by the simultaneous light irradiation and thermal treatment at 160 °C. The thermal effect during photodegradation was not only the simple addition of two effects, but also the elevated temperature multiplied the effect of photodegradation. The greatest difference was revealed in the redness change.

The Arrhenius plots of all three colour coordinates had a breaking point close to 100 °C, showing that above this temperature the chemical changes are more complex than below this value. The redness changes could be described by the Arrhenius law, indicating that both light and thermal degradations of the extractives are exponential functions of the applied temperatures. The yellowness change caused by pure thermal treatment followed the Arrhenius law; however, the simultaneous photodegradation and thermal degradation did not follow the Arrhenius law.

2.6.3 Air Humidity Dependence of Photodegradation

To test the humidity dependence of photodegradation, Beech and Spruce samples were put into a closed quartz tube (Tolvaj et al. 2015). A water bath under the samples ensured 100 % relative air humidity within the tube (wet condition). The temperature inside the tube was measured by thermocouple. For comparison, samples were closed into a similar dry tube (without water bath). Mercury vapour lamp was used for UV irradiation. The total electric power of the applied double mercury lamps were 800 W, and the samples were located 64 cm from the lamps. The temperature was 32 °C for the first series and 53 °C for the second series within the wet tube during the irradiation. (The temperature within the irradiation chamber was

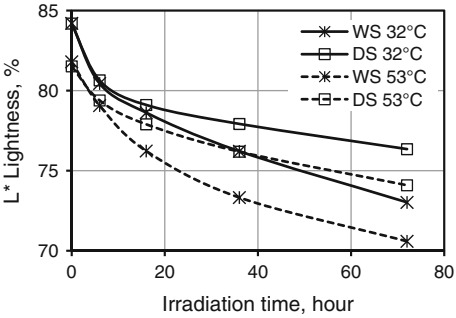

Fig. 2.69 Lightness change of Spruce (*S*) samples due to UV light irradiation under wet (*W*) and dry (*D*) conditions at the indicated temperatures

set to 30 and 50 °C.) The irradiation was interrupted after 6, 16, 36 and 72 h for colour and IR measurements. Five replicates were cut from the same board for both species with a dimension of 30 × 10 × 5 mm. The initial colour data of samples were slightly different used at 32 and 53 °C. The initial moisture content of the samples was 12 ± 1 %, and it increased up to 16 ± 2 % during the treatment at 50 °C.

The usual decrease in lightness was observed in all cases and for both examined species (Fig. 2.69). The rapid decrease in lightness at the beginning was followed by a moderate decrease. The wet condition caused considerably greater darkening than the dry condition at both temperatures. The treatment at higher temperature produced greater differences in lightness between wet and dry condition in the 10–60 h of irradiation.

The wet condition generated greater red colour change than the dry condition for all examined species at both temperatures (Fig. 2.70). The elevated temperature (53 °C) produced more rapid redness increase at the beginning of the treatment than the lower one (32 °C). After 36 h, the trend lines were close to parallel.

The yellow colour change of the samples was similar for both examined species at both temperatures (Fig. 2.71); nevertheless, the wet condition produced a slightly greater change than the dry condition. The treatments generated similar differences at both applied temperatures.

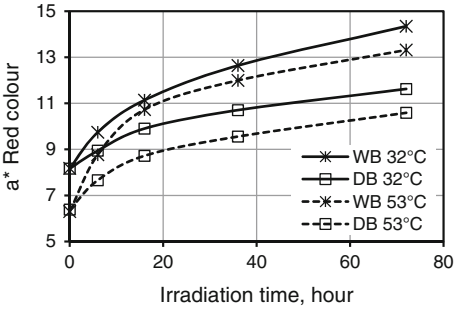

Fig. 2.70 Change in the redness of Beech (*B*) samples due to UV light irradiation under wet (*W*) and dry (*D*) conditions at the indicated temperatures

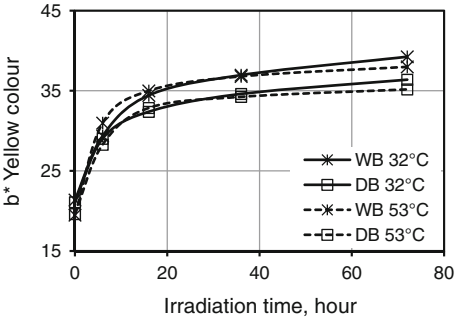

Fig. 2.71 Yellowness change of Beech (*B*) samples due to UV light irradiation under wet (*W*) and dry (*D*) conditions at the indicated temperatures

The wet condition produced considerably greater colour change than the dry condition. This finding is especially important as the air humidity in tropical countries is much higher than in continental climate. Consequently, results of different outdoor weathering tests are not comparable unless the air humidity data are carefully monitored.

Figures 2.72, 2.73 and 2.74 represent the difference IR absorption data of the samples produced by 36-h UV treatment. The UV light induced lignin degradation is clearly shown by the absorption decrease at 1507 cm^{-1} for both wood species.

The wet condition generated greater lignin degradation than the dry condition, i.e. the difference was greater at 53 °C than at 32 °C (Figs. 2.72 and 2.73). This finding is in good correspondence with the colour change data (Figs. 2.69, 2.70 and 2.71). The degradation products of lignin undergo rapid oxidation creating carbonyl groups. These carbonyl groups absorb the IR radiation between 1680 and 1820 cm^{-1}. According to the lignin degradation, the wet condition should generate greater absorption increase in the carbonyl region than the dry condition. It happened only to a small extent. The peak at 1706 cm^{-1} was a little higher in wet condition than in dry condition. The behaviour of the other peak at 1767 cm^{-1} was the opposite. The deviation was even greater at 53 °C. It seems that some parts of the carbonyl groups suffer further degradation.

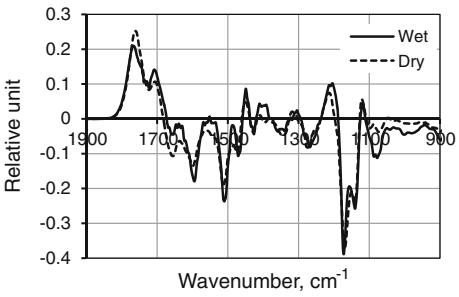

Fig. 2.72 Difference IR spectra of Beech samples caused by 36-h UV treatment at 32 °C under wet and dry conditions

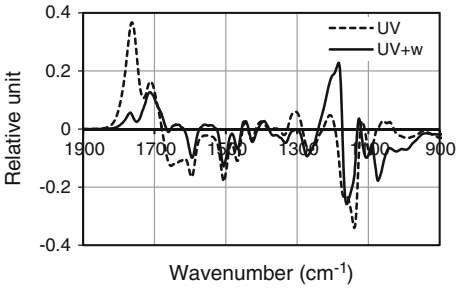

Fig. 2.73 The difference IR spectra of Beech samples caused by 36-h UV treatment at 53 °C under wet and dry conditions

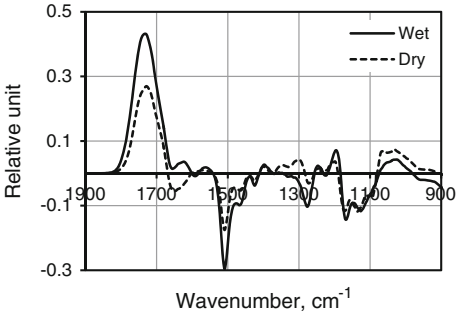

Fig. 2.74 Difference IR spectra of Spruce samples caused by 36-h UV treatment at 53 °C under wet and dry conditions

This is the "leaching" effect of the water molecules. This effect is discussed in details in the Sect. 2.6.4. Liquid water is able to leach out those chemical compounds containing carbonyl groups, which absorb around 1767 cm^{-1}. It seems that water molecules being in the air are able to remove carbonyl groups from the surface of the wood as well. The elevated temperature (53 °C) produced a more intensive removal than the lower (32 °C). The reason is that the vapour molecules move faster at higher temperature.

There are both absorption increases and decreases in the 1100–1300 cm^{-1} wavenumber region (Fig. 2.73). The absorption increases are mainly generated by the irradiation under wet condition. These are not real absorption increases. The increased roughness elevated the spectrum in this region. (Detailed explanation of the phenomenon can be found in the end part of Sect. 2.5.1.) This lifting effect reduced the intensity of the negative peak at 1157 cm^{-1}. The intensity of this negative peak should increase with elapsed irradiation time. But this intensity was −0.18, −0.21 and −0.22 after 16-, 36- and 72-h UV irradiation, respectively. The roughness increase was determined by optical method described in Sect. 2.5.1. The roughness values (Eq. 2.31) were 1.31, 1.34, 1.38 and 1.4 after 6-, 16-, 36- and 72-h irradiation, respectively.

Spruce samples (Fig. 2.74) have shown partly different behaviour than Beech. The lignin degradation at 1506 cm^{-1} was similar, but the absorption increase of the carbonyl groups differed considerably. The wet condition generated greater absorption increase of the carbonyl groups than the dry condition. This is opposite compared to what we have seen in the case of Beech. The 36-h UV treatment in wet condition produced 1.6 times greater absorption increase than in dry condition. This multiplication factor was 1.7 and 1.4 with 16 and 72 h treatment, respectively. The decrease of this multiplication factor indicates the existence of removal effect. The main difference between the IR spectra of Beech and Spruce is that there is no increasing absorption peak at 1760 cm^{-1} for Spruce (see Fig. 2.74). This is the band which was reduced by the leaching effect in the case of Beech.

Our results show that the presence of water vapour intensifies the degradation of lignin. Some parts of carbonyl groups (generated by the lignin degradation) are not stable, and the presence of vapour decreases the number of this chemical group. The increasing temperature amplifies this removing effect.

Nowadays, many papers represent the colour change only by the total colour change ΔE^*. However, the ΔE^* is not always reliable by itself. In some cases, ΔE^* values do not match to the visual observations. Human eyes are highly sensitive to the changes of hue determined by the alterations of a^* and b^*. The total colour change is mainly determined by the change of the dominant component. In the photodegradation of wood, the yellowing is the dominant change since the red colour shift is usually much smaller. These statements are well demonstrated in Fig. 2.75. This figure represents the colour changes of Beech caused by UV irradiation at 53 °C under wet condition (100 % air humidity).

It is clearly seen that the total colour change ΔE^* is mainly determined by the yellowness change. The total colour change was calculated without the redness change ($\Delta E'$) as well. The difference between these two curves (ΔE^* and $\Delta E'$) is negligible. It suggests that the effect of redness change is also negligible for the total colour change. This redness change is large enough to be visible to the naked eye. This example shows the disadvantage of using total colour change as one single indicator.

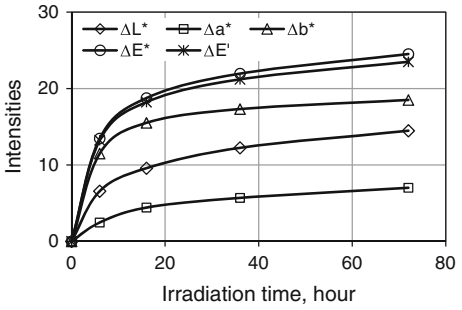

Fig. 2.75 The change of colour parameters for Beech caused by UV light irradiation under wet condition at 53 °C (ΔL is the absolute value of the lightness change and $\Delta E'$ is the total colour change calculated without the redness change)

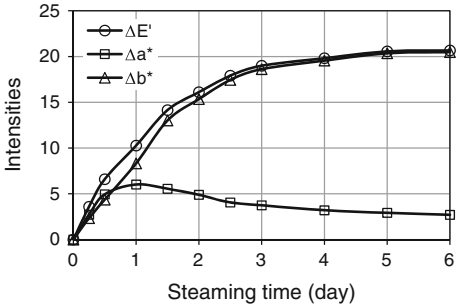

Fig. 2.76 The change of colour parameters for Black locust caused by steaming at 115 °C (Δb^* is the absolute value of the yellowness change and $\Delta E'$ is the total colour change calculated without the lightness change.)

As the changing tendencies of all three colour coordinates are similar, their ratio within the total colour change is not visible in Fig. 2.75. Another example is given in Fig. 2.76. The colour of Black locust can be considerably modified by steaming. During the process, its dominant unattractive yellow colour decreases, while the redness increases during the first day but decreases during the remaining period of the treatment. The total colour change ($\Delta E'$), calculated without the lightness change, does not follow the redness change. However, it is determined by the more intensive yellowness change.

These examples prove the weakness of the total colour change as one single parameter for monitoring colour alterations. The total colour change is determined mainly by the dominant changes and it disregards the small but visible alterations. Therefore, the three colour coordinates supply much more and detailed information than the total colour change.

2.6.4 Effect of Water Leaching

Beside sun radiation, the leaching effect of the rain is the second harmful factor effecting the degradation of outdoor wood. These effects were simulated by the following experiments. Samples were irradiated by mercury lamp and then plunged into distilled water for 1 day. Figure 2.77 represents the effect of the 1-day UV treatment of Spruce earlywood followed by 1-day of leaching in distilled water. The same initial spectrum was subtracted from the treated spectrum to calculate the difference spectra in both cases. The first difference spectrum presents the effect of UV treatment alone, while the second one shows the effect of UV treatment and the subsequent water leaching together. The UV light induced lignin degradation represented by the absorption decrease at 1507 cm^{-1} is clearly visible (Fig. 2.77). The water leaching did not affect this peak. The UV treatment produced great absorption increase in the unconjugated carbonyl region (1670–1820 cm^{-1}).

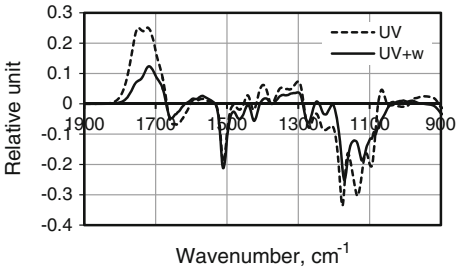

Fig. 2.77 Absorption change of Spruce earlywood after 1-day UV treatment (*UV*) and 1-day UV treatment followed by 1-day water leaching (*UV+w*) (the initial spectrum was the reference in both cases)

Two peaks arose close to each other during the one-day treatment. (The longer treatment unites these bands into one band with a maximum at 1720 cm^{-1}.) The intensity of this band was reduced considerably by leaching. The intensity of both peaks (1713, 1736 cm^{-1}) decreased but to a different extent. The peak at 1713 cm^{-1} lost half of its intensity, while the other peak at 1736 cm^{-1} almost disappeared and remained only as a shoulder. The little shoulder at 1680 cm^{-1} became clearly visible after leaching, strengthening the claim that three peaks arose in the unconjugated region as the result of photodegradation. This third peak was hardly affected by water leaching. The UV treatment generated absorption decrease in the ether bond region (1070–1200 cm^{-1}). Three negative bands occurred representing the splitting of the ether bond in the cellulose chain, in the pyranose ring and in the aromatic system.

Examining the photodegradation and leaching properties of Beech (Fig. 2.78), similar changes were found compared to Spruce earlywood. The lignin content was not affected by the water leaching. It is exemplified by the negative peak at 1596 and 1508 cm^{-1}. The water leaching does not change the intensity of these lignin peaks. Here, the apparent difference is visible because of baseline shift. The UV radiation degraded the conjugated carbonyl groups in the extractives presented here

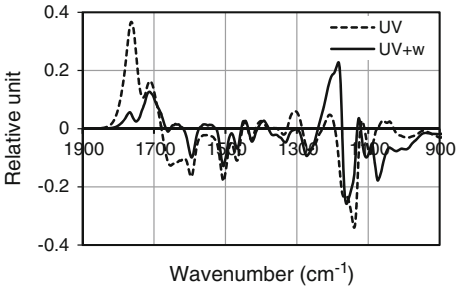

Fig. 2.78 Absorption change of Beech after 1-day UV treatment (*UV*) and 1-day UV treatment followed by 1-day water leaching (*UV+w*) (the initial spectrum was the reference in both cases)

by the absorption decrease around 1650 cm^{-1}. The subsequent water leaching eliminated this negative peak. An absorption band of water is located here as well. Probably, the moisture content of the samples after leaching and drying was not exactly the same as the initial moisture content of the untreated samples. The absorption increase of the water overlapped the absorption decrease of the conjugated carbonyls creating zero difference. This effect is visible in Figs. 2.72 and 2.74 but in different quantity.

Two peaks were grown up in the non-conjugated carbonyl region (1670–1820 cm^{-1}) as a result of the UV light induced lignin degradation. The stability of these two peaks is not equal. The peak at 1706 cm^{-1} was hardly affected by the water leaching, while the other peak at 1767 cm^{-1} was mostly removed by the water leaching. This erosion of the surface allows the photodegradation of the next layer. As the earlywood is more degradable than the latewood, the outdoor surface of wood will become rougher during the years.

The interpretation of the changes in the ether band region (1100–1200 cm^{-1}) is difficult. Although the absorption intensities were calculated from the diffuse reflectance spectra using the K-M theory, this theory does not work well in this region where the absorption of wood is strong (see Sect. 2.5.1). The increasing roughness lifts up the difference spectrum confusing the real changes. The water leaching (and drying) produces roughness increase too (see later in Sect. 4.10). The swelling lifts up the cut end of the fibres, and the drying does not bring them back creating a microlevel increase in roughness. The lifting effect is more visible in Figs. 2.79 and 2.80.

To monitor the effect of repeated rainfall, the samples were irradiated by mercury lamp (first time 1 day) followed by water leaching (always 1 day). The repeated light irradiations were for 2 days followed by 1 day water leaching. For comparison, continuous light irradiation (without leaching) was also carried out. Results of light irradiation are presented here until the 7th day (4 cycles). Small samples (30 × 10 × 5 mm) were dried at room temperature for a week after water leaching for IR measurement. The changes were always compared to the untreated

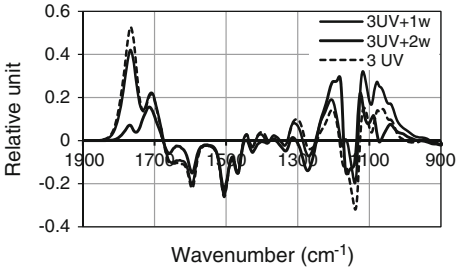

Fig. 2.79 Absorption change of Beech after different treatments (the reference is the initial spectrum in all cases.). *Legend* 3 UV = 3-day UV treatment; 3UV+1w = 1-day UV irradiation, 1-day leaching followed by 2-day UV irradiation; 3UV+2w = 1-day UV irradiation, 1-day leaching, 2-day UV irradiation followed by 1-day leaching

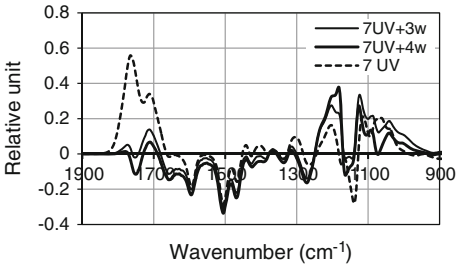

Fig. 2.80 Absorption change of Beech after different treatments (the reference is the initial spectrum in all cases). *Legend* 7 UV = 7-day UV treatment; 7UV+3w = 1-day UV irradiation and then 1-day leaching followed two times by the combination of 2-day UV irradiation and 1-day leaching and then finished with 2-day UV irradiation; 7UV+4w = 1-day UV irradiation and then 1-day leaching followed three times by the combination of 2-day UV irradiation and 1-day leaching

samples independently of the numbers and type of treatment. Always the initial spectrum was subtracted from the treated one to create the difference spectrum.

The lignin degradation (presented by the absorption decrease at 1505 cm^{-1}) was similar for both continuous UV treatment and UV treatment interrupted by water leaching in the case of all cycles. This experience confirms that the lignin degradation was not affected by water leaching. The results of the second series of treatment are presented in Fig. 2.79. The 1 + 2-day light irradiation produced similar but only a little greater changes than the 1-day light irradiation. The 3-day continuous UV treatment created a little greater absorption increase at 1767 cm^{-1} than the treatment interrupted by leaching. The only important difference between Fig. 2.78 and Fig. 2.79 is that the K-M transformation lifts up the difference spectrum between 1070 and 1200 cm^{-1} because of the increasing surface roughness of the samples. The lignin degradation was continuous with increasing light irradiation for both UV treatment types (with and without leaching). The absorption of carbonyl groups at 1767 and 1706 cm^{-1} increased continuously only for continuous UV treatment.

The UV treatment interrupted by leaching created a declining rate of production of carbonyl groups. The intensity of the peak at 1706 cm^{-1} decreased slowly after the second cycles, but the intensity of peak at 1767 cm^{-1} decreased rapidly. This phenomenon can be interpreted by the lack of the lignin molecules on the surface of the sample. The reduction of the absorption increase at 1767 cm^{-1} is clearly visible in Fig. 2.80. This absorption increase was negligible even before the water leaching during the fourth cycles (7UV+3w). The next leaching reduced this small positive peak as well. The fourth day of leaching created a negative peak at 1750 cm^{-1}.

This absorption decrease did not originate from the carbonyls created by photodegradation, but displays the degradation of carbonyl groups being originally in the untreated wood. This negative peak was never found before. Our suggestion was that the water leaching generated this negative peak independently from photodegradation. To clarify the reason for the absorption decrease at 1750 cm^{-1},

wood samples were put into distilled water to find out the effects of pure water leaching. After a 3-day leaching, a small absorption decrease at 1750 cm^{-1} was detected, and it became clearly visible after the fourth day of leaching. This finding proves that the rain is able to leach out not only the carbonyl groups created by photodegradation but also some type of carbonyls originally present in the wood.

2.7 Hardness of Wood Surfaces

The durability and mechanical resistance of wood surfaces against different kind of loadings (static, dynamic, concentrated, frictional, etc.) considerably depend on their hardness. Hardness measurements are widely used in the metal industry, and several standardised methods are known. Due to the structural properties of wood, hemispherical indenters are more suitable for hardness determination in the wood industry. The diameter of indenters varies generally between 25 and 35 mm, and the earlier users have often used inch dimensions (e.g. 5/4 inch).

Hardness measurement of wood materials have been begun 100 years ago thanks to the pioneering work of Janka (Janka and Wien 1912; Janka et al. 1915) who proposed and introduced the application of hemispherical indenter in 1912. The hemispherical shape also allows a more accurate mathematical treatment although the combined elastic–plastic deformations taking place in the wood material gives rise to some difficulties in the evaluation of the measurement results.

The mode of loading on the surface by spherical indenters may be static or dynamic (Fig. 2.81). With static loading, the indenter is pushed into the surface with low velocity, and the force is recorded as the function of displacement. If the sinkage of indenter is prescribed, then the measurement of the maximum force is also sufficient.

Performing dynamical measurements, a metal sphere with a mass m is dropped onto the surface from given height h having the kinetic energy of:

$$E = mgh = \frac{m}{2} v_0^2$$

The hardness is a secondary mechanical property due to its complicated multi-axial stress state, the anisotropy of wood and permanent deformations. Its numerical measure considerably depends on the measurement technique used.

The calculations are based on a simplified engineering mechanics (Hertz and Boussinesq problems) supposing small deformations. In spite of these simplifications, however, the hardness of wood is a useful mechanical property for comparing different wood species concerning their surface stability and durability.

Using the static measurement method, a spherical indenter with a radius R is pressed into the wood surface and, according to the Hertz theory, the force F is calculated with the following relationship:

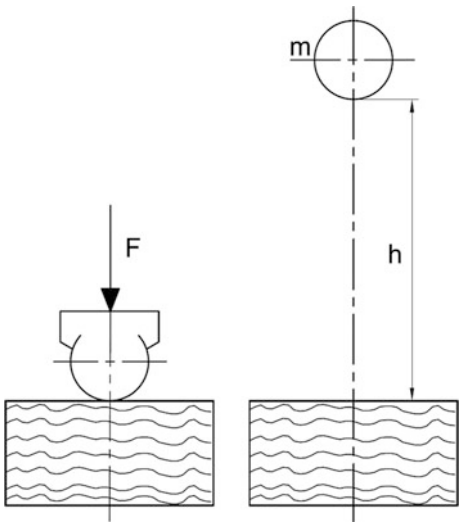

Fig. 2.81 Static and dynamic measurement method for hardness

$$F = \frac{4}{3}\frac{E}{1-v^2}\sqrt{R}z^{3/2} = Bz^{3/2} \tag{2.34}$$

where E and v are the modulus of elasticity and Poisson's ratio, respectively, and z is the deformation under the indenter.

In Hungary, a spherical ball of 5/4 inch dia. has long been used with a fixed 2-mm deformation. In this case, the hardness H_w is characterised by the material property $E/(1 - v^2)$, and it is given by:

$$H_w = \frac{E}{1-v^2} = \frac{F}{\frac{4}{3}\sqrt{R}z^{3/2}} = \frac{F}{15} \quad \mathrm{N/mm^2} \tag{2.35}$$

where F is the force for the given deformation of $z = 2$ mm.

From Eq. (2.35), the reference surface area under the indenter is given as follows:

$$A = \frac{4}{3}\sqrt{R}z^{3/2}$$

Sometimes, the contact surface of the indenter as a reference area was proposed. The surface of the spherical calotte (A_c) is given by the equation:

$$A_c = 2\pi Rz$$

which fundamentally differs from the above reference area equation and indicates that the use of this latter surface area is theoretically not correct.

The dynamic measurement method generally uses a metal sphere with the mass m, and it is dropped onto the surface from given height h. Using the energy equation, we may write as follows:

$$mgh = \int_0^{z_0} F(z)\mathrm{d}z$$

where the force function is given by Eq. (2.34). Integrating the above equation yields as follows:

$$H_\mathrm{d} = \frac{E}{1-v^2} = \frac{mgh}{\frac{8}{15}\sqrt{R}z_0^{5/2}} \quad \mathrm{J/cm^3 or\ N/cm^2} \tag{2.36}$$

Now, the denominator has the dimension of cm^3, but this volume again is not identical with the volume of the spherical calotte. The maximum deformation z_0 can be obtained from the measured radius of the imprint (Fig. 2.82) by the simple relation:

$$z_0 = R - \sqrt{R^2 - r^2}$$

The maximum deformation can also be expressed from Eq. (2.36) as follows:

$$z_0 = \left(\frac{2.5\,mgh}{B}\right)^{0.4} \tag{2.37}$$

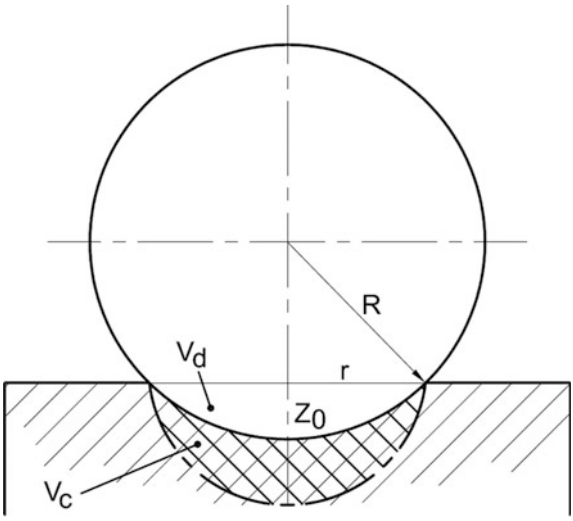

Fig. 2.82 Deformations under spherical indenter

Table 2.3 Calculated hardness values

	r mm	z_0 (mm)	H_d (N/mm^2)	V_d (mm^3)	F_{max} (N)	T (s)	v (m/s)
Ash	5	0.57	2835	22.5	7674	12.76×10^{-4}	2.1
Spruce	7.5	1.305	358	116.44	3354	6.19×10^{-4}	2.1

Keeping in mind Eq. (2.34), the maximum impact force can be obtained as follows:

$$F_{max} = B^{0.4}(2.5\,mgh)^{0.6} \tag{2.38}$$

The use of the above method is demonstrated with the following example: using a steel ball of 7/4 inch dia. (R = 22.2 mm), its mass is 0.357 kg and the drop height is 0.5 m. The potential energy is mgh = 1.751 Nm. Measurements were performed on strip flooring elements made of Ash and Spruce. The radii of permanent deformations were 5 and 7.5 mm, respectively. The calculated values are summarised in Table 2.3.

The wood is viscoelastic material over time. Therefore, it is interesting to calculate the average loading velocity which is determined by the deformation z_o and the impact duration T:

$$v = z_0/T \quad \text{and} \quad T = 0.946\frac{\pi}{2}\frac{z_0}{v_0}$$

where v_0 is the falling velocity ($v_0 = \sqrt{2gh} = 3.132$ m/s).

The impact duration somewhat shorter compared to the linear elastic case (note that the exponent in Eq. (2.34) is 1.5). As Table 2.3 shows, the loading velocity in both cases is 2.1 m/s. This value with all probability is not far from the critical speed corresponding to the infinitely high loading velocity (Sitkei 1994b). Therefore, in this case, the viscoelastic effect should not be taken into consideration.

From certain point of view, the energetic concept might be used also here. The energy transmitted to the body is consumed by permanent deformations which consist of two parts: the visible displaced volume and a compacted volume accommodating the displaced volume (Fig. 2.82). The specific absorption energy is expressed in the following form:

$$E_w = \frac{mgh}{V_d + V_c} = \frac{mgh}{(\psi + 1)V_d} \quad \text{J/cm}^3 \tag{2.39}$$

where the displaced volume is given by:

$$V_d = \pi z_0^2\left(R - \frac{z_0}{3}\right) \tag{2.40}$$

and the compressed volume below the surface is approximated as follows:

$$V_c = \psi V_d \quad \text{and} \quad \psi = \frac{\rho_w}{\rho_0 - \rho_w} \tag{2.41}$$

where ρ_0 is the density of compressed wood below the surface, and ρ_w is the volume density of wood.

The compressibility of wood against the infinite half space is an interesting question, and to our best knowledge, it was never investigated. Some observations on the surface compaction of wood due to blunt tool edges, however, have shown that the compacted wood density generally varies between 1.1 and 1.2 g/cm^3. Figure 2.83 shows the expected values of the factor ψ as a function of volume density of wood. Hardwood and softwood show a considerable difference in their compressibility: the Ash has ψ values around 2.2, while the Spruce only around 0.65. Using these values, the total deformed values amount to 0.072 and 0.192 cm^3, respectively, and the specific absorbed energies have values of 24.3 and 9.12 J/cm^3, respectively.

It can be stated that both methods are suitable to characterise wood hardness with acceptable accuracy and resolution. The hardness based on the modulus of elasticity, Eq. (2.36), has better resolution, and it is more suitable to distinguish individual specimens within wood species.

The hardness measurement methods of Janka and Brinell–Mörath are often used also today. They can easily be interpreted in terms of engineering mechanics described above.

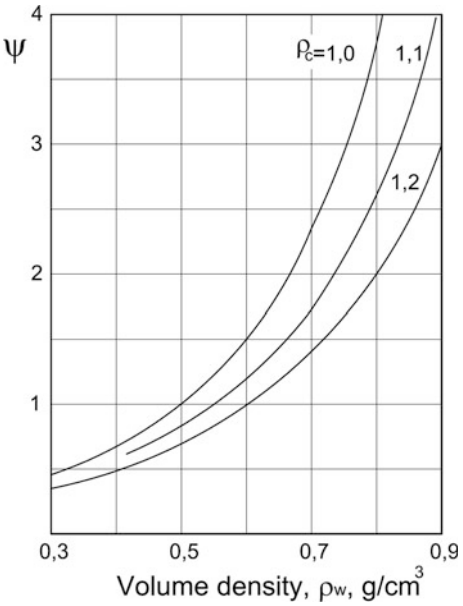

Fig. 2.83 The relative compressibility of wood as a function of initial volume density

Janka (Janka 1912; Janka et al. 1915) used a steel ball of 11.284 mm diameter and pressed half into the wood surface, and the deformed cross section was 100 mm^2. The hardness H_J was defined as the required force F divided by the deformed cross section:

$$H_{\mathrm{J}} = \frac{F}{100} \quad \mathrm{N/mm^2}$$

Substituting the known values into Eq. (2.34), we get

$$\frac{E}{1-\nu^2} = \frac{F}{42.44} \quad \mathrm{N/mm^2}$$

and a comparison of the above equations yields as folows:

$$H_{\mathrm{J}} = 0.4244 \frac{E}{1-\nu^2}$$

giving a linear relationship between the two methods.

The Brinell–Mörath method uses a 10-mm-dia. steel ball and presses it into the wood surface with a given force of 500 N, and the depth of deformation is measured. The force divided by the deformed surface as a spherical calotte gives the hardness, that is

$$H_{\mathrm{BM}} = \frac{F}{D\pi z} \quad \mathrm{N/mm^2}$$

where D means the diameter of the deformed surface. Using Eq. (2.34), it can be shown that in this case

$$H_{\mathrm{BM}} = 0.5235 \left(\frac{E}{1-\nu^2} \right)^{2/3} \quad \mathrm{N/mm^2}$$

which results in a nonlinear relation between the Brinell–Mörath hardness and the deformation modulus. The following Table 2.4 summarises average hardness values in N/mm^2 for comparison concerning different wood species.

Due to the high portion of plastic deformation at the Janka's method, values of H_{J} and H_{BM} are hardly comparable. The dynamic method (see Table 2.3) gives higher H_{d} values, with all probability, due to the elastic recovery which lowers the perceptible deformation and so increases the apparent hardness.

Table 2.4 Comparison of different hardness values

Species	H_J	H_{BM}	$E/(1-\nu^2)$
Spruce	25	14	140
Pine	33	18	200
Larch	37	20	240
Linden	25	15	155
Beech	60	32	480
Oak	70	34	520
Ash	70	34	520
Hornbeam	75	36	570
Sugar maple	80	40	670
Black locust	100	48	880
Blue gum	80	40	670
Ironwood	130	75	1700
Guaiacum off.	180	86	2100

Note Ironwood = *Olea capensis*, 1020 kg/m^3

2.8 Abrasion Resistance of Wood Surfaces

Utility surfaces of various wood products such as horizontal surfaces of kitchen furniture and flooring in living room are subjected to different, mostly frictional loadings causing wear. The wear process is associated with material loss, deterioration of surface coating, change in colour, loss of gloss and appearance of scratches. All these changes may severely lower the overall utility value of the product, especially its aesthetical value.

The loading conditions of utility surfaces may be quite different, and they are always occasional, concerning a given surface area of probabilistic nature. Therefore, the surface appears to be not evenly worn. Due to the dominating frictional forces, the wear process is mainly abrasive, sometimes enhanced by heat and moisture. Local damages of the surface are generally due to sharp or pointed tools.

The design of utility surfaces requires the careful selection of materials that offer maximum abrasion resistance to all expected loadings. For this reason, the knowledge of abrasion resistance of different wood species is indispensable. If necessary, the abrasion resistance of natural wood surface can be improved using various surface treatments and coatings.

The abrasion resistance of wood surfaces can be determined by the use of different laboratory equipments attempting to imitate real loading conditions. Key factors that must be considered in developing and using an abrasion test include as follows:

- time and kind of contact between the material and the abrading surface,
- the normal load on the abrading surface,
- the speed of the sliding action between the surfaces,

– the temperature at the interface,
– minimum alteration in the surface of abrading material,
– an easy and uniquely defined evaluation of wear and
– a possible correlation between laboratory test results and real wear experiences.

These requirements can only be partially satisfied. Till now, only one standard abrasion procedure is accepted, that is the Taber Abraser. The abraser consists of two rollers coated with sanding paper and mounted on a self-balanced axle. The grade of abrasive material is specified for solid wood, coated and laminated surfaces. The axle is loaded with a given vertical force, and the sample is rotating under the rollers as shown in Fig. 2.84. It is important that the axis of the wheels is shifted from the centre of rotation by about 3/4 inch and the drifting angle is around 30°. The abraded surface is an annulus, and the wear is assessed in terms of quantity of material lost for a given standard condition.

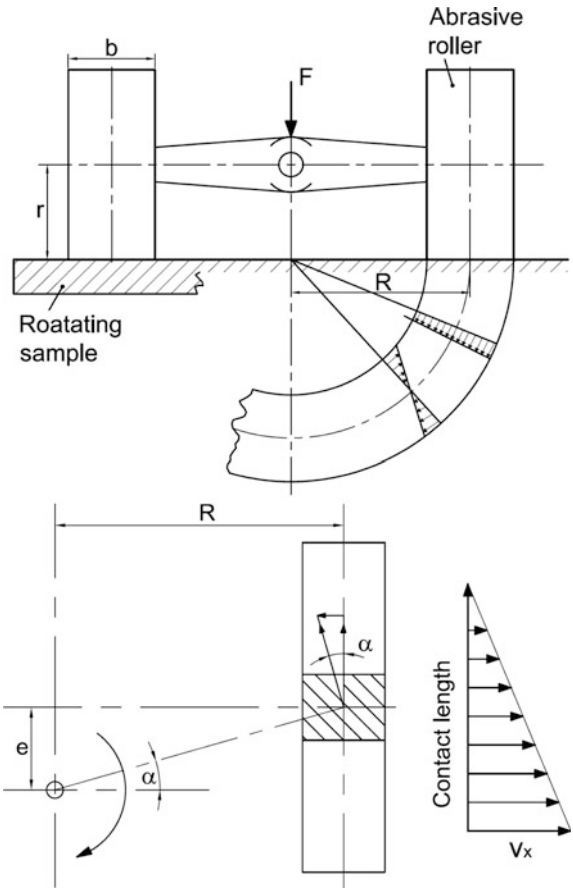

Fig. 2.84 Working principle of Taber Abraser

The sliding action between the material and abrasive rollers is due to the relative motion between them which is characterised by the wheel slip. The resultant slip has three components. The first is due to the rolling resistance of rollers, and the second one is due to the circular motion of the rollers with finite width. The first component is not more than 2–4 %, while the second component is depending on the ratio of the roller width to the diameter of rotation path:

$$S = \pm \frac{b}{2R} \tag{2.42}$$

where
S is the slip,
b is the roller width and
R is the radius of the wheel centre line.

The slip changes its sign at the outer and inner side and has values between 12 and 20 %. It is clear that the slipping of rollers across the width is not constant.

The third slipping component is due to the drifting motion of wheels. The resultant slip in the abraded annular track governs the trajectory of grits during their contact with the wood sample which are depicted in Fig. 2.85. Due to the opposite direction of wheel rotations, the trajectories are crossing each other almost perpendicularly. Using rough sandpaper grade (P-40), the trajectories are fully visible on the abraded surface.

Using the general theory of the sanding process, the working process of the Taber Abraser can be approximated. The quantity of removed material related to the unit width is given by the following equation (Csanády and Magoss 2013):

$$\frac{V\gamma}{b} = BLpv_c t \tag{2.43}$$

where
V is the removed material volume,
γ is volume weight of the wood material,

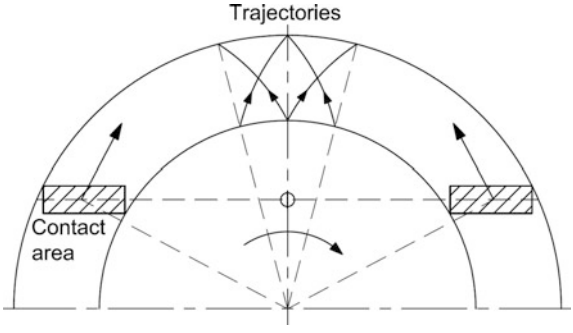

Fig. 2.85 Grit trajectories in the annular track

b is the width of rollers,
B is a material constant related to the unit width, 1/cm,
L is length of sanding path,
p is the surface pressure,
v_c is the sanding velocity and
t is the elapsed time.

The length of the sanding path is equal to the distance done in one rotation, $L = 2R\pi$. An estimate for the sanding velocity requires some considerations. The velocity of rollers is simply given by the relation:

$$v_r = 2R\pi n \quad \text{cm/min}$$

where n is the rotation speed, rpm. The actual sliding velocity is proportional to the slip, and therefore, the sanding velocity is approximated as follows:

$$v_c = 2R\pi nS \tag{2.44}$$

where S is the average slip in the contact surface.

The estimation of the contact pressure may also cause some troubles. The contact pressure for a cylindrical body contacting the plane surface is proportional to the square root of the line load on the wheels. At the same time, the contact width and thus the contact surface is also proportional to the square root of the line load. Therefore, theoretically, the line load on the wheels proportionally increases the removed material. The theory assumes, however, that the rollers are rigid and the surface is perfectly smooth. None of these assumptions are valid in this case.

The rollers are covered with sandpaper, and its deformation behaviour under loading may be very uncertain. The sandpaper by its own deformation increases the contact surface and lowers the pressure in the contact area.

A further fundamental problem is the surface roughness of the wood sample. With rigid wheel and smooth surface, the deformations under the rollers fall into the range of 0.5–1.0 μm, which is much smaller than the roughness heights of the surface.

Examining the Abbott material ratio curves (see Fig. 4.12 in Sect. 4.4), we see that using sharp tools at least to a depth of appr. 20 μm, we may expect layers dense enough to carry the given load. Taking deformation of 20 μm, the corresponding contact width will be appr. 2 mm. Nevertheless, it seems to be well-established that the pressure under the wheels is at least one magnitude higher than those used in the common sanding operation.

It was observed that after a "running-in" period (some 100 revolutions), the surface roughness in the track will have a stationary value corresponding to the given conditions related to sandpaper grade, load on the rollers and the abraded material. In this case, the wear process on the surface will also be stationary and only the continuous wear of the abrasive material decreases the removed material as

Table 2.5 Roughness of the machined Beech sample and the abraded surface

	R_z	R_a	R_q/R_a	R_{ku}	R_{sk}	R_{pk}	R_k	R_{vk}	$R_a/\sqrt{R_k R_z}$
Initial	40.3	5.1	1.37	4.9	−1.1	4.6	12.7	15.7	0.226
	40.6	4.3	1.47	8.5	−1.2	5.9	9.5	9.5	0.218
Track	74.7	11.9	1.25	3.2	−0.4	10	37	23.5	0.226
5 N/cm	76.5	11.2	1.3	3.8	−0.04	14.3	36.5	20.5	0.211
Track	77.3	12	1.3	3.8	−0.5	10.5	40.7	25	0.213
10 N/cm	70	10.9	1.3	3.8	−0.6	10.1	32.5	24.5	0.23

a function of time. The latter can be described with exponential function which makes possible the evaluation of measured results.

As an example, Table 2.5 shows roughness measurements on a machined Beech sample in two directions perpendicular to each other and in the track abraded with 5 and 10 N/cm line load. It is interesting to note that a load change from 5 to 10 N/cm in the same abrading process has made an abnormal wear process in the next 100 revolutions. The difference in roughness shown in Table 2.5, would give no reasons for a deviation in the wear process. A closer look at the grit trajectories in the track, however, revealed that the slightly higher slip at 10 N/cm load will rearrange the trajectories, and the grits recarve the ridges running along the previous trajectories. As a consequence, the amount of the abraded material will be considerably higher than in the stationary process.

As it is already mentioned above, the performance of sandpapers does not remain constant as a function of time. It decreases, with good approximation, according to an exponential function of the form:

$$\frac{\mathrm{d}G}{\mathrm{d}t} = G_0 \mathrm{e}^{-\beta t} \tag{2.45}$$

where G_0 is the initial wear rate and β characterises the decrease in the performance of the sandpaper. The reciprocal value of β is the often used time constant T.

The integral of the above equation gives the removed material as a function of time:

$$G = \frac{G_0}{\beta}(1 - \mathrm{e}^{-\beta t}) \quad \mathrm{mg/cm} \tag{2.46}$$

Figure 2.86 shows experimental results on Beech samples with two different loads on the rollers as a function of rotation number. The course of the material loss fully obeys Eq. (2.46), except the first point at $N = 100$ rotations. From these results, the time constant β and the material constant G_0 can uniquely be determined. Their values are $\beta = 0.0339$ 1/min (or $T = 29.5$ min) and $G_0 = 37$ mg/cm min.

A stationary wear process was assumed, and the variation in material loss was attributed to the continuous wear of the sand paper. In the first phase of the wear

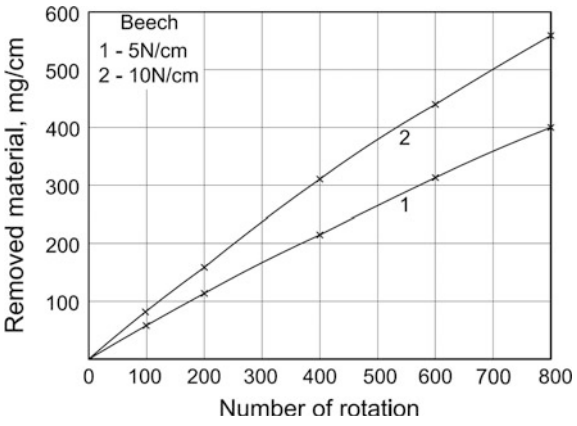

Fig. 2.86 Material loss of Beech samples as a function of number of rotations with two axle loads

process, however, the surface roughness may enhance the wear significantly. In Fig. 2.86, the material loss at N = 100 rotations was 9 % higher than value extrapolated from the overall courses of the wear curve. This deviation is probably due to the influence of the initial roughness on the dynamics of the wear process.

Using rough abrasive materials (P-32, P-40) with grit diameters around 400 μm, in the initial phase each particle can bite a full chip from the relatively smooth surface. As the surface becomes rough with deep furrows, the bite of some grits may be less resulting in a lower wear rate.

In the following, we assume that Eqs. (2.45) and (2.46) are formally valid also for the initial phase of the wear process with the difference that in the first, relatively short phase, the time constant is determined by the change of surface roughness due to the continuous wear. Using the experimental results for Beech wood, the approximate dynamics of the wear process is represented in Fig. 2.87. The two curves with different time constants have the common form:

$$\frac{\mathrm{d}G}{\mathrm{d}t} = G_{0\mathrm{i}}\mathrm{e}^{-\beta_{\mathrm{it}}} \quad \mathrm{mg/min} \tag{2.47}$$

where G_{0i} is the initial wear rate and β_i is the time constant in the particular section. The elapsed time (t) is given by the number of rotations t = N/60.

During the first 100 rotations, the surface roughness affects the wear rate with a time constant of β_1 = 0.154 1/min (T = 6.5 min) and the initial wear rate is 44.3 mg/min. After 100 rotations, a stationary wear process develops and the further moderate decrease in the wear rate is governed by the deteriorating performance of the abrading material. The stationary wear process would have an initial rate of 37 mg/min with a time constant β_2 = 0.0339 1/min (T = 29.5 min). It is interesting to note that the time constant of the stationary wear process is not far from those found for sanding (T varies between 30 and 60 min).

The two curves in Fig. 2.87 should be determined under the following conditions:

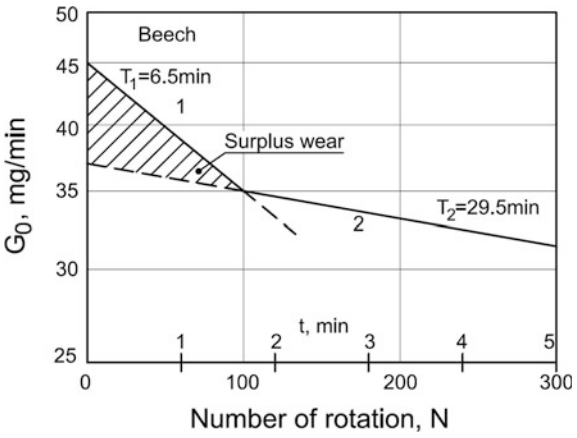

Fig. 2.87 Change of the wear rate in the initial and the stationary phase with different time constants for Beech wood. $P' = 5$ N/cm

- The stationary wear curve (2) is the best fit for all experimental points except the first point at $N = 100$ rotations.
- The curve for the initial wear phase (1) intersects the stationary curve at $N = 100$ rotations, and its integral between zero and 100 rotations gives the experimentally obtained value at $N = 100$ rotations.

The wear rate does not follow the theoretically expected values with different roller loads (0.5 or 1.0 kg). If the load is doubled, the wear rate increased by only some 40 %. There may be many reasons for this. The most important factor is probably the relatively high surface pressure in the contact area. The surface is deeply furrowed at 0.5 kg load, and with a further increased load, the grits cannot proportionally remove more material. Therefore, it is wise to use the same wheel load in comparison studies.

Coated utility surfaces (flooring parquet) were tested for abrasion resistance in the same way with the difference that a finer grade of abrasive sandpaper, P-150, was used. Figure 2.88 shows experimental results for clear coated parquet made of Jatoba (Hymenaea courbaril). To get reliable result for a detailed evaluation, the measurement was continued up to 1000 rotations with 0.5-kg wheel load. The measured points obey the exponential law and allow a reliable evaluation.

During the first 100 rotations, the running-in period, the wear rate considerably exceeds the stationary value (Fig. 2.89). Therefore, it is not recommended to form a judgement based on the results of the first 100 rotations.

The abrasion resistance of wood surfaces can be classified based on measurement results. A possible classification is given in Table 2.6.

The value of "mg/100 rotations" should be taken for the first stationary section of the curve. Generally, the second 100 rotations are suitable for this purpose. The determination of G_0 values is well defined as shown in Figs. 2.87 and 2.89. The abrasion resistance of wood materials may have correlation with their mechanical properties, especially with their hardness. Figure 2.90 represents measurement

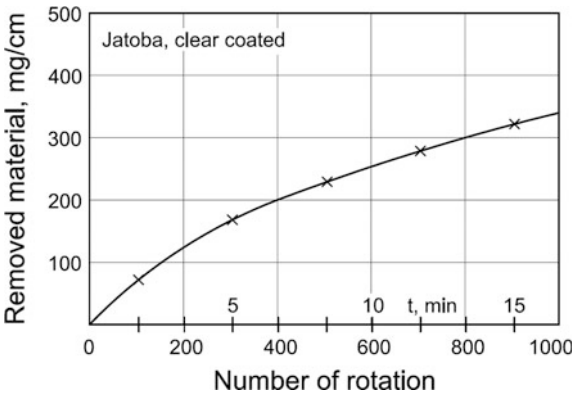

Fig. 2.88 Removed material as a function of the number of rotation on clear coated parquet

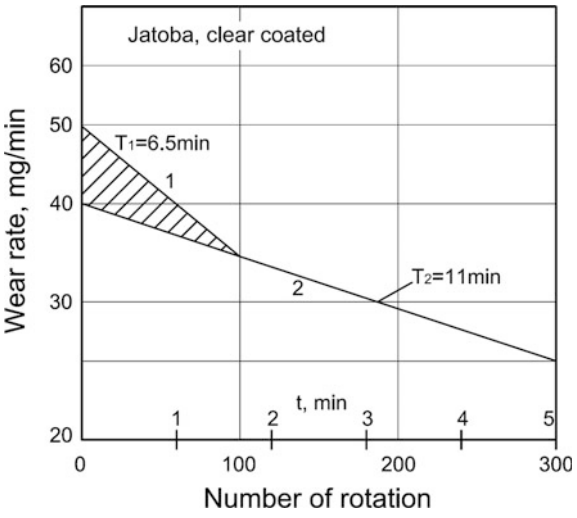

Fig. 2.89 Wear rate as a function of number of rotation for clear coated parquet

Table 2.6 Abrasion resistance classification

mg/100 rotation	G_0 (mg/min)	Classes
<80	<50	Very good
80–150	50–95	Good
150–220	95–140	Satisfactory

results using different wood species. The dynamic hardness was measured with a steel ball of 44.4 mm dia. (7/4 inch) and drop height of 0.5 m. Light conifers have H_d values between 400 and 700 J/cm^3 (or N/mm^2), but dense Pinewood over 700 kg/m^3 had hardness near 2000 J/cm^3.

Black locust has an excellent abrasion resistance at hardness values of 6000–8000 J/cm^3. The very dense Ironwood (1040 kg/m^3) possess hardness values up to 15,000 J/m^3 and correspondingly high abrasion resistance.

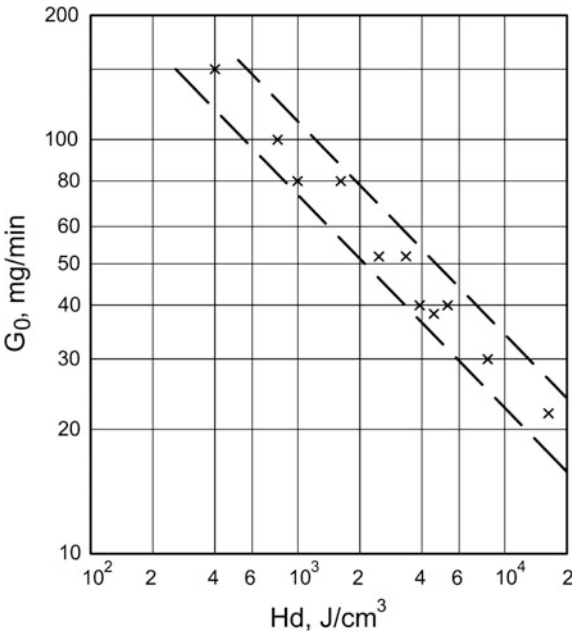

Fig. 2.90 Relation between wear rate and dynamic hardness for different wood species

It should be stressed that the dynamic hardness measurement is not very accurate. The permanent deformation can be measured, but the elastic recovery remains unknown. The size and mass of the ball and the energy of impact may also have a given influence on the obtained result. Furthermore, equation of the contact mechanics used for calculations are only valid, strictly speaking, for small deformations. In this respect, a bigger size is more favourable. Nevertheless, Fig. 2.90 gives a good orientation and overview of abrasion resistance for practical purposes.

References

Agresti, G., Bonifazi, G., Calienno, L., Capobianco, G., Lo Monaco, A., Pelosi, C., Picchio, R., Serranti, S.: Surface investigation of photo-degraded wood by colour monitoring, infrared spectroscopy, and hyperspectral imaging. J. Spectrosc. **1**(1), Article number 380536 (2013)

Ayadi, N., Lejeune, F., Charrier, F., Charrier, B., Merlin, A.: Colour stability of heat-treated wood during artificial weathering. Holz als Roh- und Werkstoff **61**, 221–226 (2003)

Bak, M., Németh, R., Csordós, D., Tolvaj, L.: Effect of treatment medium on the moisture uptake rate and colour change during natural weathering of heat treated wood, pp. 80–86. In: Conference of COST Action FP0904, Rogla, Slovenia, 16–18 Oct 2014

Bak, M., Németh, R., Tolvaj, L.: The colour change of oil-heat-treated timber during weathering. Óbuda Univ. E-Bull. **3**(1), 339–345 (2012)

Béldi, F., Bálint, J.: Einige Sorptionseigenschaften von Zementgebundenen Spanplatten. Acta Facultatis Ligniensis **1**, 25–38 (1986)

Béldi, F, Szabó, J.: Forgécslapok páradiffúziós vizsgálata. Experimental investigation of water-vapour diffusion of particle boards, pp. 43–49. EFE Tudományos Közleményei (1979)
Béldi, F., Bálint, J.: Über einigen Sorptionseigenschaften der Akazie. Acta Facultatis Ligniensis, **1**, 15–27 (1984)
Burmester, A., Olsen, C.: Verbesserung der Formbeständigkeit von Buchenholz durch Tränkung mit Diisocyanat. Holz als Roh- und Werkstoff, S. 84–89 (1971)
Calienno, L., Lo Monaco, A., Pelosi, C., Picchio, R.: Colour and chemical changes on photodegraded beech wood with or without red heartwood. Wood Sci. Technol. **48**, 1167–1180 (2014)
Carslaw, H., Jäger, J.: Conduction of Heat in Solids. Oxford University Press, New York (1959)
Chang, T.C., Chang, H.T., Wu, C.L., Chang, S.T.: Influences of extractives on the photodegradation of wood. Polym. Degrad. Stab. **95**, 516–521 (2010)
Christensen, G., Kelsey, K.: Die Geschwindigkeit der Wasserdampfsorption durch Holz. Holz als Roh- und Werkstoff, S.178–188 (1959)
Cloutier, A., Fortin, Y.: A model of moisture movement in wood. Wood Sci. Technol. **27**, 95–114 (1993)
Cloutier, A., Fortin, Y.: Moisture content—water potential relationship from saturated to dry conditions. Wood Sci. Technol. **25**, 263–280 (1991)
Csanády, E., Magoss, E.: Mechanics of Wood Machining. Springer, Berlin (2013)
Fowkes, F.M.: Acid-base interactions in polymer adhesion. In: Mittal, K.L. (ed.) Physicochemical Aspects of Polymer Surfaces, vol. 2, pp. 583–603. Plenum Press, NY (1983)
Gardner, D.J.: Application of the Lifshitz—van der Waals acid-base approach to determine wood surface tension components. Wood Fiber Sci. **28**(4), 422–428 (1996)
Gardner, D.J., Generella, N.C., Gunells, D.W., Wolcott, M.P.: Dynamic wettability of wood. Langmuir **7**, 2498–2502 (1991)
Garrett, H.: Contact angles and their significance for adhesion, pp. 19–41. In: Proceedings of Northampton College of Advanced Technology (1964)
Gindl, M., Sin, G., Gindl, W., Reiterer, A., Tschegg, S.: A comparison of different methods to calculate the surface free energy of wood using contact angle measurement. Colloids Surf. A **181**, 279–287 (2001)
Good, R.J.: Contact angle, wetting, and adhesion: a critical review. In: Mittal, K.L. (ed.) Contact Angle, Wettability and Adhesion, pp. 3–36. VSP, Utrecht (1993)
Hill, C.A.S.: Wood Modification: Chemical, Thermal and Other Processes. Wiley, London (2006)
Huang, A., Zhou, Q., Liu, J., Fei, B., Sun, S.: Distinction of three wood species by Fourier transform infrared spectroscopy and two-dimensional correlation IR spectroscopy. J. Mol. Struct. **883–884**, 160–166 (2008)
Huang, X., Kocaefe, D., Kocaefe, Y., Boluk, Y., Pichette, A.: Study of the degradation behavior of heat-treated jack pine (*Pinus banksiana*) under artificial sunlight irradiation. Polym. Degrad. Stab. **97**, 1197–1214 (2012)
Huang, X., Kocaefe, D., Kocaefe, Y., Boluk, Y., Krause, C.: Structural analysis of heat-treated birch (*Betula papyrifera*) surface during artificial weathering. Appl. Surf. Sci. **264**, 117–127 (2013)
Janka, G.: Härteprüfung des Holzes mittels Kugeldruckverfahren. Wien (1912)
Janka, G.: Die Härte der Hölzer, Wien (1915)
Kataoka, Y., Kiguchi, M., Fujiwara, T., Evans, P.D.: The effect of within-species and between-species variation in wood density on the photodegradation depth profiles of sugi (*Cryptomeria japonica*) and hinoki (*Chamaecyparis obtusa*). J. Wood Sci. **51**, 531–536 (2005)
Kataoka, Y., Kiguchi, M., Williams, R.S., Evans, P.D.: Violet light causes photodegradation of wood beyond the zone affected by ultraviolet radiation. Holzforschung **61**, 23–27 (2007)
Kubovsky, I., Kacík, F.: Colour and chemical changes of the lime wood surface due to CO_2 laser thermal modification. Appl. Surf. Sci. **321**, 261–267 (2014)
Liptáková, E., Kúdela, J.: Analysis of the wood-wetting process. Holzforschung **48**, 139–144 (1994)

Masuda, M.: Why human loves wood grain figure? Extraction of vision-physical characteristics deeply related to impression, pp. 11–23. In: ICWSF Conference, Ljubljana, 5–7 Sept 2001

Matsuo, M., Umemura, K., Kawai, S.: Kinetic analysis of color changes in keyaki (*Zelkova serrata*) and sugi (*Cryptomeria japonica*) wood during heat treatment. J. Wood Sci. **60**, 12–20 (2014)

Matsuo, M., Yokoyama, M., Umemura, K., Gril, J., Yano, K., Kawai, S.: Color changes in wood during heating: kinetic analysis by applying a time-temperature superposition method. Appl. Phys. A **99**, 47–52 (2010)

Mitsui, K.: Changes in the properties of light-irradiated wood with heat treatment. Part 2. Effect of light-irradiation time and wavelength. Holz als Roh- und Werkstoff **62**, 23–30 (2004)

Mitsui, K., Tsuchikawa, S.: Low atmospheric temperature dependence on photodegradation of wood. J. Photochem. Photobiol. B **81**, 84–88 (2005)

Mitsui, K., Takada, H., Sugiyama, M., Hasegawa, R.: Changes in the properties of light-irradiated wood with heat treatment. Part 1. Effect of treatment conditions on the change in color. Holzforschung **55**, 601–605 (2001)

Mitsui, K., Murata, A., Tolvaj, L.: Change in the properties of light-irradiated wood with heat treatment. Part 3. Monitoring by DRIFT spectroscopy. Holz als Roh- und Werkstoff **62**, 164–168 (2004)

Mitsui, K., Tolvaj, L., Papp, G., Bohus, J., Szatmári, S., Berkesi, O.: Changes in the properties of light-irradiated wood with heat treatment. Part 4. Application of laser. Wood Res. Slovakia **50**, 1–8 (2005)

Müller, U., Rätzsch, M., Schwanninger, M., Steiner, M., Zöbl, H.: Yellowing and IR-changes of spruce wood as result of UV-irradiation. J. Photochem. Photobiol. B **69**, 97–105 (2003)

Nakshabandi, G., Kohnke, H.: Thermal conductivity and diffusivity of soils as related to moisture tension. Agr. Meteorol. **2**, 271–279 (1965)

Németh, K.: Rolle des Feuchtigkeitsgehaltes des Holzes in der Hygroskopizität von Polyuretan-Holz-Kompositen. Acta Facultatis Ligniensis Sopron, S. 55–64 (1986)

Pandey, K.K.: Study of the effect of photo-irradiation on the surface chemistry of wood. Polym. Degrad. Stab. **90**, 9–20 (2005a)

Pandey, K.K.: A note on the influence of extractives on the photo-discoloration and photo-degradation of wood. Polym. Degrad. Stab. **87**, 375–379 (2005b)

Pandey, K.K., Vourinen, T.: Comparative study of photodegradation of wood by a UV laser and a xenon light source. Polym. Degrad. Stab. **93**, 2138–2146 (2008)

Persze, L., Tolvaj, L.: Photodegradation of wood at elevated temperature: colour change. J. Photochem. Photobiol. B: Biol **108**, 44–47 (2012)

Popescu, C.M., Popescu, M.C., Vasile, C.: Structural analysis of photodegraded lime wood by means of FT-IR and 2D IR correlation spectroscopy. Int. J. Biol. Macromol. **48**(4), 667–675 (2011)

Popescu, M.-C., Froidevaux, J., Navi, P., Popescu, C.-M.: Structural modification of *Tilia cordata* wood during heat treatment investigated by FT-IR and 2D IR correlation spectroscopy. J. Mol. Struct. **1033**, 176–186 (2013)

Sell, J.: Physikalische Vorgänge in wetterbeanspruchten Holzbauteilen. Holz als Roh- und Werkstoff, S. 259–267 (1985)

Sitkei, G. (ed.).: Faipari műveletek elmélete (Theory of wood processing), pp. 105–141. Szaktudás Kiadó Budapest (1994a)

Sitkei, G.: Non-linear rheological method describing compaction processes. Int. Agrophys. **8**, 137–142 (1994b)

Srinivas, K., Pandey, K.: Photodegradation of thermally modified wood. J. Photochem. Photobiol. B **117**, 140–145 (2012)

Stamm, A.: Passage of liquids, vapours and dissolved materials through softwoods. USDA Bull. **929**, 1946

Tolvaj, L., Faix, O.: Artificial ageing of wood monitored by DRIFT spectroscopy and CIE L*a*b* color measurements. I. Effect of UV light. Holzforschung **49**, 397–404 (1995)

Tolvaj, L., Mitsui, K.: Surface preparation and direction dependence of DRIFT spectra of wood. Appl. Spectrosc. **58**, 1137–1140 (2004)

Tolvaj, L., Mitsui, K.: Light source dependence of the photodegradation of wood. J. Wood Sci **51**, 468–473 (2005)
Tolvaj, L., Mitsui, K.: Validity limits of Kubelka-Munk theory for DRIFT spectra of photodegraded solid wood. Wood Sci. Technol. **45**, 135–146 (2011)
Tolvaj, L., Varga, D.: Photodegradation of timber of three hardwood species caused by different light sources. Acta Silvatica et Lignaria Hungarica **8**, 145–155 (2012)
Tolvaj, L., Molnar, S., Nemeth, R., Varga, D.: Color modification of black locust depending on the steaming parameters. Wood Res. Slov **55**, 81–88 (2010)
Tolvaj, L., Z, Molnar, Nemeth, R.: Photodegradation of wood at elevated temperature: infrared spectroscopic study. J. Photochem. Photobiol. B **121**, 32–36 (2013)
Tolvaj, L., Molnar, Zs., Magoss, E.: Measurement of photodegradation-caused roughness of wood using a new optical method. J. Photochem. Photobiol., B **134**, 23–26 (2014a)
Tolvaj, L., Nemeth, R., Pasztory, Z., Bejo, L., Takats, P.: Colour stability of thermally modified wood during short-term photodegradation. Bioresources **9**(4), 6644–6651 (2014b)
Tolvaj, L., Popescu, C.M., Molnar, Zs., Preklet, E.: Dependence of the air relative humidity and temperature on the photodegradation processes of beech and spruce wood species. Bioresources (in print) (2015)
van Genuchten, M.: A closed-form equation for predicting the hydraulic conductivity of unsaturated soils. Soil Sci. Soc. Am. J. **44**, 892–898 (1980)
Van Oss, C.J., Chaudhury, M.K., Good, R.J.: Monopolar surfaces. Adv. Colloid Interface Sci. **28**, 35–64 (1987)
Varga, D., van der See, M.E.: Influence of steaming on selected wood properties of four hardwood species. Holz als Roh- ond Werkstoff **66**, 11–18 (2008)
Tolvaj, L., Tsuchikawa, S., Inagaki, T., Varga, D.: Temperature dependence of photodegradation of wood monitored by colour measurement. Wood Sci. Technol. doi:10.1007/s00226-015-0749-1 (in print)
Yildiz, S., Yildiz, U.C., Tomak, E.D.: The effects of natural weathering on the properties of heat-treated alder wood. Bioresources **6**(3), 2504–2521 (2011)
Zavarin, E., Jones, S.J., Cool, L.G.: Analysis of solid wood surfaces by diffuse reflectance infrared Fourier transform (DRIFT) spectroscopy. J. Wood Chem. Technol. **10**, 495–513 (1990)
Лыков, А.В., Михайлов, Ю.: А. Теория переноса энергии и вещесва Изд. АН. БССР, Минск, 1959. (Theory of energy and mass transfer)
Шубин, Г.: Физические основы и расчет процессов сушки древесины, pp. 271–279. Лесная промышленностъ, Москва (Physical background of wood drying) (1965)

http://www.springer.com/978-3-319-22418-3

Quality of Machined Wood Surfaces

Csanády, E.; Magoss, E.; Tolvaj, L.

2015, X, 257 p. 273 illus., 20 illus. in color., Hardcover
ISBN: 978-3-319-22418-3